

**Functionalized Thermo-responsive Polymer Core-shell Materials for use in
Controlled Dye Release, Thin-film Composite Membranes, and Water Desalination**

by

Madeline Tuai

A thesis submitted in partial fulfillment of the requirements for the degree of

Master of Science

Department of Chemistry

University of Alberta

©Madeline Tuai, 2024

Abstract

This thesis focuses on the varied applications of core-shell structured stimuli-responsive polymer materials and their applications in water treatment. The relevant background and introduction to stimuli-responsive polymers, core-shell particles and morphologies, and membrane separations systems is detailed in Chapter 1.

Chapter 2 explores the effect of shell thickness on the uptake and release of dye loaded into pNIPAm-based microgels. The modified core is designed for the uptake of oppositely charged dye species where the release of the dye can be triggered by changes in pH. The release profiles from the loaded microgels free in solutions as well as immobilized on a gold surface at temperatures below and above the LCST was observed.

Chapter 3 utilized a similar morphology core-shell nanogel where a poly(N-3-aminopropyl)methacrylamide polymer shell was added to a pNIPAm core that could be covalent crosslinked to the selective polyamide layer used in thin-film composite (TFC) membranes. The feed temperature of the pressure-driven nanofiltration membranes was heated above the LCST of the nanogels to observe the changes in flux and salt rejection when the nanogels were incorporated within the polyamide structure. Further, the nanogels were localized on the surface of the polyamide to observe the impact they had on improving the antifouling properties of the TFC membrane.

The final project detailed in Chapter 4 utilizes a spherical pNIPAm hydrogel coated in the polyamide skin layer to create a self-driven water filtration system. The clean water absorbed by the hydrogel can be recovered by heating the hydrogels. The salt rejection was evaluated by ICP-AES and confirmed excellent rejection performances for the optimized polyamide layer against a variety of salt species.

Acknowledgements

I would like to express my deepest appreciation to my supervisor, Dr. Michael Serpe, for his guidance, patience, and support throughout my time working in his lab. I am grateful to him for sharing his invaluable knowledge and for having faith in me to be able to succeed in his group. I also would like to sincerely thank Dr. Mohtada Sadrzadeh and his research group for sharing their lab and expertise with me. Working collaboratively with the Advanced Water Research Lab on several projects and the opportunity to learn from them during my program was a true privilege. And my deepest appreciation to Dr. Jonathan Veinot for being on my committee, and for generously sharing kind words of support and feedback.

I would like to extend thanks to Dr. Pooria Karami from the AWRL for generously sharing his time and knowledge with me. And to Dr. Krista Freuhauf, my heartfelt thanks for your mentorship and steadfast support. I would also like to give a special thanks to my undergraduate research supervisor Dr. Kingsley Donkor and to Dr. Sharon Brewer from Thompson Rivers University who both inspired me to pursue research and have been instrumental influences throughout my academic career.

To my fellow Serpe group lab mates, thank you for all the encouragement and camaraderie these past years with a special thanks to Haley Hunter, Alyssa Fu, and Nicholas Balasuriya. And to all my friends in the department, the hours of conversation and laughs will always be cherished.

Lastly, to my parents, grandparents, and my sister, thank you for your unwavering love and support. I could not have done this without you.

Table of Contents

Abstract	ii
Acknowledgements	iii
Table of Contents	iv
List of Tables	vi
List of Figures	vii
List of Abbreviations	x
Chapter 1 Introduction to Thermo-responsive Polymers and Composite Membranes.....	1
1.1 Introduction to Stimuli-Responsive Polymers.....	1
1.1.1 Stimuli-Responsive Polymer Materials	1
1.1.2 Thermo-responsive Polymers.....	2
1.1.3 pNIPAm-based Polymer Materials	4
1.1.4 pH Responsive Materials	4
1.2 Core-shell Materials	6
1.2.1 Functionalities of Different Layers of Core and Shell.....	6
1.2.2 Synthesis of Core-shell Materials.....	8
1.3 Background on Thin-film Composite Membranes for Water Treatment.....	11
1.3.1 Modified Membrane Separation Systems.....	11
1.3.2 Modification of Polyamide Selective Layer with pNIPAm	12
1.3.3 Hydrogels for Water Treatment	14
1.4 Conclusion	16
Chapter 2 Poly(<i>N</i>-isopropylacrylamide)-based Core-shell Microgels for Controlled Release of Dyes	17
2.1 Introduction	17
2.2 Experimental Section	20
2.2.1 Core-shell Microgel Synthesis	21
2.2.2 Dye Uptake Experiments	22
2.2.3 Dye Loading and Release from Free Solution Microgels	23
2.2.4 Dye Loading and Release from Immobilized Microgels	24

2.2.5 Characterization of Microgels	24
2.3 Results and Discussion	27
2.4 Conclusion	36
<i>Chapter 3 Coupling Thermo-responsive Core-shell Nanogels with Thin-film Composite Membranes for Improved Thermal and Anti-fouling Behaviour</i>	<i>37</i>
3.1 Introduction	37
3.2 Experimental Section.....	38
3.2.1 Core-shell Nanogels Synthesis	39
3.2.2 Preparation of Composite Membranes	40
3.2.3 Temperature Ramp Nanofiltration experiments	41
3.2.4 Antifouling Nanofiltration Experiments.....	43
3.2.5 Characterization of Nanogels and Membranes	44
3.3 Results and Discussion	45
3.4 Conclusion	56
<i>Chapter 4 Self-driven Water Filtration and Clean Water Recovery using Polyamide-coated Thermo-responsive Polymer Hydrogels.....</i>	<i>57</i>
4.1 Introduction	57
4.2 Experimental Section.....	59
4.2.1 Preparation of Spherical Hydrogels and Polyamide Coating	59
4.2.2 Preparation of Flat Hydrogels	60
4.2.3 Filtration Experiments and Data Treatment	60
4.2.4 Characterization.....	62
4.3 Results and Discussion	64
4.4 Conclusion	74
<i>Chapter 5 Conclusions and Future Work</i>	<i>75</i>
<i>References</i>	<i>78</i>

List of Tables

Table 2.1 Hydrodynamic diameter of microgel cores and core-shells at different pH, temperature, and polymerization yields	25
Table 3.1 Summary of membrane properties for temperature ramp experiments	42
Table 3.2 Summary of membrane properties for antifouling experiments.....	43
Table 3.3 Summary of data of core and core-shell nanogels for measuring the hydrodynamic size at different temperatures and pH's and zeta potential results.....	45

List of Figures

Figure 1.1 Structures of comonomers that have LCST properties	4
Figure 1.2 Structures of common anionic monomers and cationic monomers	6
Figure 1.3 Schematic illustrations of multi-step polymerization methods to generate core-shell materials (a-d) and (e) is a scheme of microfluidic one-step polymerization of core-shell spheres. Both reprinted with permission from Ref. 46 © 2015 IEEE	10
Figure 1.4 Scheme of pressure-driven membrane separation stages	12
Figure 2.1 Illustration of the swelling and shrinking mechanism of (a) acrylic acid comonomer and (b) N-(3-aminopropyl)methacrylamide in response to changes in pH above and below the respective pK_a	20
Figure 2.2 Polymerization reaction scheme for the fabrication of (a) functional pNIPAm cores and (b) pNIPAm shell addition to make core-shell microgels.....	22
Figure 2.3 Illustration of dye release experiment set up	23
Figure 2.4 Brightfield TEM image of dried microgel samples (a) AAc-core and (b) APMA core	26
Figure 2.5 AFM images of the immobilized (a) AAc-core, (b) AAc-20, (c) APMA-core, and (d) APMA-20 on a gold-coated glass slides with the approximate dry microgel radius	26
Figure 2.6 Bar graph depicting the change in absorbance of a dye solution before (blue, left bar) and after (orange, right bar) adding microgel samples to it. (a) The addition of AAc-core, AAc-5, AAc-10, and AAc-20 to 22 μ M CV at pH 3 and pH 6.5. (b) The addition of APMA-core, APMA-5, APMA-10, and APMA-20 to 45 μ M OII at pH 5.5 and pH 11	29
Figure 2.7 Plot of absorbance versus time for the dye release of (a) crystal violet dye release at 590 nm from AAc-core (blue), AAc-5 (red), AAc-10 (green), and AAc-20 (purple) at 25 °C (solid line) and at 40 °C (dashed line). (b) orange II dye release at 486 nm from APMA-core (blue), APMA-5 (red), APMA-10 (green), and APMA-20 (purple). The absorbance plots for 5 μ M concentrations of (c) CV at pH 6.5 adjusted to pH 3 after 1 min of circulating and (d) OII at pH 5.5 adjusted to pH 11 after 1min of circulating at 25 °C (blue) and 40 °C (red)	32

Figure 2.8 Absorbance profiles with time collected via UV-Vis to measure the dye release from (a) immobilized AAc-containing microgels and (b) APMA -containing microgels below the LCST (solid line) and above the LCST (dashed line).	35
Figure 3.1 Polymerization scheme for (a) pNIPAm core and (b) APMA shell addition.	40
Figure 3.2 Nanofiltration set up used for testing the TFC membranes.....	42
Figure 3.3 (a) Brightfield TEM image of the core-shell nanogels and (b) bromophenol blue staining test for amines on the core-APMA shell (right) and the pNIPAm core (left). (a) Brightfield TEM image of the core-shell nanogels and (b) bromophenol blue staining test for amines on the core-APMA shell (right) and the pNIPAm core (left).	45
Figure 3.4 Interfacial polymerization scheme for the formation of the polyamide on the membrane support	48
Figure 3.5 The change in flux with increasing temperature plot for (a) 1% PIP base and modified membranes and for (b) 0.5% PIP base and modified membranes. The % salt rejection at 25 °C (blue) and at 50 °C (red) for (c) 1% PIP membranes and (d) 0.5% PIP membranes.	50
Figure 3.6 (a) dynamic contact angle and (b) zeta potential data for the base and modified membranes. AFM and SEM images for the base membrane (c & g), 400/400 (d & h), 400 s-mod (e & i), and the 800 s-mod membrane (f & j).....	53
Figure 3.7 Change in flux with time where the initial flux was recorded (0-20 min), the impact of fouling on the flux (20-80 min), and the recovered flux after washing (80-100 min) for the base (blue) and modified membranes	55
Figure 4.1 Images of a pNIPAm hydrogel with a 1% MPD-0.4% TMC PA coating swelling in water captured every 15 min for 2 hr and after 24 hr.	62
Figure 4.2 FTIR spectra of the bare hydrogel (in red) and the hydrogel coated in 2% MPD-0.4% TMC polyamide composition (in green)	63
Figure 4.3 FESEM images of the polyamide layer on a dried flat hydrogel for (A) 1% MPD-0.1% TMC, (B) 1% MPD-0.4% TMC, (C) 2% MPD-0.1% TMC, and (D) 2% MPD-0.4% TMC (with high mag. inset).....	64

Figure 4.4 Polymerization and polyamide coating scheme.....65

Figure 4.5 SEM images for the (a) bare hydrogel, (b) 1%MPD-0.1% TMC, (c) 1% MPD-0.4% TMC, (d) 2% MPD-0.1% TMC, and (e) 2% MPD-0.4% TMC polyamide layers separated from the spherical hydrogels.....67

Figure 4.6 AFM images to determine surface roughness of the (a) the bare hydrogel, and the polyamide coatings of (b) 1% MPD-0.1% TMC, (c) 1% MPD-0.4% TMC, (d) 2% MPD-0.1% TMC, and (e) 2%MPD-0.4% TMC68

Figure 4.7 Calculated flux of the hydrogels with (a) 1% MPD-0.4% TMC and (b) 2% MPD-0.4% TMC PA coating in various feed concentrations (in blue) and the percent water taken up by the gel within the time scale (in green)69

Figure 4.8 Images of PA coated hydrogels in (A) 1% MPD-0.1% TMC, (B) 1% MPD-0.2% TMC, (C) 1% MPD-0.4% TMC, (D) 2% MPD-0.1% TMC, (E) 2% MPD-0.2% TMC, (F) 2% MPD-0.4% TMC, and (G) a bare hydrogel after 2 hr in 10 ppm reactive red solution. Bar graph is rejection plot of reactive red for each gel71

Figure 4.9 (a) The performance of different PA compositions after one filtration and recovery cycle. (b) The selectivity of 1% MPD-0.4% TMC against different salts. The mole ratio of salt of the PA coated hydrogel (in blue) and a bare hydrogel control (in red) bar graph, where a ratio ≥ 1 is indicative of a selective PA. Both 1% MPD-0.4% TMC (c) and 2% MPD-0.4% TMC (d) were able to withstand 3 filtration and heat recovery cycles. The % water recovered in presented in green on for each respective heat cycle.....73

List of abbreviations

4-VP	4-vinylpyridine
AAc	Acrylic acid
AFM	Atomic force microscopy
AM	Acrylamide
APMA	N-(3-aminopropyl) methacrylamide
APS	ammonium persulfate
BIS	N,N'-methylenebisacrylamide
CA	contact angle
CTAB	Cetrimonium bromide
CV	Crystal violet
DI	Deionized water
DLS	Dynamic light Scattering
ED	Electrodialysis
FTIR	Fourier-transform infrared spectroscopy
GPTA	Glycerol propoxylate triacrylate
HCl	Hydrochloric acid
ICP-AES	Inductively coupled plasmon atomic emission spectrometer
IP	Interfacial polymerization
IS	Ionic strength
K _a	Dissociation constant
LCST	Lower critical solution temperature
MA	Maleic acid
MAAc	Methacrylic acid
MF	Microfiltration
MG	Microgel
MPD	m-phenylenediamine
MW	Molecular weight
NaOH	Sodium Hydroxide
NF	Nanofiltration

NG	Nanogel
OII	Orange II
PA	polyamide
pDEAAm	poly(N,N'-diethylacrylamide)
PEGDA	poly(ethylene glycol) diacrylate
PEI	polyetherimide
PES	polyethersulfone
PET	poly(ethylene terephthalate)
PGLA	poly(lactic-co-glycolic acid)
PIP	piperazine
pNIPAm	poly(N-isopropylacrylamide)
PSf	polysulfone
PTA	Phosphotungstic acid
pVCL	poly(N-vinylcaprolactam)
RO	Reverse osmosis
SA	Sodium alginate
SDS	Sodium dodecyl sulfate
SEM	Scanning electron microscopy
TCE	Tetrachloroethylene
TEA	Triethylamine
TEM	Transmission electron microscopy
TEMED	tetramethylethylenediamine
TFC	Thin-film composite
T _g	Glass transition temperature
TMC	Trimesoyl chloride
UF	Ultrafiltration
USCT	Upper critical solution temperature
V50	2,2'-azobis(2-amindinopropane) dihydrochloride
ZP	Zeta potential

Chapter 1 Introduction to Thermo-responsive Polymers and Composite Membranes

1.1 Introduction to Stimuli-Responsive Polymers

Stimuli-responsive polymer materials have been incorporated in many different systems to integrate “smart” characteristics made possible by the intrinsic properties of the material to respond to changes repeatedly and reversibly in the system environment. For example, these polymers can undergo physical or chemical changes in response to temperature, light, pH, or magnetic fields. The focus of this chapter is to explore the general characteristics of temperature responsive pNIPAm-based polymer materials as they pertain to studies of dye release and water treatment systems.

1.1.1 Stimuli-Responsive Polymer Materials

Stimuli-responsive polymers can be synthesized through the polymerization of specific monomers that possess such properties, or by incorporating them physically or chemically into a pre-existing matrix. Like many polymer materials, the 3-D structures can often be tuned and manipulated to fit the desired system. Whether it be large macro-scale hydrogels or micro-scale nanoparticles, the flexibility of the size of material is a key advantage when exploring the applications in controlled drug delivery,^{1,2} sensing,³ biomimetic actuators,⁴ separation,⁵ and water treatment.⁶

Generally, the polymeric structures are formed by crosslinking hydrophilic polymer chains by chemical or physical interactions. The resulting sponge-like structure can absorb and retain up to 10^3 times the dry polymer weight in water without dissolving depending on the crosslinking density and hydrophilic nature of the bulk polymer.⁷ Without the presence of a barrier, the porous structure will allow for the transport of ions and small molecules into and out of the polymer matrix depending on the mesh size.

Consider a hydrogel in pure water without a hindering selective layer to influence the swelling kinetics of the system. In this case, the Flory-Rehner theory describes the equilibrium swelling of the hydrogel as the enthalpy of polymer-solvent mixing and limited

by the elasticity related to the degree of crosslinking, represented by the following equation (1.1).⁸

$$(1.1) \quad \Delta G_{tot} = \Delta G_{el} + \Delta G_{mix}$$

Where the Gibbs free energy of the system (ΔG_{tot}) is the summation of ΔG_{el} and ΔG_{mix} which are the elastic and mixing forces, respectively. When a dry hydrogel contacts water, the swelling pressure, or osmotic pressure, of the polymer drives the absorption of water until a maximum at equilibrium swelling. When a stimuli-responsive hydrogel responds to a change in the environmental conditions, the swelling equilibrium shifts and the water absorption ratio decreases, as a measure of mass of water absorbed in relation to the mass of the polymer (g/g dry gel). This effect can be induced by changes in UV exposure, magnetic fields, temperature, pH, ionic strength, and other physical or chemical stimuli depending on the chosen polymer.⁹

1.1.2 Thermo-responsive Polymers

Thermo-responsive polymers are widely studied due to their ability to reversibly undergo significant changes in solubility, volume, and refractive index with varying changes in temperature. This class of polymer will change phase at a given lower or upper critical solution temperature (LCST or UCST, respectively), or both. The LCST can be described as the lower bound temperature interval in which all components of the polymer are soluble in the solvent environment that transitions to insoluble at temperatures above the LCST. The inverse is true for a polymer with a USCT where it transitions from insoluble to soluble as the temperature is increased above the USCT.¹⁰⁻¹²

Popular LCST polymers include poly(N- isopropylacrylamide) (pNIPAm), poly(N,N'-diethylacrylamide) (pDEAAm), and poly(N-vinylcaprolactam) (pVCL). The structures of these LCST thermos-responsive polymers are shown in Figure 1.1. Polymers with LCST behaviour typically contain both hydrophilic and hydrophobic groups that contribute to the rearrangement structure when they undergo solubility transitions. This can be thermodynamically described by the Gibbs free energy equation (Equation 1.2).

(1.2)

$$\Delta G = \Delta H - T\Delta S$$

Where ΔG represents the interactions with the polymer in solvent, ΔH corresponds to the change in enthalpy, T is the temperature in Kelvin, and ΔS is the change in entropy. The polymer is soluble when ΔG is negative and water molecules are hydrogen bonded to the hydrophilic regions of the polymer chain, in combination with the hydrophobic effect where water molecules form a cage-like arrangement around the hydrophobic regions of the chain, resulting in an exothermic arrangement and decreased entropy. As the temperature increases, the increased entropy dominates resulting in a positive ΔG as an increase in polymer-polymer and solvent-solvent interactions is observed. The hydrophilic-hydrophilic and hydrophobic-hydrophobic interactions results in a spontaneous rearrangement, collapsing the polymer network on itself, and expelling the bound water molecules in an endothermic process.¹¹⁻¹³

The LCST of a polymer is subjective to the hydrophilic and hydrophobic substituents of the monomer unit as the transition is largely dependent on the hydrogen bonding between the solvent and the polymer. Generally, the LCST is increased with the addition of more hydrophilic groups or polar groups present in the polymer.¹⁴ The opposite is true when increasing the hydrophobicity of the polymer, the LCST will decrease. This can tune the polymer system to a targeted transition temperature depending on the system. For example, the LCST of pNIPAm is around 32°C, near physiological temperatures, which makes it highly useful for targeted drug delivery in vivo. By increasing the LCST by adding hydrophilic units such as polyacrylamide, the LCST increases to near 40 °C and imparts a pH sensitivity to the polymer allowing for a triggered release of loaded species only under the right conditions of pH and temperature.¹⁵ LCST can also be impacted by co-solvent systems, crosslinking density, size, and structure of the polymer.

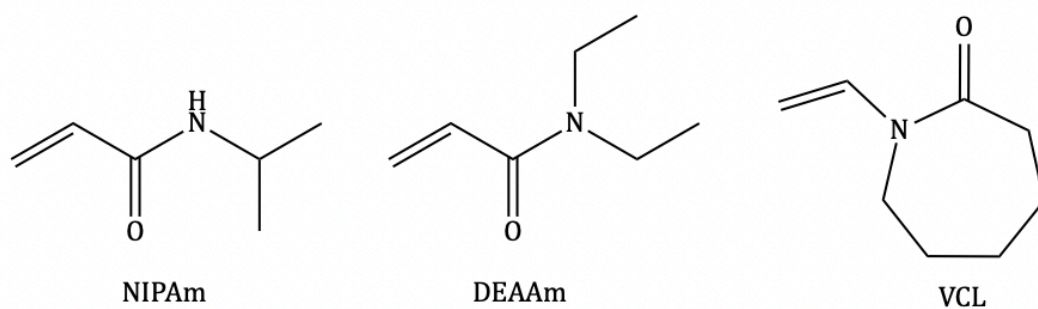


Figure 1.1 Structures of common monomers that have LCST properties. (prepared in ChemDraw)

1.1.3 pNIPAm-based Polymer Materials

pNIPAm is the most widely studied thermo-responsive polymer and as a result there are many innovative applications exploiting its properties such as its biocompatibility, its high-volume phase transition, and easily tunable size and shape. The LCST behaviour allows for it to be easily polymerized into spherical nanogels or microgels ranging from <100 nm up to several μm in diameter, respectively, via free-radical polymerization. These small, soft materials respond rapidly to temperature and retain a large volume transition ratio when heated above LCST in comparison to larger hydrogel structures. The larger scale pNIPAm hydrogels have been used in artificial muscles and biomimetic systems that behave as living organisms do in nature, responding to external stimulus like Venus flytraps that snap shut when touched.¹⁶ Systems that utilize pNIPAm can chemically modify the bulk polymer by incorporating pH and light sensitive monomers,^{15,17,18} chelating-agents for analyte specific detection or capture and release,^{19,20} and DNA-grafts for sensing and target treatment in vitro.²¹

1.1.4 pH Responsive Polymers

The addition of pH sensitive monomers to pNIPAm produces a polyelectrolyte polymer. Where pNIPAm alone is nonionic, the addition of charged, ionic monomer units will increase the LCST above that of pure pNIPAm and dominate the deswelling kinetics via electrostatic repulsion.^{14,22,23} Although, this may be favourable as increased Coulombic

repulsion between the immobilized ionic moieties will increase the water absorbance capacity of the polymer and the increase in swelling pressure allows for rapid hydration compared to pure pNIPAm. Some common ionic comonomers are acrylic acid (AAc), methacrylic acid (MAAc), maleic acid (MA), 4-vinylpyridine (4-VP), and N-(3-aminopropyl) methacrylamide hydrochloride (APMA) (Figure 1.2). The carboxylic acid groups, or the amine group in DMAEMA and APMA, are ionizable depending on the dissociation constant (K_a) of the group. The incorporation of the ionic monomer imparts a reversible pH dependent swelling responsive behaviour that is triggered at approximately the pK_a of the monomer.²⁴⁻
²⁶ In the case of a pNIPAm-*co*-AAc polymer, the pK_a of AAc is ~ 4.3 . Therefore, at a pH below the pK_a , majority of the carboxylic acid group of AAc are protonated. By increasing the pH above the pK_a , the carboxylic acid will be deprotonated, and an increased swelling capacity is observed in the polymer network.

This variety of polyelectrolyte polymer will also respond to the presence of ions or small molecules of opposite charge. If the majority of the AAc groups in a polymer are deprotonated and in the presence of NaCl, the dissociated Na^+ ions will interact the negative charges, this is known as Debye screening.^{27,28} This assumption that the pH triggered transition in the presence of salt is relative to the pK_a is highly dependent on the composition ratio of ionic and non-ionic monomers and the ionization state of the groups in the surrounding environment. A polyelectrolyte with a high charge density is also very sensitive to ionic strength as the pK_a can shift to several magnitudes higher for an acidic polymer or inversely, lower for a basic polymer. For example, the pK_a for pAAc in 1 mM NaCl is closer to 11 than the 4.3 of a single pAAc chain.²⁴ In the interest of species uptake and pH triggered release in functionalized polymer particles, as is the focus of the work detailed in Chapter 2 of this thesis, the dramatic change in pH is enough to overcome the Debye screening and disrupt other polymer-ion interactions to observe rapid deswelling of the material.

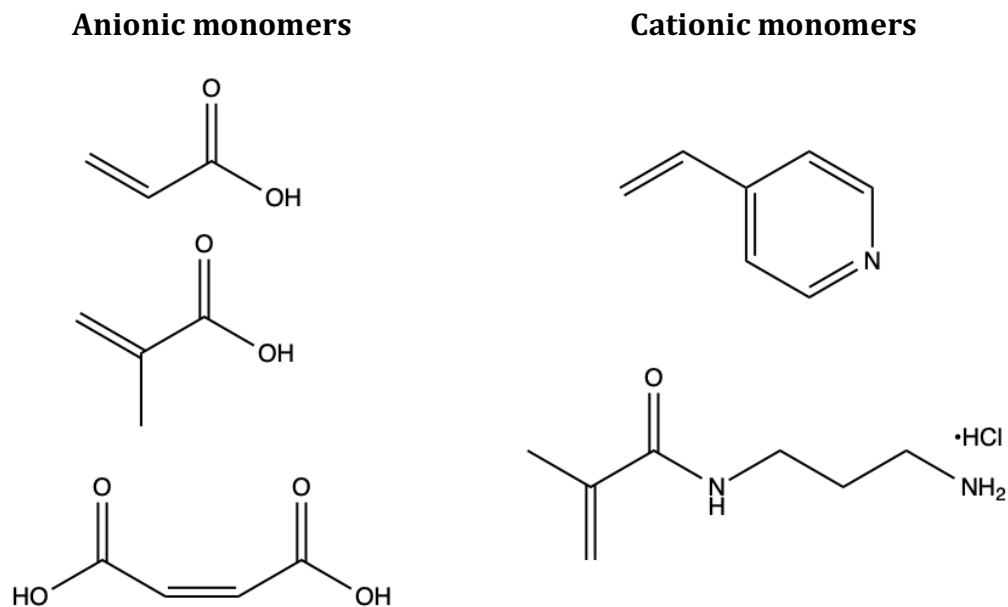


Figure 1.2 Structures of common anionic monomers (left) and cationic monomers (right).

1.2 Core-shell Materials

Core-shell structures are particles that consist of two or more different material layers that are unique in their flexible composition and size. The ability to selectively tune the functionalities of both the core and shell layer to suit is highly useful when developing smart materials. These materials have practical applications in the food and cosmetic industry, biomedical purposes like drug encapsulation and delivery, as well as materials for aiding in water treatment systems.²⁹

1.2.1 Functionalities of Different Layers of Core and Shell

The composition and morphology of spherical core-shell particles can vary by the nature of the core, the shell, and number of shell layers to customize the particle for the desired application. The core of the particle can be hollow, or gas filled, which are typically formed by etching away a solid core template after the shell(s) have been formed around it. Hollow particles can act as protective membrane for active compounds like proteins and enzymes, or nutrient encapsulators such as probiotics that can be protected from the gastric environment by a polymer shell until delivery to the small intestine.³⁰ The core can also be a liquid phase where the shell is often a nonpermeable layer to protect the core contents from

the surrounding environment. The liquid cores are very interesting as they can be used in artificial cells.³¹ One study found that a liquid core-hydrogel shell microsphere was able to significantly improve embryonic stem cell proliferation within 7 days when compared to immobilized cultured cells or 3D microgels without the core-shell morphology.³² A core-shell particle can also have a solid core that can be made of metal,³³⁻³⁵ silica,^{36,37} and polymer materials like polystyrene or, in the context of this work, pNIPAm.³⁸⁻⁴¹ The solid core increases the particle integrity, and the added layer increases the potential for multifunctionalized use.

The shell can similarly be tailored in several ways by composition and number of shell layers. The shell must be a solid phase and can be an organic layer like the natural polymer chitosan. Chitosan is biocompatible, biodegradable, and non-toxic making it an excellent material candidate for drug transport and release. A study by Yang et al. reported a core-shell microparticle that contained both free drug molecules as well as drug-loaded poly(lactic-co-glycolic acid) (PGLA) nanoparticles. The particle-within-a-particle system was designed so that the pH triggered release of the free drug and PGLA-drug nanoparticles resulted in both an immediate release of the drug as well as the time-delayed release of the drug as the PGLA slowly degraded.⁴² Alternatively, an inorganic shell like silica or metal species like gold, copper, or nickel, will improve the thermal stability and thermal conductivity.⁴³ The presence of a gold shell has applications in in-vivo NIR imaging due to its biocompatibility and photo absorbing properties.⁴⁴ The versatility of core-shell materials will be further discussed in the scope of the work to follow where a core-shell structure of solid polymer core and shell can be used for both dye molecule uptake and release, incorporation in thin-film composite membranes for water treatment, and as a novel core-shell structure for self-driven water treatment.

1.2.2 Synthesis of Core-shell Materials

There are several synthetic methods for making a core-shell structure including physical methods such as layer-by-layer assembly, sol-gel templating, spray drying and electrospray, as well as chemical polymerization routes. Herein only chemical polymerization routes were used and will be discussed in detail.

Microfluidics is a common route for fabricating uniform core-shell nano- and microspheres that have narrow size distribution and precise control over shell thickness.⁴⁵ This is usually done in a one- or two-step sequence where uniform droplets of an emulsion of monomer and crosslinker are suspended in an immiscible phase where the surface tension maintains the droplet shape until the polymerization is complete. Successive polymerizations can be done to add one or more shells in a multi-step synthesis. Recently there have been methods developed that allow for the core and shell to be polymerized in a one-step polymerization. An example that well represents the general process of a one-step fabrication method was presented by Zhou et al. where aqueous droplets of dissolved core monomer (PEGDA) and photoinitiator are directed into a continuous immiscible toluene phase containing dissolved shell monomer (GPTA) and surfactant as seen in **Figure 1.3-e**. UV exposure activates the photoinitiator contained in the core droplet, generating radicals that diffuse throughout the polymer core. Eventually the radicals will migrate towards the edge of the core, through the surfactant layer, triggering the polymerization of the GPTA to form the shell.⁴⁶ Microfluidic platforms have also been used to create particles with surface microstructures (i.e. folds, pits, bubbles, protruding “tentacle” growths) to increase the surface area and show great potential for bioapplications.^{47,48} There are clear advantages to using microfluidics to synthesize core-shell structures including uniform and tunable size and thickness, but this is limited in production rates for large scale synthesis.

Alternative methods to microfluidics are large-scale polymerizations that still utilize the same fundamental radical polymerization techniques but without the microfluidic platform. Free radical precipitation polymerization is a common method and was used to prepare the materials presented in this work. In a two-step method, the cores were first synthesized from an aqueous volume of dissolved monomer (pNIPAm), N,N'-

methylenebisacrylamide (BIS) crosslinker, and cetrimonium bromide (CTAB) as a surfactant. The volume was heated to 70 °C then initiated with 2,2'-azobis(2-amidinopropane) dihydrochloride (V50). The spherical cores grow from small aggregates of collapsed crosslinked pNIPAm polymer, as the reaction temperature is above the LCST, resulting in outward growth to a stable and decently monodisperse precipitation method with good yields. The second step shell addition occurs must like the first where the collapsed core particles act as nuclei for further polymerization rather which is preferential over new growth (Figure 1.3-a).⁴⁰

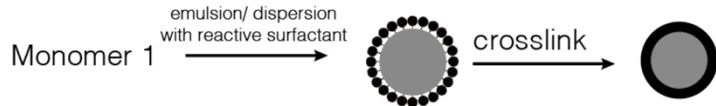
Other multi-step polymerizations can generate interesting surface morphologies on the shell as is done in stepwise hetero-coagulation procedures. For this design, cationic polymer units are packed onto an anionic core polymer when heated above the glass transition temperature (T_g) of the cationic shell particles.⁴⁹ The shell morphology for particles made by this route can vary from relatively smooth and uniform, to a bulky “raspberry-like” appearance depending on the size and packing density of the shell polymer (Figure 1.3-c).^{37,50}

Block copolymerization methods can also be used to form core-shell materials as seen in Figure 1.3-d. Block copolymers self-assemble to form micelles in solvents appropriate to solvate one of the blocks. Usually, the core forms a micelle which can be crosslinked while the soluble shell blocks form a corona shell around it.³⁹ The ends of the shell polymer chains can be functionalized for multiple applications or for further modification. Alternatively, the core-shell structure can be achieved by crosslinking the shell rather than the core.³⁸

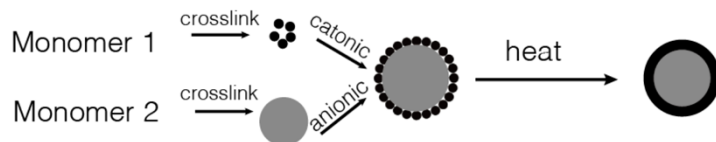
a) Two stage emulsion polymerization



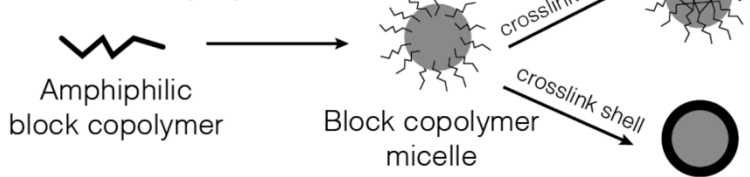
b) Emulsion polymerization with reactive surfactant



c) Step-wise hetero-coagulation



d) Block copolymerization



e)

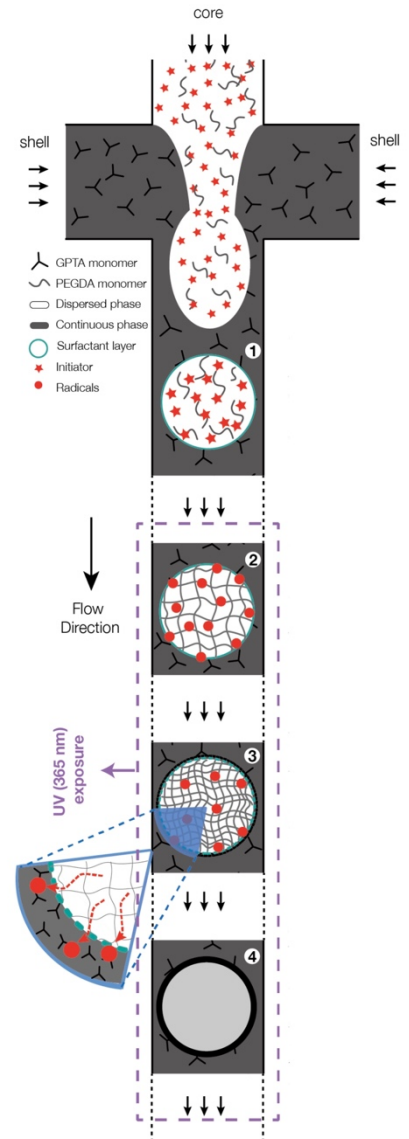


Figure 1.3 Schematic illustrations of multi-step polymerization methods to generate core-shell materials (a-d) and (e) is a scheme of microfluidic one-step polymerization of core-shell spheres. Both reprinted with permission from Ref. 46 © 2015 IEEE.

1.3 Background on Thin-film Composite Membranes for Water Treatment

The demand for new and innovative advancements for water treatment has grown significantly in recent years to meet the stresses for clean water globally. Not only will this impact the human population, but also wildlife, agriculture and food systems, and industrial sectors.^{51,52} A filtration membrane must be robust enough to withstand long-term filtration cycles, be resistant to fouling of organic and inorganic matter, and maintain selectivity to produce a clean permeate, while being cost-effective to produce. The details in this chapter section summarizes relevant background information on thin film composite membranes for pressure driven filtration systems as well as self-driven systems utilizing hydrogels.

1.3.1 Modified Membrane Separation Systems

Thin-film composite (TFC) membranes are semi-permeable materials that allow the passage of water molecules but excludes larger solutes when a driving force is applied to the membrane, forces such as pressure, temperature, concentration gradients, or electrical potential. Pressure-driven filtration is the most common as it can be tailored for the removal of different sized solutes based on the desired level of separation. Microfiltration (MF), ultrafiltration (UF), nanofiltration (NF), and reverse osmosis (RO) will separate solutes of decreasing size from $> 1 \mu\text{m}$ down to dissolved salt ions that are $< 1 \text{ nm}$ in diameter, schematically represented in Figure 1.4. As the solute size decreases, the applied pressure increases to drive the separation.⁵³ While the selectivity of the membrane is important to evaluate performance, the flux and permeability is also significant and can be affected by the feed temperature or by fouling that can occur on the membrane surface.

Improving the thermal stability of TFC membranes is of interest to meet the demand of industrial separation processes that maintain high feed temperatures. For example, food process water is typically maintained at temperatures above $80 \text{ }^\circ\text{C}$ to deter the growth of microorganisms.⁵⁴ The structure of a TFC is a polymer bilayer consisting of a membrane support, commonly polyethersulfone (PES), polysulfone, (PSf), or polyetherimide (PEI), and a selective polyamide (PA) layer that is formed on the membrane support by interfacial polymerization (IP). The polyamide is responsible for the separation of solutes where the support layer improves the integrity of the material during high pressure and temperature

filtration.⁵³ Both layers can be modified and optimized to enhance thermal stability. There are numerous examples in the literature reporting the improved thermal stability of membranes by incorporating inorganic materials such as antimony-doped tin oxide nanoparticles,⁵⁵ zeolites,⁵⁶ or modified silica nanoparticles.^{57,58} The same can be said for organic materials like modified polystyrene nanoparticles⁵⁹ or with thermo-responsive polymer materials of varied morphologies such is the focus of the work herein.^{3,60-65} The modified membranes not only enhance the thermal stability but often mitigate the impact of membrane fouling.

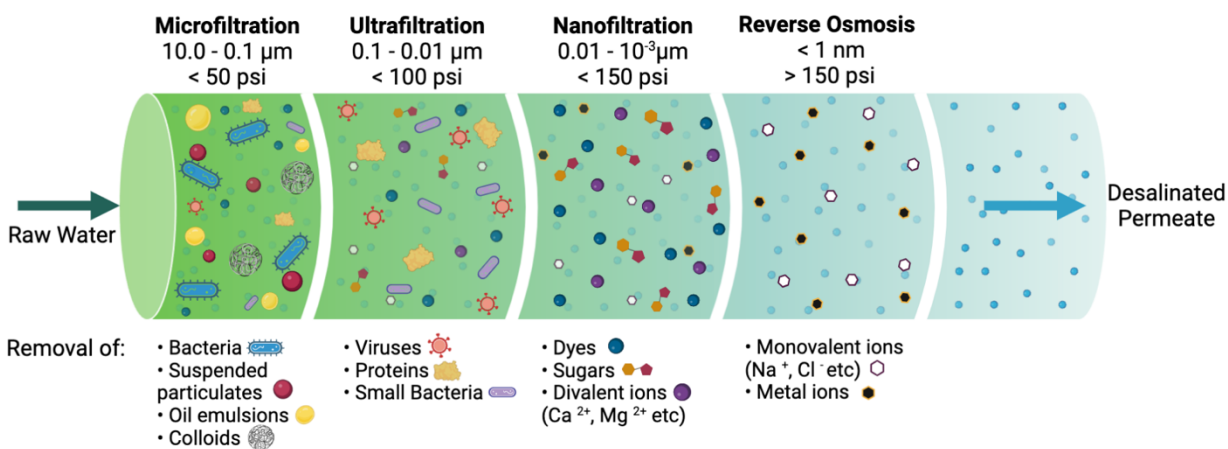


Figure 1.4 Scheme of pressure-driven membrane separation stages. Created with BioRender.

1.3.2 Modification of Polyamide Selective Layer with pNIPAm

Membrane fouling occurs when feed solutes accumulate on the membrane and block the passage of water, compacted by the applied pressure driving the separation. Often the hydrophilic-hydrophilic, hydrophobic-hydrophobic, or electrostatic charge interactions will result in the deposition of colloidal, organic, or dissolved macro-materials on the membrane surface. There have been developments in physical coatings and chemical grafting techniques to impart antifouling properties on membranes to prolong the performance lifetime. While physical coating methods are generally simpler, adaptable to many substrates, and inexpensive, the weak attachment interaction is not a good long-term solution as it can be washed away during filtration.⁶⁶ Chemical grafting methods are more

sophisticated as they typically use tailor-made functionalized materials that can be chemically crosslinked to or from the membrane surface to create a stronger more robust attachment between the two materials. In the scope of this work, unreacted acyl chloride groups (-COCl) from the trimesoyl chloride (TMC) used in the IP reaction to form the polyamide selective layer is available to covalently bond with any amine modified material. It is often the case that the materials will increase the hydrophilicity of the membrane, decreasing the attachment of hydrophobic solutes, as well as decreasing the negative charge that is intrinsic of an unmodified polyamide due to the high density of carboxylic acids (from hydrolyzed acyl chloride groups).⁶⁷ While there have studies that report an antifouling membrane with pNIPAm incorporated into the support layer of the membrane,⁶⁵ or layered underneath the polyamide,⁶⁸ it is more common to modify the polyamide itself where the material will be in direct contact with the feed.^{62,64,69}

While the addition-elimination reaction discussed above is the most convenient chemical grafting method, there are others reported in the literature. For example, a study by Tripathi et al. reported a thermo-responsive ultrafiltration membrane that grafted amino-terminated pNIPAm chains via polydopamine.⁶² The physical deposition of polydopamine on a PET membrane allowed for the covalent grafting of the terminal amine on the modified pNIPAm chain. The grafted pNIPAm was found to decrease the pore size, which consequently increased when the feed temperature was raised to 45 °C because of pNIPAm chain collapse. Additionally, the rejection of bovine serum albumin, a hydrophobic foulant, significantly increased when comparing the base membrane to the pNIPAm modified membrane due to the increased concentration of water localized around the pNIPAm chains below LCST, decreasing the fouling behaviour.

In other instances, pNIPAm nanogels were incorporated directly into the bulk membrane or polyamide by non-covalent interactions. Luo et al. reported the trapping of pNIPAm nanogels in the membrane bulk by casting a homogeneous mixture of lyophilized nanogels with polyethersulfone in solution via vapour-induced phase separation. This technique controls the temperature, humidity, and exposure time to tailor the microstructure of the membrane pores that will produce a membrane with “smart gates”

that will open and close in response to temperature.⁶³ Alternatively, Wu et al. modified a commercial TFC membrane for reverse osmosis by letting an aqueous solution of pNIPAm-co-Am microgels sit on the surface of the membrane for 24 h at 25 °C. They reported that the physical adhesion via hydrogen bonding between the carbonyl groups and amine/amide groups present in both the polyamide and microgels will be strong enough to withstand RO filtration at 100 psi.⁶⁴ While these and other similar literature examples can achieve excellent rejection and antifouling properties, the fabrication and modification steps are lengthy whereas the simple covalent crosslinking can be done during or in succession of fabricating the membrane.

1.3.3 Hydrogels for Water Treatment

Traditional pressure driven membrane-based systems have been optimized and readily employed for large scale water treatment worldwide.^{70,71} To compensate for the high energy costs of running pressure-driven systems, research focus has shifted to both modifying commercial membrane, as discussed above, as well as exploring new materials to increase the efficiency of water treatment processes. Employing thermo-responsive hydrogels for self-driven filtration is an interesting niche of water treatment research as it does not require the same energetic costs of continuous pressure or electric forces.

Forward osmosis desalination is driven solely by the osmotic potential of a concentration gradient across a membrane where water moves from regions of low osmotic pressure to high, or from feed to draw. In a simple FO system, water (feed) will move across a semi-permeable membrane to high osmotic pressure saline solution (draw). But this is not effective in recovering clean water, rather it is just diluting the brine and further desalination treatment is required, such as RO. Instead, draw agents have been employed which work to induce high osmotic pressure and therefore a high water flux that can be recovered and reused from the draw volume, solutes such as sugars⁷² or ammonium bicarbonate.⁷¹ Unfortunately, draw agents will often experience reverse ion diffusion, resulting in contaminated feed solutions and generating the same problem as in a simple water/brine system. This issue has been recently addressed by incorporating highly hydrophilic polymer layers on FO membranes, creating high osmotic potentials, and eliminating reverse ion

diffusion. For example, Razmjou et al. fabricated a double-layer of pNIPAm-*co*-sodium acrylate and pure pNIPAm as draw agents on an FO membrane. The high osmotic potential of the absorptive polyelectrolyte pSA hydrogel layer will draw water from the feed. The second pNIPAm layer will act as a dewatering layer whereby solar energy can heat the hydrogels above the LCST to recover the clean water.⁷¹ The potential to use renewable solar energy to recover clean water and scale this membrane framework up to achieve essentially zero-cost water desalination.

Hydrogels have also been used as independent filtration materials without coupling to a membrane. Polyelectrolyte hydrogels have been used in several studies for clean water uptake due to the high ionic charge density contained within the polymer that creates a high osmotic pressure within the gel.^{7,73-76} While it seems counterintuitive, the Donnan exclusion of salt ions in the feed can be rejected from the hydrogel matrix due to the charge density, even those of opposite charge and the water taken up by the gel is salt-depleted in comparison to the feed. pAAc hydrogels have a reported rejection of 35% but the mode to reclaim the salt-depleted water for polyelectrolyte hydrogels is only through mechanical squeezing.⁷³ Attempts to copolymerize these ionic polymers with thermo-responsive polymers like pNIPAm in hopes to recover clean water by heating are largely unsuccessful due to the electrostatic repulsion dominating the dewatering transition when heated and with decreased ionic character, both the swelling ratio and rejection decreased without any significant recovery where for example pNIPAm-*co*-SA hydrogel could similarly achieve up to 20% salt rejection but only 9% water recovery.⁷ Attempts to improve the rejection of polyelectrolyte hydrogels was done by coating the hydrogels in a polyamide skin layer identical to that used in TFC membranes to create a core-shell structure. This selective skin layer allowed for >90% rejection of both monovalent and divalent salt species but the water contained in the hydrogels could not be recovered without damaging the PA layer.⁷⁴ Gupta et al. reported an optimized method for forming a robust PA layer on a pNIPAm hydrogel that could withstand up to 100 heating cycles without showing signs of cracking or delamination by incorporating branched polyethyleneimine to anchor the PA to the hydrogel.⁷⁶ However, they were only able to selectively reject larger divalent salt species, not Na⁺ or Li⁺. To combat the challenges outlined here, Chapter 4 details a thermo-responsive

hydrogel that is capable to rejecting both monovalent and divalent salts and can withstand the heat cycling to recover clean water 3 times.

1.4 Conclusion

In this chapter, the relevant background on thermo-responsive polymers and how they work, how they can be used in sensing, and how they can be structured in core-shell morphologies for different applications has been detailed. Additionally, thin-film composite membranes for water remediation were introduced and how they can be modified with different polymeric materials to achieve better thermal stability, rejection, and antifouling properties. And finally, the use of larger scale hydrogels for self-driven filtration for desalination was discussed.

For the scope of work detailed herein, the temperature dependent swelling and deswelling of the polymer pNIAPm in an aqueous environment is the focus and how various core-shell morphologies of this material can be used in the controlled release of small molecules and for water treatment and remediation purposes. Specifically, in Chapter 1 the dye uptake and release of free-solution and immobilized functionalized pNIPAm cores with varying shell thicknesses is evaluated under different pH and temperature conditions. Similar core-shell nanogels with an APMA shell were fabricated for the incorporation into a thin film composite membrane via covalent crosslinking between the nanogel and the membrane system to evaluate flux behaviour and salt rejection with increasing feed temperatures. Additionally, the localization of the same nanogels on the surface of the membrane was evaluated for antifouling performance is detailed in Chapter 2. Lastly, a novel core-shell structure of pNIPAm hydrogel cores coated in a polyamide shell was evaluated for monovalent and divalent salt rejection as well as its ability to withstand multiple heating cycles to recover the clean water taken up by the gel.

Chapter 2 Poly(N-isopropyl acrylamide)-based Core-shell Microgels for Controlled Release of Dyes

2.1 Introduction

Polymer materials have been used in a wide range of applications from drug delivery to contaminant uptake for environmental treatment. Previously, the Serpe group has explored the uptake and release of organic dyes from pNIPAm-based microgels and assemblies.⁷⁷⁻⁷⁹ Organic dye species like crystal violet (CV) and orange II (OII) are considered environmental contaminants due to their use in many industries but most notably the textile industry as fabric dyes. Both are toxic and genotoxic and are becoming increasingly present in soil and water where they persist for long periods of time.^{52,80} The concern for wildlife, agriculture, and human exposure has led to management options for the uptake or degradation of these dye species and others like it.

In the context of mechanistic uptake and release, the previously mentioned studies found that OII uptake in pNIPAm microgels was limited compared to pNIPAm-*co*-AAc microgels.⁷⁷ The argument being that the increased size of the pNIPAm-*co*-AAc network allowed for more dye molecules to enter the microgel due to the increased electrostatic repulsion between the deprotonated carboxyl groups in AAc at a pH above the pK_a , which is ~ 4.3 , compared to when the carboxyl group is protonated below the pK_a . A schematic representation of acrylic acid (AAc) containing microgels in response to changes in pH is presented in Figure 2.1-a. The uptake was also dependent on the environmental temperature due to the LCST properties of pNIPAm as discussed in detail in section 1.1.2, where uptake was greater below the LCST when the polymer is in the swollen hydrated state. This study also found that there was a significant amount of leaching of the dye molecules with time, where 25.6% of retained dye was lost to the surrounding water environment.⁷⁷ This is likely due to the negative charge of the deprotonated carboxyl group and the anionic OII dye contributing additional repulsion interactions despite the additional volume of the microgel in this state. An additional study by the same authors was done exploring the uptake efficiency of the individual pNIPAm-*co*-AAc microgel particles compared to aggregates formed from crosslinking the microgels with N,N'-methylenebisacrylamide. The

uptake of the microgels increased from 29.5% to 44.2% when in aggregates at room temperature and even more so when heated above the LCST.⁷⁸ This result is interesting and prompted the idea that there may be a difference in both loading and release behaviour for similar microgel materials, such as core-shell structures of pNIPAm polymer, free in solution and when immobilized on a gold surface which may mimic the aggregates previously studied.

The loading and subsequent release of dye from immobilized microgels sandwiches between gold layers in an etalon structure was also explored. pNIPAm microgels have been employed in etalons for colorimetric sensing of many different target species such as heavy metal species (Pb^{2+} , Hg^{2+} , and Cr^{3+}),⁸¹ hormone species,^{82,83} and other organic dyes like methylene blue.⁷⁹ Etalons are unique in their sensitivity to small changes in distance between the two gold layers will result in visible colour change. The stimuli-responsive pNIPAm microgels are an ideal material for the middle dielectric layer that change size rapidly in response to different stimuli.^{84,85} In the literature, a sulfide group is usually employed to create a strong interaction between pNIPAm based materials to a gold surface either by modifying the terminal ends of the polymer chains with a -SH group or utilizing a disulfide bridge from a specific crosslinker to create a monolayer to polymer on gold surfaces.^{86,87} But it has been observed that there is some non-covalent binding that occurs between pNIPAm and gold surfaces that allows pNIPAm based microgels to be painted onto a gold surface with good adhesion for exploring the properties when immobilized. It is hypothesized that the immobilization of pNIPAm on a gold is due to the interaction between the lone pairs of the amide group and the Au surface.⁸⁸ The impact of ionic strength (IS) and charge contained within the microgels themselves will alter the microgel-microgel and microgel-surface interactions in turn altering the packing density and assembly on the gold surface. If the pH is above the pK_a of AAc and the ionic strength is low, as it is in the experiments detailed below, the formation of microgel aggregates is lower as is the packing density.⁸⁹ This idea that immobilized microgels may behave as aggregates and will have improved loading compared to individual microgel particles as was determined in the previously mentioned study, led to the work presented in this chapter. In this work, a core-shell microgels were made by copolymerizing pNIPAM with acrylic acid (AAc) or N-(3-

aminopropyl) methacrylamide hydrochloride (APMA) to create a spherical core, followed by the addition of a pNIPAm shell of varying thickness. As some leaching of the loaded dye was observed from both the microgels and the aggregates, the addition of the shell may help in preventing leaching of the dye.^{77,78}

The design of the experiment is using the same theory of loading the microgel modified with AAc or APMA when the comonomer is charged as was done in the previous dye loading studies, where the chosen dye carries an opposite charge to that inside the polymer to improve the loading and prevent leaching. The model system of loading pNIPAm-co-AAc microgels with cationic crystal violet (CV) and pNIPAm-co-APMA with anionic orange II (OII) dye was chosen. The behaviour of the modified cores is compared to the same cores with added pNIPAm shells to observe the impact of the shell thickness on the release of the target dye both below and above the LCST and whether the shell will have a greater influence on the dye release in solution or when immobilized. The free solution and immobilized sample methodology, dye uptake study, TEM and most DLS characterization, and all core-shell microgel sample synthesis was performed by Dr. Krista Freuhauf. The dye release experiments, remaining DLS, AFM, and data processing was performed by me.

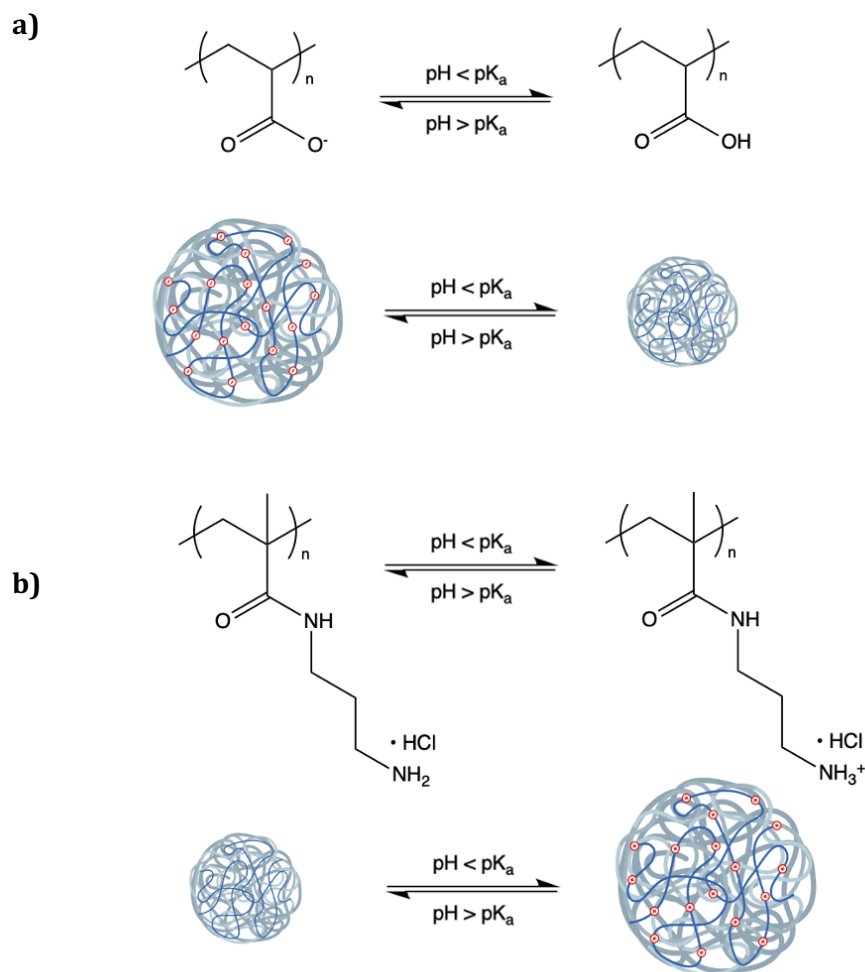


Figure 2.1 Illustration of the swelling and shrinking mechanism of (a) acrylic acid comonomer and (b) N-(3-aminopropyl)methacrylamide in response to changes in pH above and below the respective pK_a .

2.2 Experimental Section

Materials: N-isopropylacrylamide (NIPAm) purified by recrystallization from hexanes (ACS reagent grade, EMD, Gibbstown, NJ) before use. N,N'-methylenebisacrylamide (BIS, 99%), acrylic acid (AAc, 99%), N-(3-aminopropyl)methacrylamide hydrochloride (APMA), ammonium persulfate (APS, $\geq 98\%$), sodium dodecyl sulfate (SDS, 99%) and sodium hydroxide (NaOH) were obtained from Sigma-Aldrich (Oakville, Ontario) and were used as received. Hydrochloric acid (HCl) was purchased from Caledon Lab. Deionized (DI) water

with a resistivity of 18.2 M Ω cm was obtained from a Milli-Q Plus system and was used for all experiments. A pH meter (JENCO 6173) was used to tune solution pH.

2.2.1 Core-shell Microgel Synthesis

Core-shell microgels were synthesized in a two-step precipitation polymerization. Two different microgel core compositions, pNIPAm-*co*-AAc and pNIPAm-*co*-APMA, were synthesized. NIPAm (11.7 mmol and 12.6 mmol for *co*-AAc and *co*-APMA, respectively) and BIS (0.7 mmol) and either AAc (0.7 mmol) or APMA (0.7 mmol) were dissolved in Milli-Q water (98 mL) and transferred to a round bottom flask. 1 mL of SDS (0.2 mmol) was added to the pNIPAm-*co*-AAc core synthesis only at this time. The solution was heated to 70 °C in an oil bath and sparged with N₂ gas for 30 min. The volume was initiated with APS (1 mL, 0.1 mmol) under an N₂ atmosphere maintained at 70 °C for 3 h. After 3 h, the flask was removed from the bath to cool to room temperature before opening to air to quench. Volume was filtered through Whatman no. 1 filter paper then transferred to 12 kDa dialysis tubing for a minimum of 8 water changes over 1 week. The yield and concentration were determined by lyophilization.

The pNIPAm shell additions with increasing concentration were added to the as-prepared cores (5 mM, 10 mM, and 20 mM). The diluted core samples (9 mL, ~ 62 mg) were heated to 70 °C under nitrogen before adding the monomer solution containing NIPAm (0.09 mmol, 0.2 mmol, and 0.38 mmol) and BIS (0.02 mmol). After 30 min of heating, the volume was initiated with APS (0.04 mmol) and allowed to proceed at constant temperature for 3 h in nitrogen atmosphere. The volume was cooled to room temperature before opening to air to quench the reaction. The core-shell microgels were purified by centrifugation 3 times.

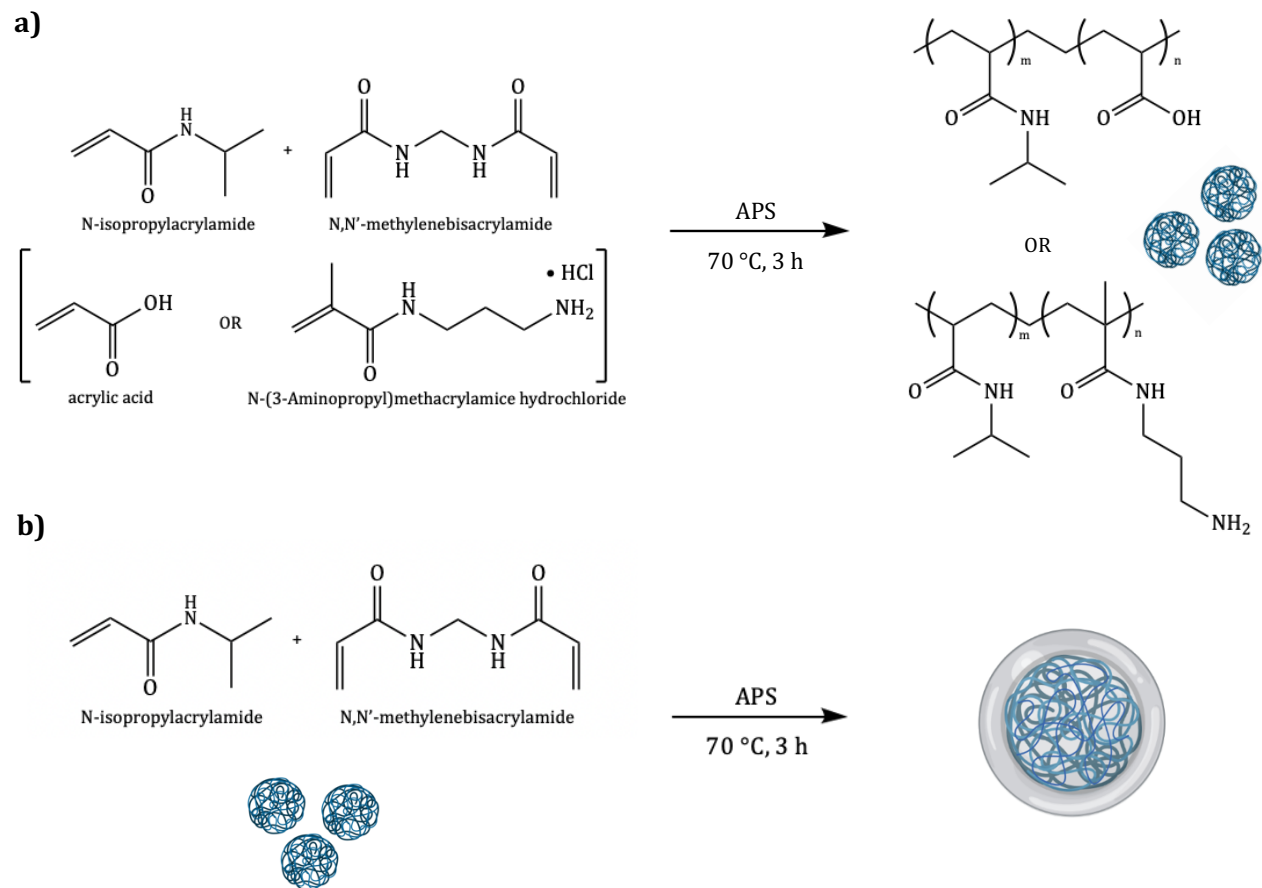


Figure 2.2 Polymerization reaction scheme for the fabrication of (a) functional pNIPAm cores and (b) pNIPAm shell addition to make core-shell microgels.

2.2.2 Dye Uptake, Loading, and Release Experiments

A solution of the as-prepared cores and core-shell microgels (0.25 mg/mL) were incubated with the appropriate dye at a pH above and below the respective pK_a of the polymer for 30 min. The AAC containing gels were incubated with 22 μM CV at pH 3 and 6.5. The APMA containing gels were incubated with 45 μM OII at pH 5.5 and 11. The pH of Milli-Q water was adjusted with 0.01 M NaOH and 0.01 M HCl and monitored by pH probe. After 30 min, the volume was centrifuged at 14k rpm for 20 min. The supernatant was measured before and after microgel loading with UV-Vis (590 nm for CV and 486 nm for OII) to determine the uptake.

2.2.3 Dye Loading and Release from Free-Solution Microgels

In conditions similar to those of the immobilized samples, the dye release kinetics of core and core-shell microgels free in solution was observed. In an eppendorf tube, AAC microgels (1 mg/mL) were incubated in CV (1 mM) at pH 6.5 overnight. The tube was centrifuged at 12k rpm for 20 min and resuspended in pH 6.5 water overnight, this was repeated twice more to remove excess dye. The final pellet was diluted to 0.2 mg/mL (5 mL total) with pH 6.5 water. The sample was circulated by peristaltic pump with a flow rate of 2.5 mL/min through a quartz UV-Vis flow cell quartz cuvette at room temperature and blanked to ensure no dye release. 50 μ L of 0.01M HCl was added to the volume and spectra were collected every 5 s for 6 min at 590 nm. The same procedure was followed except the sample was warmed in a water bath at 40 °C before adding the HCl, and the cuvette cell was also heated to 40 °C to observe temperature effects. The same procedure was followed for the APMA microgels using 1 mM OII at pH 5.5. Adding 3 drops of 0.1 M NaOH to increase the pH to 11 before collecting spectra every 5 s for 8 min at 486 nm. The pH of the solution was measured after the experiment was completed to ensure the correct release pH was reached. A schematic illustration of the experiment setup is shown in Figure 2.3.

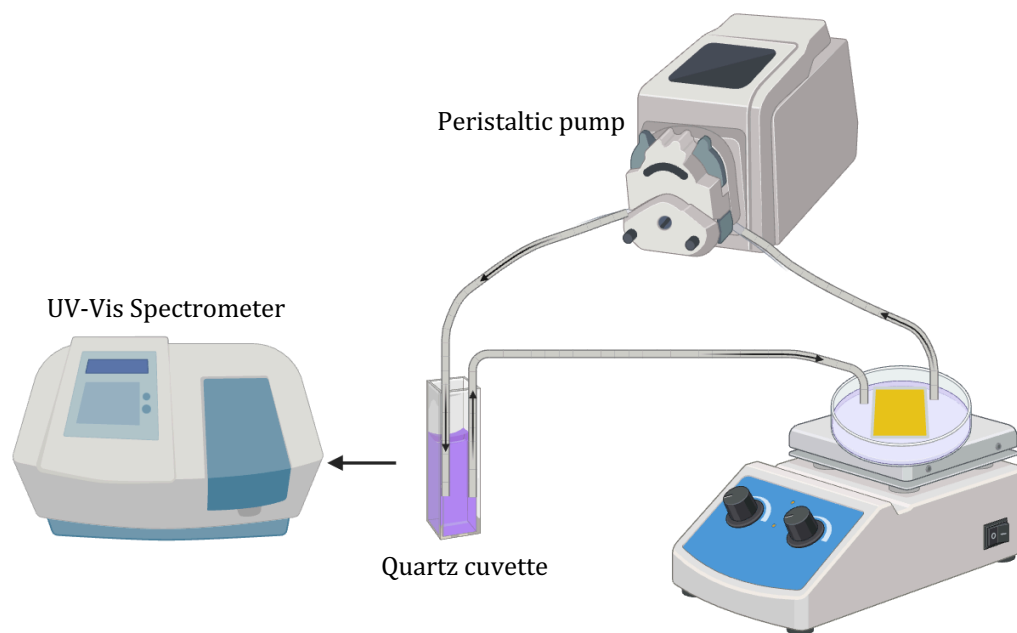


Figure 2.3 Illustration of dye release experiment set up. Created with BioRender.

2.2.4 Dye Loading and Release from Immobilized Microgels

The release kinetics of the core and core-shell gels was observed when immobilized on a gold surface. A concentrated volume of the microgels was painted glass slides with thermally deposited gold (2 nm Cr, 45 nm Au) and allowed to dry at 35 °C before soaking in water at 30 °C to remove any unbound microgels from the gold surface.

The immobilized AAc microgel cores and core-shells (4 mg/mL) were soaked in pH 6.5 CV solution (1 mM) for at least 3 days to maximize the loading. The slides were transferred to pH 6.5 water overnight to remove any excess dye not contained in the microgels. The slide was then transferred to a shallow dish containing 5 mL volume of fresh pH 6.5 water that was circulated by a peristaltic pump (2.5 mL/min) through a quartz UV-Vis flow cell at room temperature. Each sample was blanked to confirm no premature dye release before replacing the volume with 5.0 mL pH 3 water to trigger the release. The pH 3 volume was blanked again before taking measurements every 30 s for 30 min at 590 nm. This same procedure was repeated where the shallow dish was warmed to 40 °C and the holding cell for the cuvette was set to the same to measure above-LCST release kinetics. The same general procedure was followed for loading immobilized APMA microgels using 5 mg/mL OII at pH 5.5. pH 11 water was used to trigger the release of the dye and spectra were collected every 30 s for 30 min at 486 nm.

2.2.5 Characterization of Microgels

Dynamic light scattering (DLS) measurements were done to approximate the size of the microgels in solution and confirm the addition of the shell. The size of the core and the cores with 5 mM, 10 mM, and 20 mM shell additions were measured at pH below and above the pK_a of the functional comonomer as well as at temperatures below and above the LCST of pNIPAm. The yield and size of the microgels under these conditions is summarized in table 2.1.

Brightfield transmission electron microscope (TEM) images of the dried microgel cores and core-shell particles to approximate the dry diameter using a JEOL JEM-ARM200CF S/TEM. Without staining, the vague shape of the microgels can be seen (Figure 2.4). An

image of AAc core impregnated with CV was imaged (Figure 2.4-a) and did not improve the contrast in the image. While TEM is excellent for imaging small particles, the pNIPAm-based microgels are very soft materials and therefore defined edges are hard to image. Figure 2.5 summarizes the atomic force microscopy data (DI Dimension 3000) that was used to observe the packing of the microgels onto the gold surface. From the AFM the dry diameter of the immobilized microgels can be approximated.

Table 2.1 Hydrodynamic diameter of microgel cores and core-shells at different pH, temperature, and polymerization yields.

<u>Nanoparticle</u>	<u>pH</u>	<u>D_h at 25 °C (nm)</u>	<u>D_h at 40 °C (nm)</u>	<u>Yield</u>
AAc Core	3	222 ± 5	116.3 ± 0.6	72%
	6.5	321 ± 7	169 ± 8	
AAc Core/5 mM Shell	3	221 ± 2	131 ± 2	78%
	6.5	341 ± 4	306 ± 6	
AAc Core/10 mM Shell	3	219 ± 2	136 ± 19	70%
	6.5	363 ± 6	333 ± 6	
AAc Core/20 mM Shell	3	225.9 ± 0.4	124 ± 1	93%
	6.5	308 ± 3	250 ± 40	
APMA Core	5.5	880 ± 5	766 ± 8	40%
	11	715 ± 8	639 ± 4	
APMA Core/5 mM Shell	5.5	610 ± 10	540 ± 10	66%
	11	518 ± 3	480 ± 10	
APMA Core/10 mM Shell	5.5	700 ± 80	455 ± 6	66%
	11	580 ± 10	434 ± 5	
APMA Core/20 mM Shell	5.5	790 ± 20	644 ± 9	82%
	11	600 ± 20	508 ± 8	

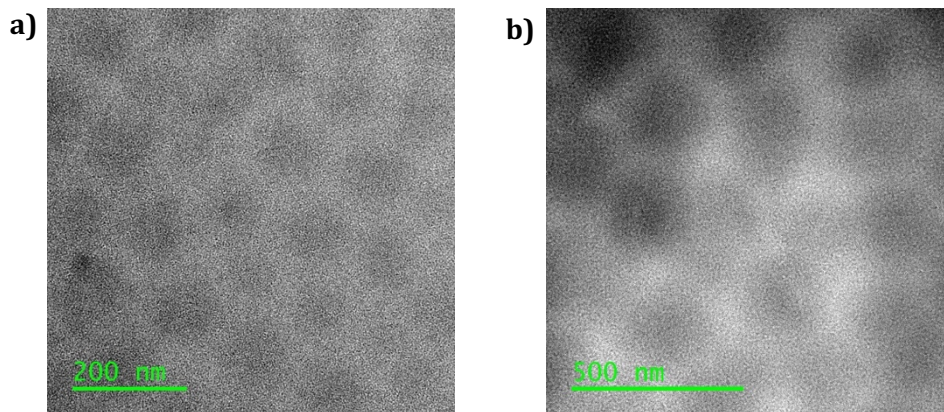


Figure 2.4 Brightfield TEM image of dried microgel samples (a) AAc-core and (b) APMA-core.

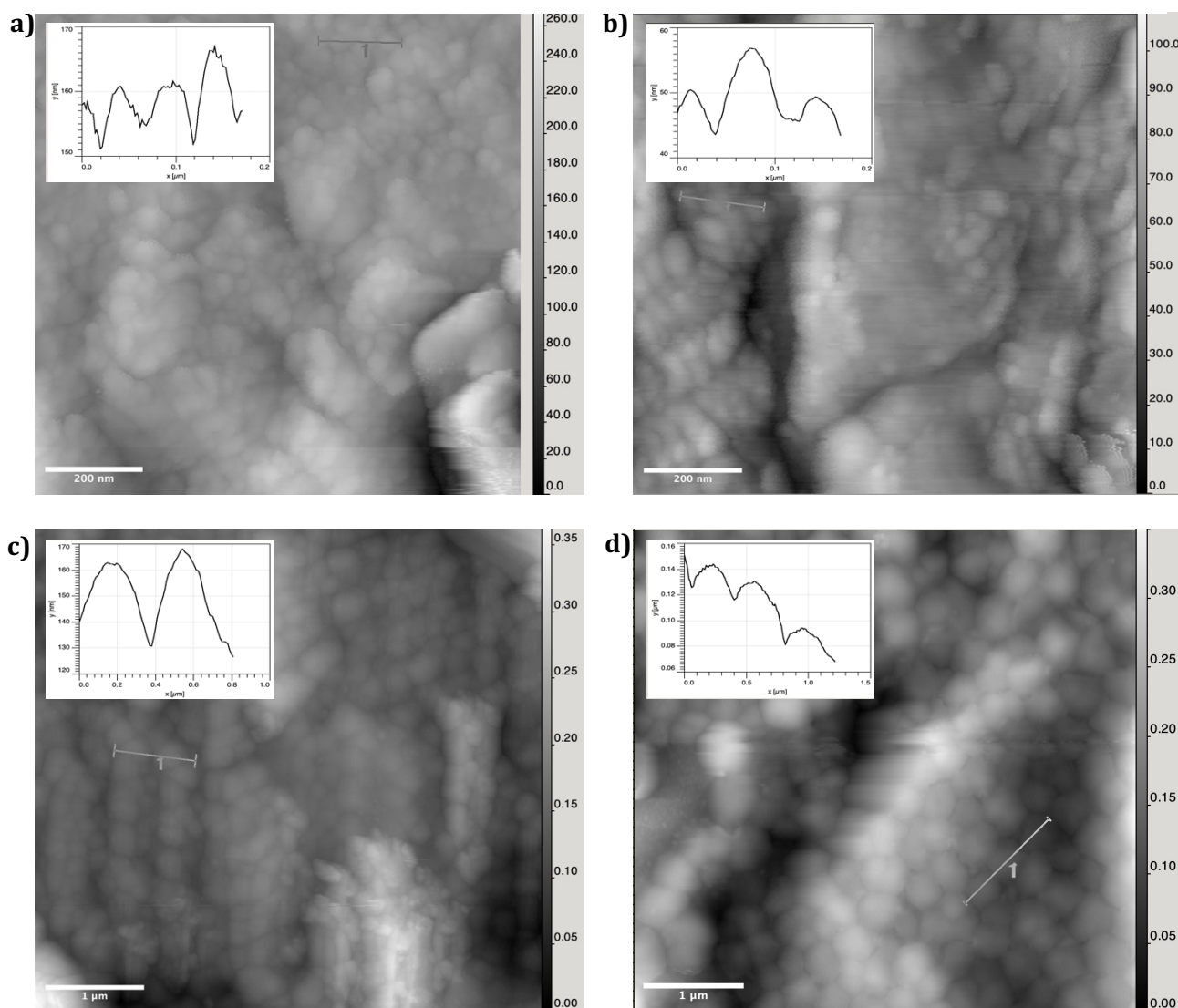


Figure 2.5 AFM images of the immobilized (a) AAc-core, (b) AAc-20, (c) APMA-core, and (d) APMA-20 microgels on a gold-coated glass slide with the approximate dry microgel radius (inset).

2.3 Results and Discussion

Eight different microgel samples were synthesized by free radical precipitation polymerization as detailed in section 2.2.1. Two pNIPAm core particles copolymerized with an anionic monomer (AAc) and a cationic monomer (APMA) were further modified with shells of pNIPAm in increasing monomer concentrations (5 mM, 10 mM, and 20 mM) to increase the shell thickness (referred to as AAc-core, AAc-5, AAc-10, AAc-20 and APMA-core, APMA-5, APMA-10, and APMA-20, herein). The core and core-shell microgels were characterized by DLS, summarized in Table 2.1. The size of AAc-Core microgels was evaluated at pH 3 and 6.5, above and below the pK_a of AAc, which is near 4.3. The size of APMA-Core microgels was measured at pH 5.5 and 11, above and below the pK_a of APMA at approximately 10. When the pH was below the pK_a of the respective functional monomer, the ionizable groups are protonated. In the case of AAc, the carboxyl group is protonated and therefore neutral in charge. When the pH is increased to 6.5, the carboxyl groups are deprotonated and create a localized negative charge density, increasing the electrostatic repulsion within the core, and increasing the observable size. The same concept is applied to the APMA containing microgels where the primary terminal amine on APMA is protonated below the pK_a and is carrying a positive charge, increasing the size of the core. When the pH is raised to 11, the amine is deprotonated and neutrally charged, resulting in a decrease in size. The effect of temperature on the size was also measured by increasing it above the LCST of pNIPAm at ~ 32 °C. The decrease in size between 25 °C and 40 °C can be observed in all samples in Table 2.1. The exact shell thickness is difficult to determine from the DLS data. The core-restricted swelling of pNIPAm-co-AAc cores with a pNIPAm shell was investigated by Jones & Lyon where they reported that the shell adds a layer of rigidity to the system that does not allow for the full volume change observed in the cores alone.⁹⁰ The shell addition is done above the LCST of the core, while it is in the collapsed deswollen state, where the swelling of the core upon cooling below the LCST will be restricted both above and below the pK_a of AAc. Consider the AAc-Core compared to AAc-20, the size at pH 3 at 25 °C is not significantly different, 222 ± 5 nm and 225.9 ± 0.4 nm, respectively. Increasing the pH to 6.5 at 25 °C, the size of AAc-20 is smaller than AAc-core, 308 ± 3 nm and 321 ± 1 nm, respectively. The shell restricted swelling is even more obvious in the APMA samples, where APMA-

5/10/20 all are smaller than APMA-core when in the protonated state at pH 5.5 at 25 °C. Decreasing from 880 ± 5 nm of the core to 610 ± 10 nm, 700 ± 80 nm, and 790 ± 20 nm for APMA-5, APMA-10, and APMA-20, respectively. Additionally, the pH responsive cores will undergo a smaller volume transition when heated above the LCST due to the charge repulsion resisting complete collapse of the pNIPAm chains around them. But the addition of a the pNIPAm shell will compress the core even when in the charged state above the LCST. Again, this is best seen in the APMA samples where the charged APMA-core at pH 5.5 at 40 °C is 766 ± 8 nm in diameter compared to 540 ± 10 nm, 455 ± 6 nm, and 644 ± 9 nm for APMA-5, APMA-10, and APMA-20, respectively. All showing a decreased diameter, or increased volume transition, due to the compression of the core even when charged. Taking this into consideration, while the exact shell thickness cannot be determined, the DLS results do confirm the presence of a shell in agreement with the trends reported for core-shell materials of this nature.⁹⁰ Brightfield TEM images for the microgel cores and core-shells seen in Figure 2.4 are not well-defined spheres as pNIPAm polymer materials are very soft and intensity of the electron beam will typically penetrate through the material. But the approximate dry diameter of the samples can be determined. Other studies have used stains such as phosphotungstic acid (PTA) for pNIPAm polymer materials to produce higher contrast images, but this was done in this work.⁹¹

Utilizing the negative charge in the AAc samples or the positive charge in the APMA samples, the uptake of oppositely charged species can be explored by the electrostatic interactions. For AAc, the deprotonated carboxyl group will attract positively charged dye molecules like crystal violet, the same phenomena will be observed between the protonated amine group in APMA and negatively charged dye species like Orange II. This was validated by performing a dye uptake test under different pH conditions by measuring the absorbance of the feed before and after adding microgel sample to a dye solution of known concentration by UV-Vis. As seen in Figure 2.6-a, the loading of CV into the AAc microgels was best achieved at pH 6.5 above the pK_a compared to below at pH 3, as expected. There is a small amount of uptake that can be seen at the “neutral” pH which could be due to a small amount of negative charge imparted by the APS initiator incorporated into the polymer attracting some dye or not achieving complete protonation of all the AAc groups after adjusting the pH. The same

trend is observed for the APMA containing microgels where a largest change is seen when the gel is positively charged at pH 5.5 compared to pH 11 in Figure 2.6-b. The observed uptake at pH 11 could be explained similarly to the AAc samples where not all the amine groups were deprotonated at this pH. With this proof of concept, the investigation on the release of dye from the different core and core-shell microgels immobilized on a gold surface and free in solution was done.

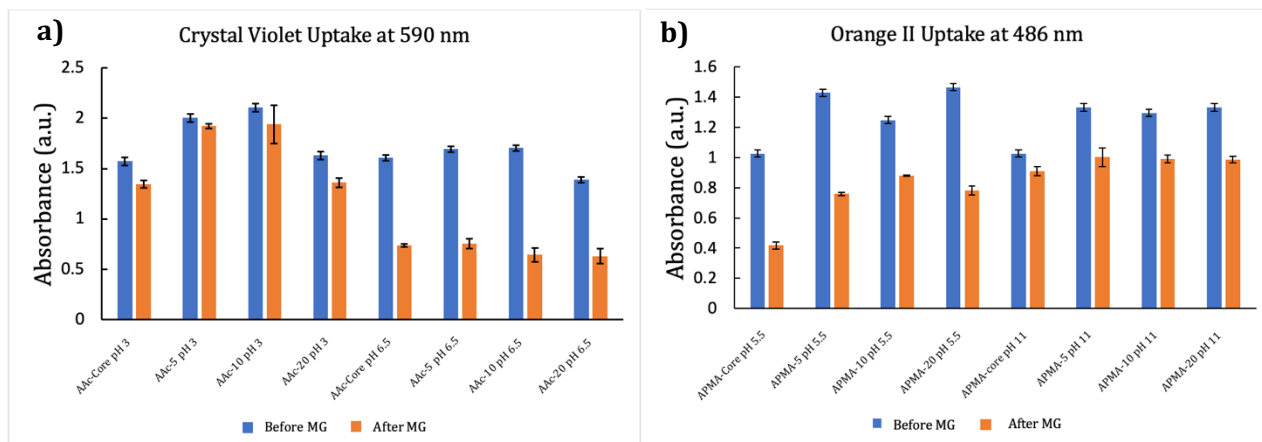


Figure 2.6 Bar graph depicting the change in absorbance of a dye solution before (blue, left bar) and after (orange, right bar) adding microgel samples to it. (a) The addition of AAc-core, AAc-5, AAc-10, and AAc-20 to 22 μM CV at pH 3 and pH 6.5. (b) The addition of APMA-core, APMA-5, APMA-10, and APMA-20 to 45 μM OII at pH 5.5 and 11.

A test experiment of 5 μM CV and OII in pH 6.5 and 5.5 water, respectively, without any microgel present was circulated through the peristaltic pump, the instrument was blanked, and circulated for 1 min before adjusting the pH. The effect of pH on the absorbance of the dye was measured at 25 $^{\circ}\text{C}$ and 40 $^{\circ}\text{C}$ and the change in absorbance with time was observed and presented in Figure 2.7-(c & d). In general, the shape of the free solution profiles is due to the mixing of the sample through the peristaltic pump. For CV, the dye will reportedly change colour from yellow to purple at pH 0-2. By decreasing the pH from 6.5 to 3, there is an observable increase in the colour intensity to the eye validating the increased absorbance at the λ_{max} (590 nm). For OII, the colour changes from a yellow-orange to deep orange-red at pH 11. This shifts the λ_{max} to a higher value as it become more red resulting

from an increase in light passing through the sample at 486 nm compared to the blank run with OII at pH 5.5, and a negative absorbance curve.

The free solution experiments consisted of 0.2 mg/mL concentration of each microgel sample loaded with the respective dye, and the release was triggered by adjusting the pH to that which would neutralize the charged group of the functional comonomer, detailed in section 2.2.3. The results of these experiments are summarized in Figure 2.7 where each presented sample is the average absorbance profile of 3 dye release experiments for each sample. Figure 2.7-a shows the absorbance profiles of each AAc sample at 25 °C (solid line) and 40 °C (dashed line). The results from these experiments show that the release of CV from the microgels with shells at 25 °C is greater, particularly AAc-5 and AAc-10, than the AAc-core alone. When the polymer is in the swollen state and the pH is changed to neutralize the carboxylic acid groups, the polymer network will shrink with reduced charge, but the shell will remain in the solvated state so that dye molecules can leave freely. It is possible that the thinner shells (ie AAc-5 and AAc-10) will allow for more dye loading when compared to the core alone where the shell may help to retain the dye molecules whereas the core might leach dye during the centrifuging and washing steps. The decreased release from AAc-20 could be due to the thicker shell hindering the uptake of dye to begin with and therefore less would be released. Measuring the exact shell thickness is difficult and was not achieved, as discussed previously, but from the reactions yields reported in Table 2.1, it may be that the improved yield of the shell addition to AAc-20 resulted in a considerably thicker shell compared to AAc-5 or AAc-10. It can be reasoned that there is a threshold for the maximum total dye uptake and release in relation to shell thickness for this system is optimal at 5 mM, comparable at 10 mM, and hindered at 20 mM. At 40 °C the release of dye dramatically decreases due to the collapsed core and shell restricting the exit of dye in combination with premature dye loss when heating the sample to 40 °C before beginning the experiment. Although when comparing the AAc-core to the samples with a shell, the average dye release is marginally greater for those with a shell which could possibly be due to some squeezing effect of the core. This trend is observed for the APMA samples as well, at 25 °C the release profiles for all APMA samples are similar to each other. But at 40 °C, the samples with a shell seem to have a larger dye release than the core alone, in this case the more negative the

change in absorbance corresponds to a larger release in OII in agreement with Figure 2.7-d. The APMA-5 microgels also showed the greatest release of dye at 25 °C although not significantly compared to the APMA-core. Therefore, the theory that there is an optimal shell thickness that will allow for the greatest uptake and release is consistent for both samples at 5 mM when free in solution. Interestingly, the absorbance for the release from microgels at 25 °C remains positive, which was not observed in the change in absorbance of OII alone at the same temperature. There may be some effect from the solvated microgels at this temperature that hinders the passage of light from hitting the detector at this wavelength even if the λ_{max} of the dye has shifted.

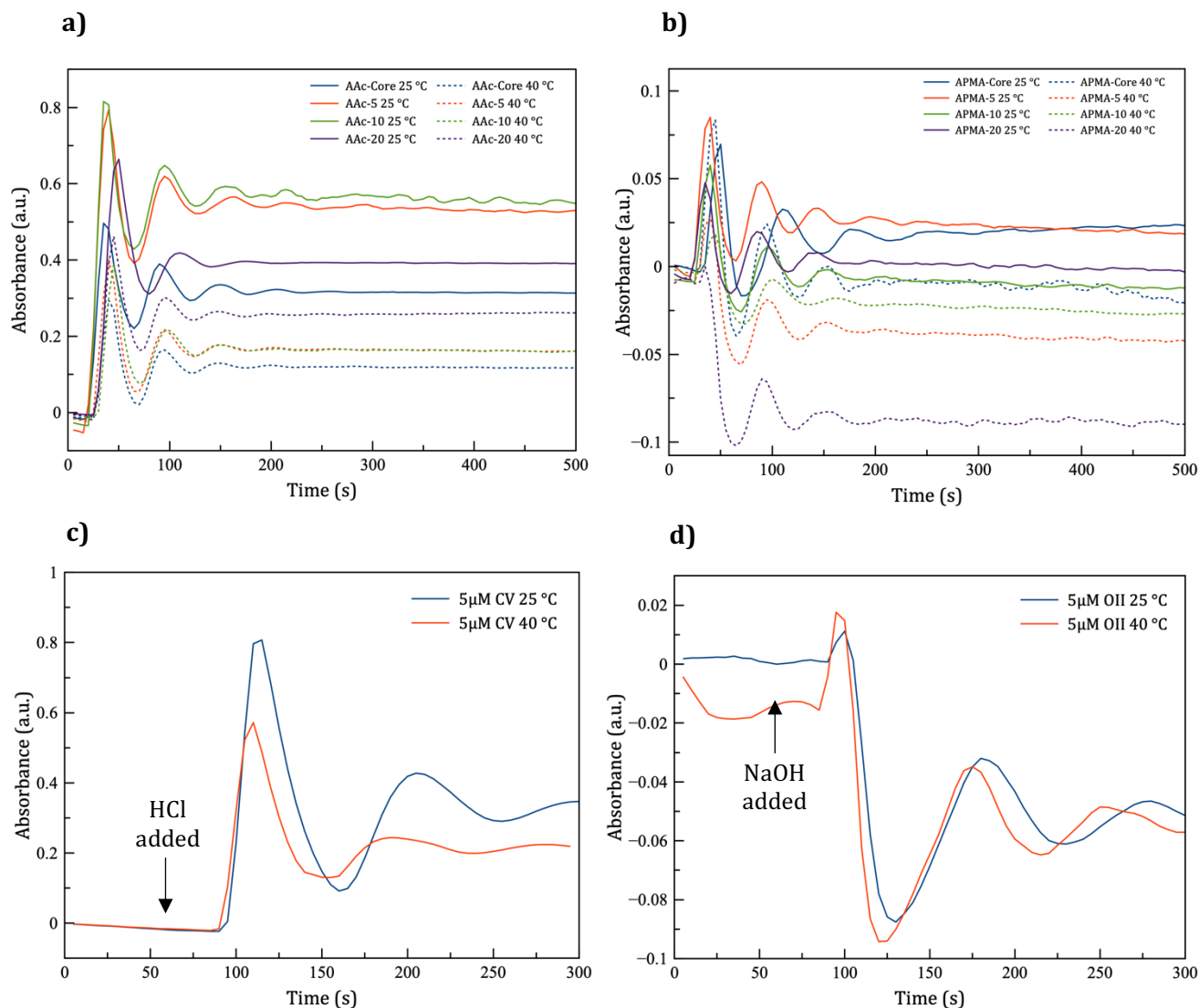


Figure 2.7 Plot of absorbance versus time for the dye release of (a) crystal violet dye release at 590 nm from AAc-core (blue), AAc-5 (red), AAc-10 (green), and AAc-20 (purple) at 25 °C (solid line) and at 40 °C (dashed line). (b) orange II dye release at 486 nm from APMA-core (blue), APMA-5 (red), APMA-10 (green), and APMA-20 (purple). The absorbance plots for 5 μ M concentrations of (c) CV at pH 6.5 adjusted to pH 3 after 1 min of circulating and (d) OII at pH 5.5 adjusted to pH 11 after 1min of circulating at 25 °C (blue) and 40 °C (red).

As mentioned previously, the immobilization interaction of pNIPAm microgels and gold is through the amide group of pNIPAm as well as some ancillary interaction between the carboxyl group of AAc or primary amine in APMA. The charge carried by the microgel at the time of painting on the gold will impact the monolayer assembly and packing density. For the AAc samples, the pH was left at ~ 6.5 where the carboxyl group was charged, and the IS was not controlled. Theoretically this would result in a more loosely packed monolayer, but the presence of the shell would seem to impact the packing as seen in the AFM images

that there is some surface morphology due to overpacking or layering of microgels on the surface. They are still discernable, but it is not a uniform monolayer as expected. The APMA microgels were not so easily immobilized on the surface. The first attempt at painting the APMA-core onto the gold, the dried layer seemed to flake off when left to soaked in water over time. Increasing the painting pH to 11, to neutralize the amine, seemed to improve the adhesion but not as densely as the AAc microgels. Spin coating was also attempted to improve the adhesion but was unsuccessful. This decreased sample loading on the gold was also observed for the APMA core-shell microgels, which is interesting as the purely pNIPAM shell should have improved the interaction with the gold. Nevertheless, there was enough sample packing on the surface to observe dye loading and release as the AFM images confirmed the presence on the gold surface. The dry diameter of the immobilized microgels can also be approximated from the AFM in Figure 2.5. The immobilized diameter can be approximated from the cross-section profiles of a small selection of the AFM image where the microgels can be seen. The dry diameter of AAc-core is ~ 49 nm (Figure 2.5-a (inset)) compared to ~ 125 nm from the TEM image (Figure 2.4-a). This aligns with the theory that the interaction between the AAc microgels and the gold is strong and will have increased packing density thereby decreasing the diameter as more microgels are packed together. The same cannot be said for the APMA-Core that have a diameter ~ 400 nm (Figure 2.5-c (inset)) compared to ~ 263 nm from the TEM image (Figure 2.4-b). It appears that the dry microgels are larger when immobilized on the surface which could possibly be due to the decreased packing density or some layering/aggregation of the microgels during the drying process as the microgel-microgel interaction is presumably greater than the microgel-surface interaction as observed in the difficulty in immobilizing the sample in the first place. Regardless, the successful immobilization of the microgels on the gold surface was done so that a more detailed insight on the dye release kinetics could be done.

The immobilized microgels on gold coated glass slides were loaded with dye and the release rate was measured as detailed in section 2.2.4. In general, the total observed release of CV was much greater than OII by several magnitudes as can be seen in Figure 2.8. This is likely due to the superior adhesion of the AAc microgels to the gold compared to the APMA microgels as discussed previously. An interesting trend of note is that since the microgels

are stuck to the gold and are not circulating through the instrument, only the dye molecules released are detected, and therefore it would be expected that the OII absorbance would be negative as it was in the control experiment (Figure 2.7-d). While this result is unexpected, it does not detract from the larger general trend of dye release from the immobilized samples below LCST is greater than that when above LCST and agrees with the free-solution experiments. This once again indicates that the collapsed polymer network after adjusting the pH to neutralize the functional comonomer will hinder the release of the dye molecules. The release of CV in the immobilized samples was much like the free solution samples where AAc-5 and AAc-10 showed a significantly larger release profile compared to the AAc-Core and AAc-20 samples. The immobilized APMA samples behaved in a more linear fashion where the APMA-Core had a larger observed dye release followed by APMA-5, APMA-10, and APMA-20 in order of increasing shell thickness. At 40 °C, the APMA samples are again showing that the release is lower than at 25 °C and in ascending order of shell thickness. It is documented that with increasing shell thickness and crosslinking density, the shell will squeeze the core to a smaller size than the core would alone when heated above LCST.⁹⁰ While the argument could be made that the increased squeezing on the core would result in greater release of dye, it is likely preventing dye release in this system of the bound microgels. The molecular size of CV is $\sim 1.4 \text{ nm}^2$ and OII is slightly smaller at 0.9 nm^2 .^{92,93} pNIPAm microgels with similar crosslinking densities (10 mol% BIS) have a reported mesh size minimum of 2.30 nm in the swollen state, the length of a single BIS chain, and as small as 0.7 nm when collapsed.⁹⁴ While the actual mesh size is highly dependent on the crosslinking and molecular weight of the polymer, and the semi-fluid state of swollen pNIPAm will allow much larger MW molecules to enter the matrix, it is reasonable to suggest that the collapsed core with the additional collapsed dense polymer shell could prevent the passage of both CV and OII out of the microgel.

The rate of dye release in the free-solution samples was clearly much faster than the immobilized samples. The release profiles for both CV and OII had stabilized after about 3 min of triggering the release. The immobilized microgels had a significantly lower rate of release, reaching equilibrium after ~ 15 min for majority of samples. This could be due to a number of contributing factors such as the hindered actuation of the microgels on the surface

when triggered or the suspected aggregates and layering of certain samples would impact the release. In general, the shell thickness appears to have a greater influence on the amount of dye released for the immobilized samples compared to the free solution experiments where APMA samples show a linear decrease in dye release with increasing shell thickness both below and above the LCST.

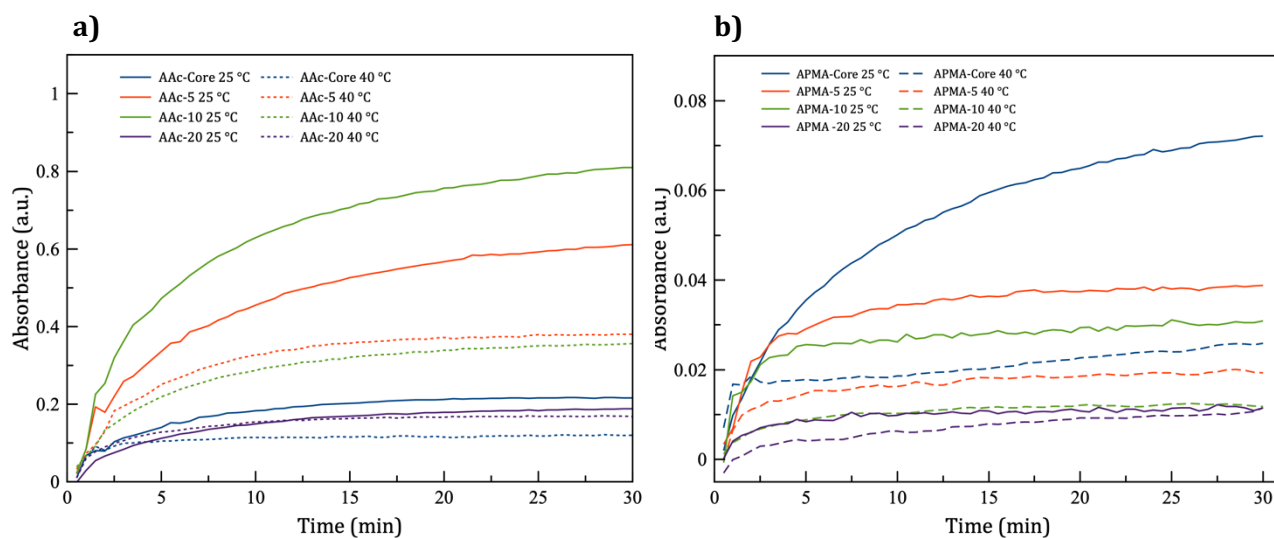


Figure 2.8 Absorbance profiles with time collected via UV-Vis to measure the dye release from (a) immobilized AAC-containing microgels and (b) APMA -containing microgels below the LCST (solid line) and above the LCST (dashed line).

2.4 Conclusion

In summary, the release of CV from AAc containing microgels and OII from APMA microgels with varying thicknesses of pNIPAm shells free in solution and immobilized on a gold surface was investigated. The microgels were characterized by DLS, TEM, and AFM to measure the size and the nature of packing on the gold surface. In general, the AAc microgels were smaller in size and displayed a higher packing density when immobilized compared to the larger APMA microgels. The release of dye from the microgels when free in solution confirmed that the collapsed core-shell structure above the LCST hindered the release of dye but the rate of release was comparable to the release below the LCST. This trend was also observed for the immobilized microgels where the APMA samples followed the trend of decreased dye release with increasing shell thickness both below and above the LCST. The rate of release from the immobilized samples were also comparable to each other but all together slower than the free solution samples due to restricted deswelling and packing/layering of the microgels in the surface.

Chapter 3 Coupling Thermo-responsive Core-shell Nanogels with Thin-film Composite Membranes for Improved Thermal and Anti-fouling Behaviour

3.1 Introduction

A variety of thermo-responsive materials have been coupled to thin-film composite membranes for both flux and antifouling improvement purposes. pNIPAm-based polymers are ideal for modifying membranes because of their hydrophilicity, simple fabrication, and tunable size and functionalities.^{65,95} The flexible properties of pNIPAm polymers allows for the incorporation into the membrane support,^{60,68} the polyamide layer,⁶⁴ or layered on top of the selective layer ^{69,96} to alter performance in response to increasing the feed temperature above the LCST. pNIPAm is highly hydrophilic and protein resistive due to the large localization of water molecules around the polymer chains below the LCST. Having a gel-like layer of pNIPAm on the surface does well to prevent the adsorption of hydrophobic foulants on the surface and prolonging the lifetime of the membrane. Alternatively, incorporating pNIPAm into the bulk structure of the membrane either in the membrane pore structures or within the polyamide will impact the flux and salt rejection. Many studies have reported using pNIPAm based materials as “smart gates” that will open and close in response to temperature.^{61,63,97} A study utilizing pDMAEMA grafted to the surface of the polyamide post IP reaction reported an increase in flux for all modified membrane at 25 °C that further increased at 50 °C where there was an observed jump in flux around the LCST.⁶¹ However, these incorporation methods usually involve a number of modification steps to the polymer and/or the membrane and can take several days to fabricate. For example, the zwitterionization of pNIPAm-*co*-polyethylenimine microgels with 1,3-propane were crosslinked to the surface of a poly(ethylene terephthalate) (PET) membrane.⁹⁵ The track-etched PET membranes were protected with a layer of Cd(OH)₂ to prevent the microgels from clogging the pores during the pressure-coating process, which has to be etched away before use. Polydopamine has also been used to graft amino-terminated pNIPAm microgels onto PET membranes, which requires 24 h coating times followed by several grafting,

washing, and curing cycles before use.⁶² The modified membranes had improved antifouling and rejection properties at 20 °C that declined at 45 °C.

To simplify the incorporation of pNIPAm in a TFC membrane for nanofiltration, a pNIPAm core-APMA shell nanogel was synthesized for coupling to the polyamide selective layer on a PES membrane support. Two different fabrication methods were explored; (1) the crosslinking of the nanogels within the bulk polyamide layer to observe the effect on flux and rejection during high temperature filtration and (2) the modification of the polyamide surface for improved antifouling properties. The nanogels can be incorporated during the IP reaction to form the polyamide or in a 10 min surface modification immediately after the IP, limiting the additional steps and keeping the fabrication time to a minimum compared to other methods. The preparation, filtration experiments, and characterization of the nanogels and membranes was performed by me apart from the SEM and TEM imaging, performed by my lab mates Haley Hunter and Alyssa Fu, respectively. The filtration experiments and membrane fabrications were performed in the AWRL lab, and this project was done in collaboration with Dr. Pooria Karami and Dr. Mohtada Sadrzadeh.

3.2 Experimental Section

Materials: N-isopropylacrylamide (NIPAm) recrystallized from hexanes, N,N'-methylenebisacrylamide (BIS, 99%), N-(3-Aminopropyl)methacrylamide hydrochloride (APMA), 2,2'-Azobis(2-methylpropionamide) dihydrochloride (V50, 98%), cetyltrimethylammonium bromide (CTAB, ≥98%), sodium dodecyl sulfate (SDS, 99%), piperazine (PIP), 1,3,5-benzenetriarbonyl trichloride (TMC), triethylamine (TEA, ≥99.5%), sodium hydroxide (NaOH, ≥97%), sodium alginate (SA), and bovine serum albumin (BSA) were obtained from Sigma-Aldrich. Calcium chloride (CaCl₂) purchased from Fisher Chemicals. Polyethersulfone membrane filters (0.03 μm, 293 mm) were purchased from Sterlitech Corp. (Auburn, WA). Deionized (DI) water with a resistivity of 18.2 MΩ cm was obtained from a Milli-Q Plus system and was used for all synthesis and monomer solutions.

3.2.1 Core-shell Nanogel Synthesis

Core-shell microgels were synthesized in a two-step precipitation polymerization presented in Figure 3.1. NIPAm (9.7 mmol), BIS (0.3 mmol) and CTAB (0.5 mmol) were dissolved in Milli-Q water (99 mL) and transferred to a 3-neck round bottom flask. The solution was heated to 70 °C in an oil bath while stirring and sparged with N₂ gas until steady temperature was reached. The volume was initiated with V50 (1 mL, 0.5 mmol) under an N₂ atmosphere maintained at 70 °C for 3 h. After 3 h, the flask was removed from the bath to cool to room temperature and opened to air to quench. Volume was filtered through Whatman no. 1 filter paper then transferred to 12 kDa dialysis tubing for a minimum of 5 water changes over 1 week.

The APMA shell was added to the as-prepared cores presented in Figure 3.1-b. The diluted core (50 mL diluted to 189 mL with DI water) was heated to 70 °C under nitrogen and stirring in a 3-neck round bottom flask before adding the monomer solution APMA (0.95 mmol) and BIS (0.05 mmol) dissolved in 10 mL DI water. After temperature was reached, the volume was initiated with 1 mL V50 (0.2 mmol) and allowed to proceed at constant temperature for 3 h in nitrogen atmosphere. The volume was cooled to room temperature and opened to air to quench the reaction. The core-shell nanogels were dialyzed again for a minimum of 8 water changes over 1 week. The pH of the volume was adjusted to 11 before lyophilizing for use.

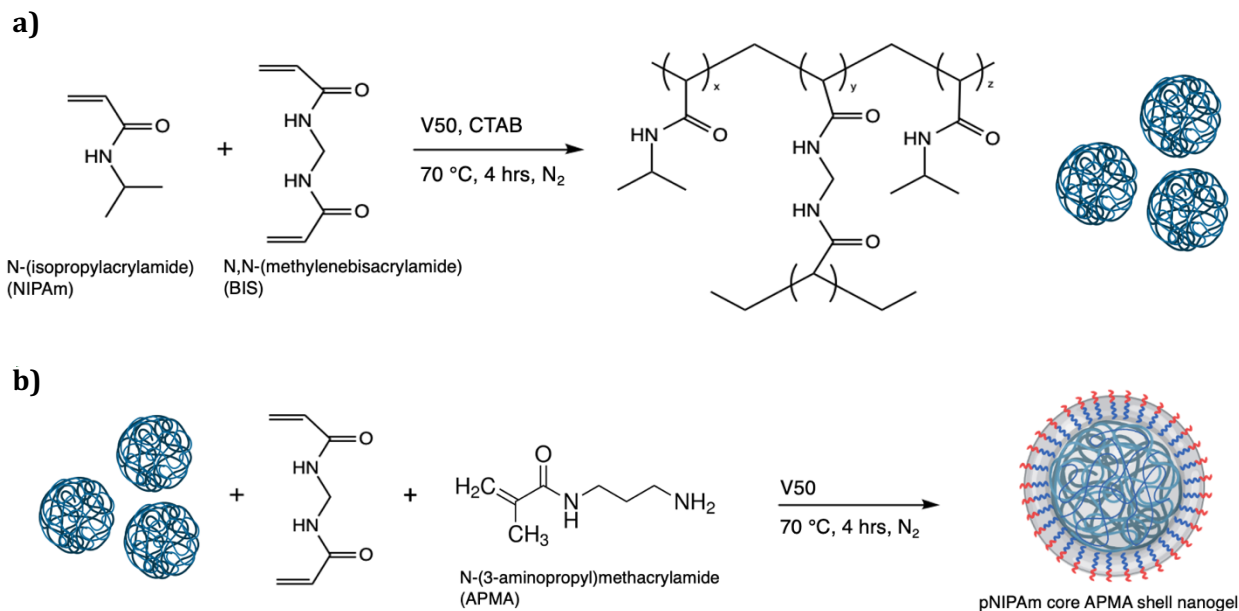


Figure 3.1 Polymerization scheme for (a) pNIPAm core and (b) APMA shell addition.

3.2.2 Fabrication of Composite Membranes

The formation of the selective polyamide (PA) layer on the surface of the polyethersulfone (PES) support membrane was done by interfacial polymerization (IP). A square portion of the commercial 0.03 μm pore size PES support was cut to fit the frames that hold the membrane during the IP reaction. A solution of aqueous monomer of desired concentration was made in aqueous volume. PIP was dissolved in solution with either 0.2 wt% SDS and 1 wt% TEA or in 0.1 M NaOH depending on the membrane. The PES membrane was impregnated with the aqueous PIP monomer solution for 9 min and excess solution was poured off. The membrane was then rolled once with an acrylic roller on paper towel and again on standard printer-type paper to remove excess monomer solution from the membrane surface. A TMC solution of desired concentration in heptane was then poured over the membrane and allowed to sit for 2 min to complete the IP reaction followed by 4 min curing in a 60 $^\circ\text{C}$ oven. The membrane was then washed for several minutes under running distilled water before storage in water overnight before using.

The incorporation of the core-shell particles was done during the IP reaction or directly after the IP to localize them on the surface. A desired concentration of lyophilized

nanogels was dispersed in the aqueous monomer phase and/or the organic heptane-TMC phase and sonicated to improve the dispersion before the IP reaction. To surface modify the membrane, the nanogels were dispersed in heptane and sonicated. Following the IP reaction after the excess heptane-TMC phase had been poured off the membrane, the surface was washed twice with 10 mL portions of heptane then the heptane-NG solution was poured over the top and allowed to react for 10 min. The membrane was cured and washed in the same procedure as detailed above.

3.2.3 Temperature Ramp Nanofiltration Experiments

The performance of the modified membranes was tested in a nanofiltration set up pictured below in Figure 3.2. To observe the effect of temperature on the flux and salt rejection, the initial flux of the membrane was measured at 25 °C for 20 min before adding Na₂SO₄ to the water feed (2000 ppm total feed concentration) and the effect of salt on the flux was observed for another ~30 min. The pressure applied was adjusted to 40 psi for the 0.5% PIP membranes, and ~90 psi for 1 % PIP membranes while the crossflow was maintained at 2.0 LPM. After initializing the flux at 25 °C, the feed temperature was ramped to 50 °C and the rate was recorded to plot the change in flux with temperature. The conductivity of the feed and permeate was measured to determine the salt rejection at 25 °C and at 50 °C using a conductivity meter (Fisher Accumet AR50 Dual Channel pH-ISE-Conductivity Meter). The membrane properties and filtration conditions are detailed in table 3.1 below.

Table 3.1 Summary of membrane properties for temperature ramp experiments.

Sample Name	[PIP] (wt%)	[TMC] (wt%)	Nanogel Modification	Pressure (psi)	Initial Flux (LMH)
0.5% PIP Base-1	0.5	0.2	-	40	~7
0.5% PIP Base-2	0.5	0.2	-	40	~8
0.5% PIP 200	0.5	0.2	200 ppm NG in heptane-TMC	40	~14
0.5% PIP 800	0.5	0.2	800 ppm NG in heptane-TMC	40	~11
0.5% PIP 2000	0.5	0.2	2000 ppm NG in heptane-TMC	40	~9
1% PIP Base	1	0.2	-	90	~15
1% PIP 800 aq.	1	0.2	800 ppm NG in aq. PIP	70	~8
1% PIP 800	1	0.2	800 ppm NG in heptane-TMC	90	~15
1% PIP 2000	1	0.2	2000 ppm NG in heptane-TMC	80	~12



Figure 3.2 Nanofiltration set up used for testing the TFC membranes.

3.2.4 Antifouling Nanofiltration Experiments

The effect of the same core-shell nanogels localized on the surface of the polyamide on antifouling of the membrane was also tested. The same nanofiltration set up was used as displayed in Figure 3.2 above. The membrane was loaded into the holding stage and the applied pressure was adjusted so that the initial flux of each tested membrane was approximately the same, around ~80 LMH, and the crossflow was held constant at 2.0 LPM. The initial pure water flux was recorded for 20 min before adding a 150 ppm sodium alginate solution, which was prepared by vigorously stirring 150 mg SA in 250 mL DI water to completely dissolve before gradually adding in 55 mg CaCl₂ and stirring for another 30 min before using in the filtration experiment. After adding the foulant, the flux decline was recorded for 60 min. The filtration was stopped, the applied pressure was reduced to 0 psi, and the feed tank was cleaned and replaced with water that was heated to 50 °C. Once at temperature, the pump was turned on with the pressure still at 0 psi and the crossflow set to 2.0 LPM as the membrane surface was washed for 20 min. The pump was once again turned off, the feed was emptied and replaced with 25 °C water, then the pressure was increased back to that what it was at the beginning of the experiment and the recovered flux was recorded for 20 min. Feed and permeate samples were collected and the conductivity was measured to determine rejection. The membrane properties and filtration conditions are detailed in Table 3.2 below.

Table 3.2 Summary of membrane properties for antifouling experiments.

Sample Name	[PIP] (wt%)	[TMC] (wt%)	Nanogel Modification	Pressure (psi)	Initial Flux (LMH)
PIP Base	0.1	0.2	-	40	~78
400/400	0.1	0.2	400 ppm NG in aq. monomer phase & heptane-TMC phase during IP	70	~80
400 s-mod	0.1	0.2	400 ppm NG surface modified	60	~82
800 s-mod	0.1	0.2	800 ppm NG surface modified	70	~81

3.2.5 Characterization of Nanogels and Membranes

The size of the core-shell nanogels were characterized by dynamic light scattering (DLS), zeta potential (ZP), and transmission electron microscopy (TEM). The DLS instrument (Zetasizer Nano S) was used to measure the hydrodynamic diameter and zeta potential of the nanogel core and the core-shell. The size was measured at temperatures below (25°C) and above (40 °C) the LCST of pNIPAm and a pH's below (6.5) and above (11) the pK_a of APMA. The ZP was measured using a dip cell. The summary of data and conditions for the size and ZP measurements is presented in Table 3.3. Brightfield TEM images captured on a 200 kV JEOL 2100 transmission electron microscope were also collected for the core-shell sample to confirm spherical morphology and to approximate the dry diameter of the nanogels in Figure 3.3-a. The presence of the APMA shell was verified by performing a bromophenol blue staining test on the core and core-shell nanogels. In the presence of an amine, the indicator will stain blue by the acid-base reaction between the basic amine and the indicator. 400 µL of 0.25 wt% bromophenol blue was added to a small amount of lyophilized core and core-shell nanogels. The sample was allowed to rehydrate in the indicator solution for 1 h before centrifuging to create a pellet and the supernatant was removed and replaced with pH 6.5 DI water. This was repeated 3 times to wash the sample and removed excess indicator. The membrane surface was characterized by a Hitachi S-4800 FESEM high resolution scanning electron microscope (SEM), a DI Dimension 3000 atomic force microscope (AFM), and contact angle (CA) (Drop Shape Analyzer DSA100) and the data is summarized in Figure 3.6 below. The SEM and AFM images are of the dry, pristine membranes to observe the surface morphology. The dynamic contact angel of both the pristine and fouled surface modified membranes was measured at time 0 s, 10 s, and 30 s, after adding the water droplet. A portion of the membrane was dried on a glass slide at 60 °C overnight before taking the measurements.

Table 3.3 Summary of DLS data of core and core-shell nanogels for measuring the hydrodynamic size at different temperatures and pH's and zeta potential.

Nanoparticle	pH	D_h at 25 °C (nm)	D_h at 40 °C (nm)	ZP (mV) *	Yield
pNIPAm core	6.5	106.4 ± 0.4	69.2 ± 0.1	0.4 ± 0.5	70%
	11	93.8 ± 0.1	63 ± 5		
pNIPAm core- APMA shell	6.5	105 ± 2	44.6 ± 0.9	7.5 ± 0.9	72%
	11	102 ± 1	90 ± 2		

* Zeta potential measured at pH 6.5 at 25 °C.

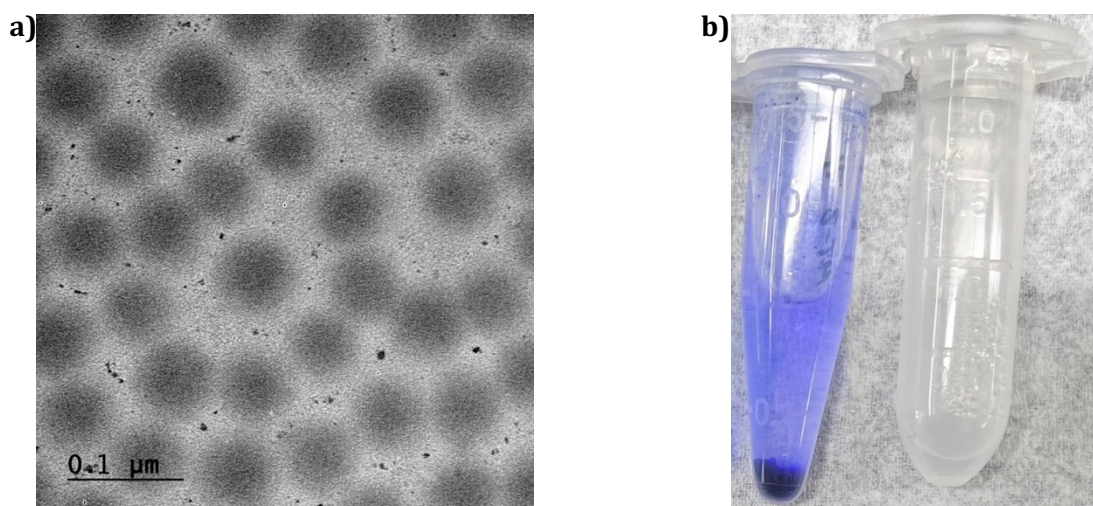


Figure 3.3 (a) Brightfield TEM image of the core-shell nanogels and (b) bromophenol blue staining test for amines on the core-APMA shell (right) and the pNIPAm core (left).

3.3 Results and Discussion

The synthesis of small thermo-responsive core-shell nanogels is detailed above in section 3.2.1. An APMA shell was added to the pNIPAm core so that the primary amine at the end of the APMA unit was accessible for further reactions without altering the thermo-responsive properties of the pNIPAm core. The core and core-shell nanogel synthesis conditions were optimized to yield a < 100 nm diameter particle by introducing a surfactant during the polymerization. The presence of the surfactant during precipitation polymerizations increases the colloidal stability of the particle nucleation sites formed in the

early stages of polymerization, which lowers the diameter and increases the number of particles formed in solution.⁹⁸ The DLS data in Table 3.3 summarizes the measured hydrodynamic size of the pNIPAm core and the core with the added APMA shell. The core alone displays a temperature dependent collapse that decreases the size from 106 nm to 69 nm when heated from 25 °C to 40 °C at pH 6.5. The measured diameter of the core at pH 11 at 25 °C and 40 °C was smaller than when in pH 6.5 solution. While pure pNIPAm does not possess any pH sensitive functional groups, the behaviour of the polymer is very sensitive to changes in pH and ionic strength. A study by Pei et al. reported that LCST of pNIPAm in a pH 10 buffer shifts from 32 °C to ~ 27 °C by disrupting the hydrogen bonding that occurs between the water molecules and the polymer chains.⁹⁹ This could explain why the core has a slightly smaller diameter under these conditions. As with the core-shell particles discussed previously in Chapter 2, the addition of the APMA shell does not appear to increase the hydrodynamic size at pH 6.5, when the primary amine is protonated and positively charged, or at pH 11, when it is neutral. Since the APMA is not incorporated into the pNIPAm polymer structure, the presence of the charge at pH 6.5 is localized to the outside of the particle shell, where it should not affect the size as much except to perhaps repel other charged groups on adjacent polymer chains surrounding it.⁴¹ This in combination with the previously discussed shell restriction on the swelling of the core both below and above the LCST, can explain why the shell thickness cannot be directly measured by DLS as the core will no longer possess the same swelling properties after the shell has been added.⁹⁰ At 25 °C, the size of the core-shell microgel appears to be about the same size at pH 6.5 and 11. Although APMA does not have any intrinsic temperature responsive properties, the diameter of the core-shell at pH 6.5 is much smaller than at pH 11 when heated to 40 °C, 45 nm and 90 nm, respectively. This seems counter to what is expected as the reduced positive charge on the outside shell at pH 11 should contribute to the deswelling of the particle by reducing the electrostatic repulsion. The contribution of charge at pH 6.5 above LCST will repel surrounding particles whereas once the shell becomes more neutral, perhaps there is increased particle-particle interactions that will inflate the observed hydrodynamic diameter. A brightfield TEM image of the core-shell nanogel was taken as seen in Figure 3.3-a where the dry diameter is approximately 65 nm across and indeed spherical. While the exact shell thickness could not be measured by DLS, the same instrument was used to measure zeta potential of the core

and core-shell nanogels. The results are included in Table 3.3 where the ZP for the pNIPAM core is nearly 0 mV which increased to 7.5 mV with the APMA shell at pH 6.5 at 25 °C. This increase ZP indicates the successful addition of an APMA shell where the positive primary amine at pH 6.5 would contribute a positive charge. Finally, a test with bromophenol blue was done on the core and core-shell nanogels. Bromophenol blue indicator can undergo and acid-base complexing with basic primary, secondary, and even aromatic amines.¹⁰⁰ The staining and washing of the core and core-shell resulted in a dark blue stained core-shell nanogel where the core alone remained colourless (Figure 3.3-b), confirming the presence of the APMA shell.

The modification of thin film composite membranes with nanomaterials is of great interest to improve the performance of the membrane during filtration. The thermo-responsive core and the primary amine modified shell allows for the modification of the polyamide (PA) selective layer in two ways; (1) incorporating the nanogels into the PA for temperature ramped filtration and (2) the surface localization of nanogels to improve antifouling performance. The formation of the PA occurs between two monomers at the interface of two immiscible layers in which they are dissolved, and the conditions are detailed in section 3.2.2. A scheme of the IP reaction is presented in Figure 3.4. TMC must be solubilized in a dry aprotic solvent that is immiscible with water to prevent the hydrolyzation of the acyl chloride groups. The aqueous monomer PIP rapidly diffuses up into the heptane-TMC phase where the amine on PIP covalently crosslinks with the acyl chloride groups on the TMC to form the polyamide. The addition of 1 wt% triethylamine or 0.1 M NaOH is present to neutralize the HCl byproduct formed by the reaction. This is convenient for when incorporating the nanogels during the IP reaction because the pH needs to be maintained above the pKa of APMA, which is ~10.2, so that the primary amine remains deprotonated and can therefore also covalently crosslink with the TMC. This method should anchor the nanogels to the PA so that they will not be washed away during pressurized filtration. The nanogels are highly soluble in polar protic solvents, but when attempts were made to add the nanogels to the heptane-TMC phase or surface modify in pure heptane, the volume was sonicated for several minutes to improve the dispersion and limit the formation of large aggregates.

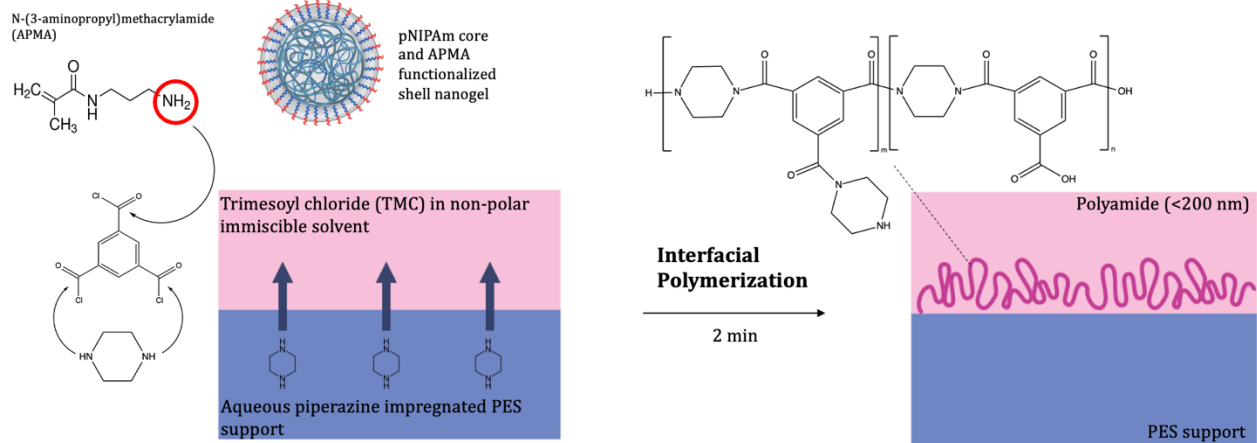


Figure 3.4 Interfacial polymerization scheme for the formation of the polyamide on the membrane support.

The details of the temperature ramped NF experiments are detailed in section 3.2.3 above. The interest behind TFC membranes with incorporated nanogels is to observe the impact of feed temperature on the performance in terms of flux and rejection during filtration. The flux of unmodified TFC membranes will increase with temperature as the mass transfer of water increases while viscosity decreases in combination with the relaxation of the polyamide chains results in a lowered salt rejection.^{53,68} The original hypothesis for the behaviour of the nanogels incorporated into the polyamide, not surface coated, was that when heated, the pNIPAm core would collapse and create a nanochannel around the particle so that the flux would significantly increase as the temperature increased above the LCST without sacrificing rejection as had been reported in other studies using similar materials.^{60,95} Many attempts to observe this flux phenomena were made by varying the monomer and nanogel concentrations, the incorporation methods (i.e. nanogels present in the aqueous monomer or heptane-TMC phase), and the filtration set up. For brevity, not all experimental data is included, but a selected comparison to represent the broad results is summarized in Figure 3.5. Membranes fabricated with 1% PIP were tested first and it was determined that incorporating the nanogels in the heptane-TMC phase performed better than when in the aqueous phase. The flux of 1% PIP 800 aq., with 800 ppm nanogel present in the aqueous PIP phase during IP, did appear to have a jump in flux around 36 °C (Figure 3 (a)) but the salt rejection of 65.7% decreased to 62.2% at high temp. filtration (Figure 3.5-

c). Comparing this membrane to the unmodified base membrane, the flux profiles are comparable, but the rejection is worse indicating that this incorporation method overall worsens membrane performance. Instead, incorporating nanogels in the heptane-TMC phase, as was done in all other modified membranes presented in these experiments, improved the salt rejection with increasing temperature. In turn, the presence of nanogels incorporated into the polyamide decreased the change in flux, which can be related to the slope of the flux change with temperature. The base membrane had a steeper slope with larger flux increase compared to 1% PIP 800 and 1% PIP 2000 seen in Figure 3.5-a. This result indicates that the initial hypothesis is not true but rather the opposite, the nanogels are crosslinked much more strongly to the polyamide that when the core collapses, the polyamide is drawn in tighter around the gel, and the pore sizes decreases. This explains both the observed increased salt rejection and the decrease in flux improvement with temperature. After this discovery, the optimization of the polyamide was done by varying the PIP concentration. The applied pressure during filtration of 1% PIP membranes was quite high for nanofiltration (80-90 psi). By decreasing the PIP concentration to 0.5%, the applied pressure was reduced to 40 psi to achieve approximately the same initial flux as the 1% PIP membranes. In figure 3.5-b, the trend of decreasing flux improvement with increasing nanogel concentration is evident. The two base membranes had comparable performances and the initial flux around 8 LMH improved to about 20 LMH, while 0.5% PIP 2000 had about the same initial flux and only improved to 12 LMH. Where all membranes modified with nanogels had an improved salt rejection with temperature while the base membranes did not. The exception being 0.5% PIP 200, which did have the improved salt rejection, but the initial rejection was 62% improving 66%. This is likely due to some inconsistency during the fabrication steps resulting in a more porous selective layer. The results from the modified membranes indicates that the incorporation of nanogels in the heptane-TMC layer will improve the salt rejection with temperature. Exploring the performance of these membranes for selective rejection of smaller salt species such as Li^+ would be of great interest in the future.

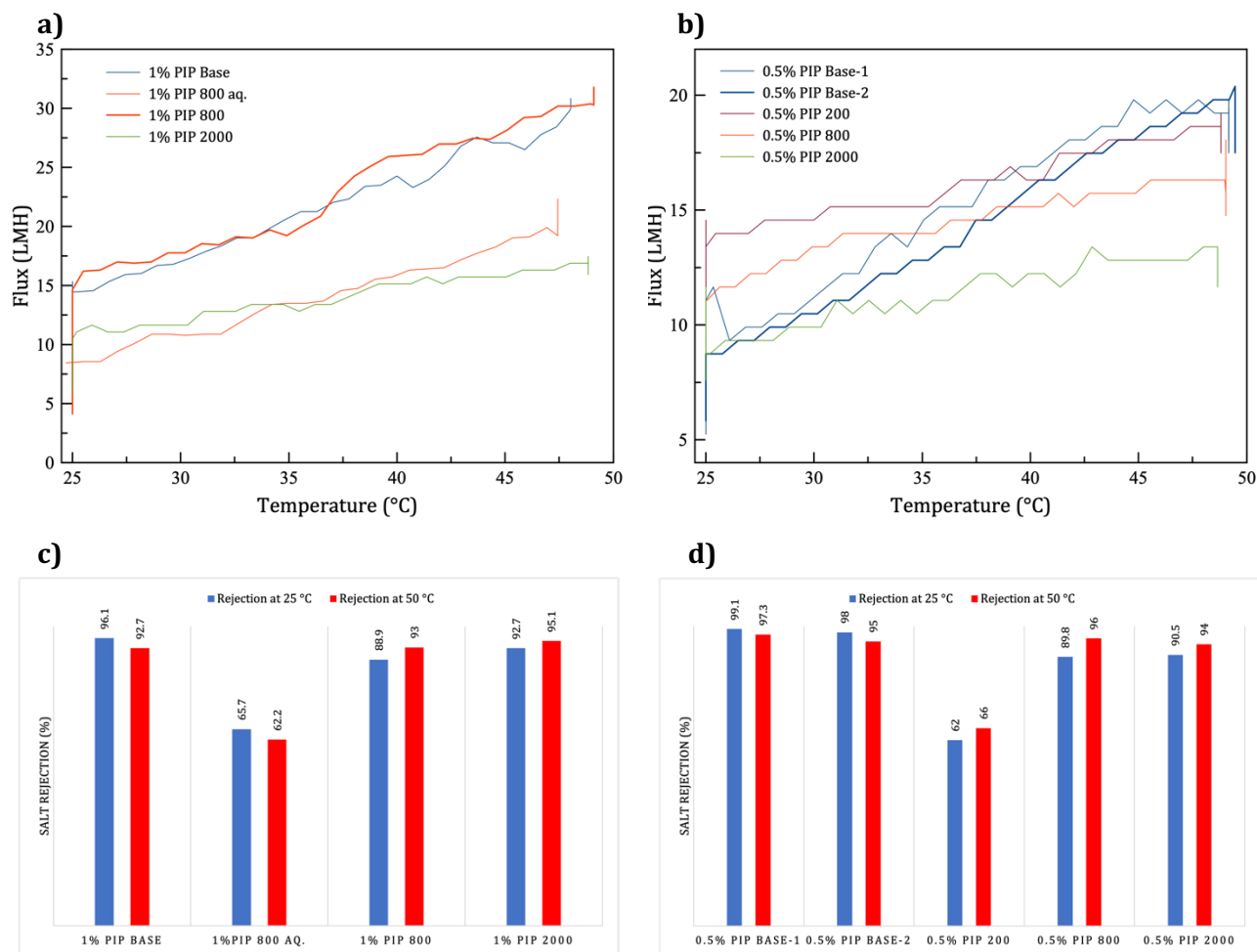


Figure 3.5 The change in flux with increasing temperature plot for (a) 1% PIP base and modified membranes and for (b) 0.5% PIP base and modified membranes. The % salt rejection at 25 °C (blue) and at 50 °C (red) for (c) 1% PIP membranes and (d) 0.5% PIP membranes.

The surface modification of the polyamide with the same core-shell nanogels was also explored for improving the antifouling properties as detailed in section 3.2.2. The idea that thermo-responsive materials can improve the antifouling properties of TFC membranes has been studied before,^{62,95,101} but the unique morphology of the core-shell nanogel modified with APMA shell for chemical crosslinking has not yet been reported to date. For these experiments, the flux recovery of the modified membrane was evaluated by varying the washing temperature to observe the effect of the swelling/deswelling actuation of the nanogels on removing the foulant cake layer. Typically, the membrane is made to be more

hydrophilic or hydrophobic depending on the foulant, so that the interaction between the membrane surface and the foulant is decreased. For example, sodium alginate is a hydrophilic foulant so the membrane would be made to be more hydrophobic to repel the foulant and make the washing more effective.¹⁰² What is not intuitive about this system is that the addition of nanogels should increase the hydrophilicity of the membrane surface as both the core and shell are hydrophilic in nature. The dynamic contact angle of the membrane was measured at time 0 s, 10 s, and 30 s after adding the water droplet to the surface to observe the change in wettability with the hydration of the nanogels, and found that the surface modified membranes were more hydrophobic compared to the base, seen in Figure 3.6-a. A contact angle $>90^\circ$ usually classifies the surface as hydrophobic but there are other factors such as surface roughness that can inflate contact angle measurements according to Wenzel's corrections made to Young's equation.^{103,104}

$$(3.1) \quad \cos\theta_r = \lambda \frac{\gamma_{sv} - \gamma_{sl}}{\gamma_{lv}} = \lambda \cos\theta$$

Where θ_r is the apparent contact angle, λ is the roughness factor or ratio of actual surface area to the projected surface area due to roughness, and the contributions to contact angle from the solid-vapour, solid-liquid, and liquid-vapour interface tensions γ_{sv} , γ_{sl} , and γ_{lv} . According to this model, when a surface is hydrophilic (CA $<90^\circ$), increasing surface roughness will decrease contact angle whereas the hydrophobic surface (CA $>90^\circ$) will have an increased contact angle with increasing surface roughness.¹⁰⁴ But there are also several reported exceptions that exist outside the confines of the model. For example, plant species that have nano- to microscale surface roughness can alter what should be a hydrophilic surface into the superhydrophobic range ($>150^\circ$).¹⁰⁵ The surface roughness was measured by AFM shown in Figure 3.6-(c-f) to better understand the surface morphology. From the AFM data, the surface modified membranes, 0.1% PIP 400 s-mod. and 0.1% PIP 800 s-mod. in particular, have an increased roughness compared to the base. Although the scale at which the roughness is increasing would not seem to be solely responsible for increasing the contact angle by nearly 40° , there does not seem to be another explanation considering the nanogels are inherently hydrophilic in nature.

While the contact angle and change in surface roughness indicates the successful coupling of the nanogels to the surface of the membrane, it was further confirmed by zeta potential. After the IP reaction, the washed PA surface was covered in nanogels dispersed in heptane for 10 min. Any residual acyl chloride groups would then be available to covalently crosslink with the primary amine on the end of APMA. On the base membrane, these acyl chloride groups would be immediately hydrolyzed to carboxylic acid group that contribute negative charges on the surface of the polyamide. The protonation state of TMC bound carboxylic acids within the polyamide is highly variable and the pK_a shifts higher as you penetrate further into the polyamide.¹⁰⁶ This explains why the zeta potential of the membrane surface becomes more negative as the pH increases as seen in Figure 3.6-b. The surface modified membranes all have a higher measured zeta potential than the base membrane, measuring more positive with increasing concentration of nanogel added. Scanning electron microscopy images were also taken to attempt to visualize the nanogels on the surface shown in Figure 3.6. From these images, there appears to be some clusters of particles that could be nanogels, most prevalent on the 0.1% PIP 800 s-mod sample, that are not seen on the base membrane. The nanogels are soft polymer materials that are difficult to image by electron microscopy techniques as the electron beam will penetrate through the material and lowering the intensity, lowered to 5 kV as in the images presented, will sacrifice the resolution.¹⁰⁷ Taking this characterization data into account, it can be reasonably concluded that the nanogels are coating the surface of the polyamide and the impact they have on antifouling of the membrane was explored.

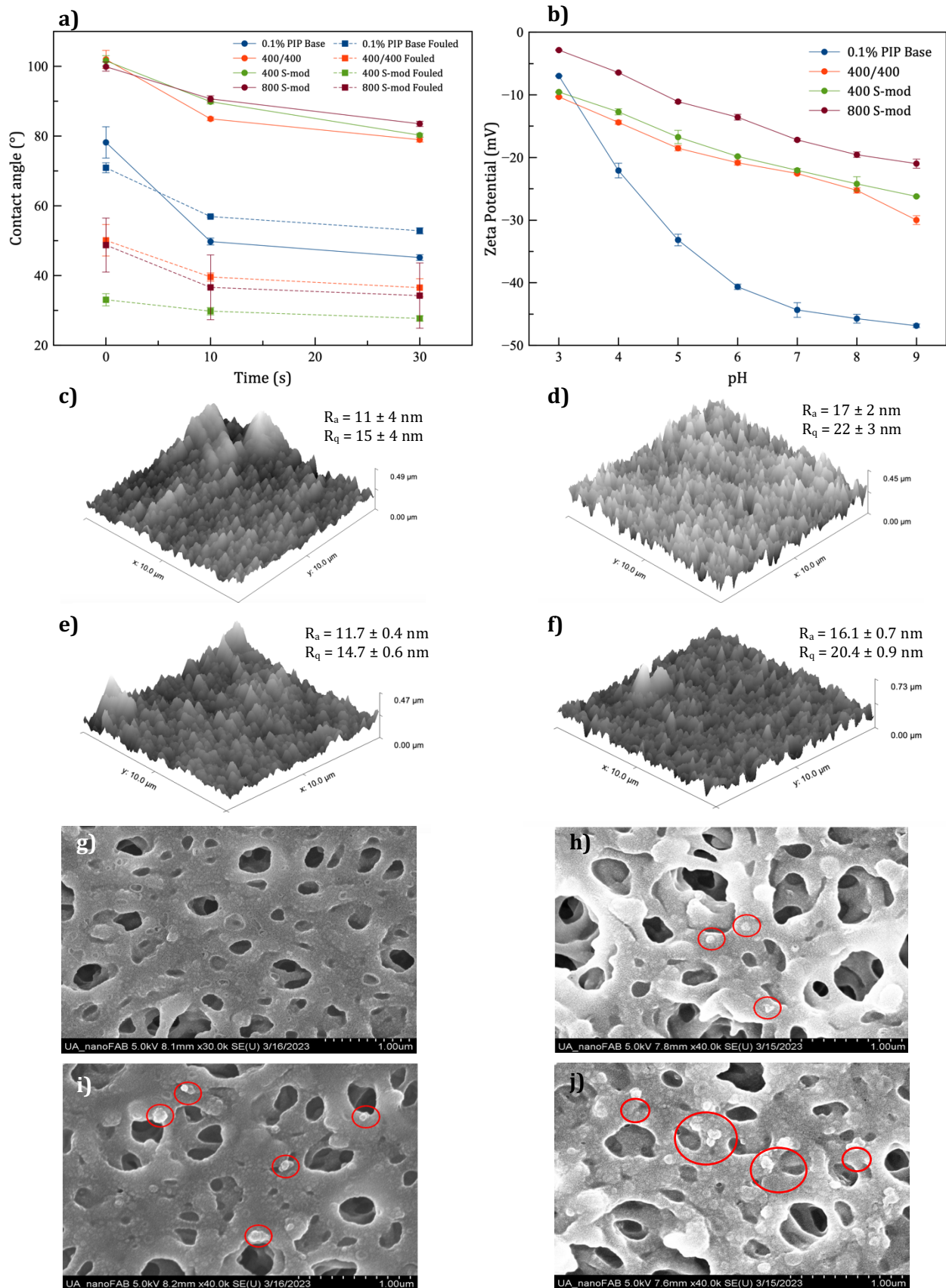


Figure 3.6 (a) dynamic contact angle and (b) zeta potential data for the base and modified membranes. AFM and SEM images for the base membrane (c & g), 400/400 (d & h), 400 s-mod (e & i), and the 800 s-mod membrane (f & j).

Details for the antifouling experiments is included in section 3.2.5 above, but briefly, the pure water initial flux was measured at 25 °C before adding crosslinked sodium alginate with CaCl₂ to foul the membrane. The feed was washed and heated to 50C to wash the membrane without any applied pressure before cooling again to 25 °C, reapplying the same initial pressure, and recording the recovered flux. The flux results from these experiments are summarized in Figure 3.7. Sodium alginate is the hydrophilic foulant used herein that is crosslinked with CaCl₂ to form a gel. The Ca²⁺ ions can also act as a bridging agent between the foulant and the membrane surface, interacting with the deprotonated carboxylic acid groups on the membrane surface.^{108,109} By reducing the net negative charge on the membrane surface, the calcium bridging effect can be mitigated.⁶⁷ The localization of the thermo-responsive nanogels on the surface of the membrane not only reduces the negative surface charge, as seen in the ZP data, but the actuation of the nanogel from swollen/hydrophilic to deswollen/hydrophobic will both reduce the severity of fouling and improve the flux recovery after washing. The base membrane (Figure 3.7, in blue) experienced the most severe fouling where the flux declined nearly 50% in 1 h and having a flux recovery of 74%. Comparing this result to the modified membranes, the impact of fouling on the flux is decreased, approximately 30%, 19%, and 15% flux decline due to fouling for 0.1% PIP 400/400, 400 s-mod, and 800 s-mod, respectively. And all achieving ≥90% flux recovery. It is not expected that the base membrane would experience much flux recovery under low temperature washing, as done in other antifouling studies with thermo-responsive materials,⁶¹ but with heating the washing feed, the sodium alginate becomes more soluble and some of the cake layer will wash away. It is when the nanogels are present, it can be reasoned that the transition from swollen to the deswollen state will aid in dislodging the foulant cake layer. There could also be some additional influence from the hydrophilic to hydrophobic transition of the pNIPAm core, despite the APMA shell that should provide some screening between the collapsed pNIPAm the surrounding environment. Referring back to Figure 3.6-a, the dynamic contact angle of the fouled membranes after filtration was measured. For the surface modified membranes, the contact angle is significantly lower than the pristine membrane, indicating that despite having a flux recovery ≥90%, there is still remnants of the hydrophilic foulant on the surface after washing. While these results are very promising, the performance of the membrane was not

ideal as the rejection for all membranes tested was $\leq 36\%$. To address this, the PIP concentration was increased but the significant impact to the initial flux was observed to the point where the applied pressure was very high, and the effects of fouling could not be observed due to the low flux. That data is not included here, but the work is ongoing and will be continued in the future.

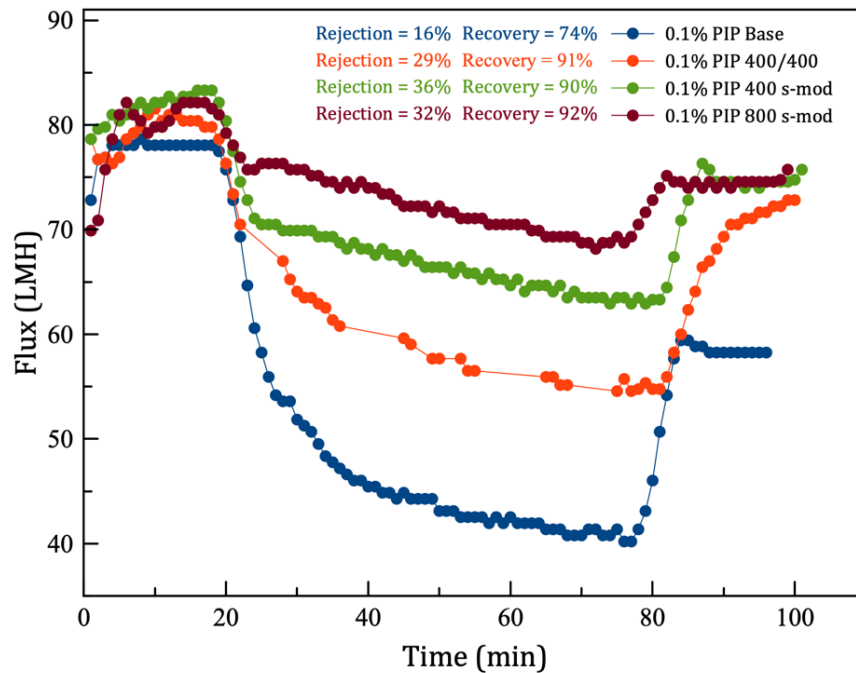


Figure 3.7 Change in flux with time where the initial flux was recorded (0-20 min), the impact of fouling on the flux (20-80 min), and the recovered flux after washing (80-100 min) for the base (blue) and modified membranes.

3.4 Conclusion

In summary, the incorporation of thermo-responsive core-shell nanogels into the polyamide of thin-film composite membranes was achieved. The presence of the nanogels in the heptane-TMC phase during interfacial polymerization incorporated the nanogels into the polyamide structure and resulted in an increased salt rejection with increased filtration temperatures. But the flux improvement with temperature was depressed with increasing nanogel concentration. Additionally, the localization of the nanogels on the surface of the polyamide reduced the severity of sodium alginate fouling and improved the flux recovery with high temperature washing. These results are not consistent with other work that couple thermo-responsive materials to a TFC membrane and should be very interesting should this work continue for exploring the combined effects of the incorporated and surface modified membranes for the rejection of smaller target species such as Li^+ ions, where research is very focused currently given the importance of lithium recovery for batteries and other manufacturing sectors.¹¹⁰

Chapter 4 Self-driven Water Filtration and Clean Water Recovery using Polyamide-coated Thermo-responsive Polymer Hydrogels

4.1 Introduction

It is recognized that membrane-based separation systems excel in a number of industrial and environmental applications. Popular membrane-based systems are pressure-driven and can achieve excellent levels of separation with high permeability and tuned properties such as pore size, selective layer morphology, and added functionalities for optimal membrane performance.^{71,111} While advancements in membrane separation are growing more rapidly than any other method for water remediation, this may not be the most practical system for addressing the major challenges we are facing globally regarding climate change, energy, and water. Where the popular processes of desalinating brackish water via reverse osmosis (RO) or electrodialysis (ED) are very effective at producing clean water, they are energetically expensive due to the high osmotic pressure of saline water and require the infrastructure to treat large volumes of water to offset the costs.¹¹² Solutions to the larger concern of global accessibility to clean water is the goal and the research community has shifted focus to explore the potential of alternative materials that will aid other sectors effected by the water crisis such as the agriculture, manufacturing, and environmental conservation industries.⁶ In this context, hydrogels have emerged as a promising alternative due to their unique properties such as tunable swelling behavior, biocompatibility, and stimuli-responsive nature.

Hydrogels are hydrophilic, cross-linked polymer structures, that can swell and take up large volumes of water but will not dissolve.⁷ The properties of the hydrogel can be tuned by altering the size, physical structure, monomer composition, and degree of crosslinking to function in the system of interest. Highly hydrophilic hydrogels capable of absorbing $< 10^3$ times their dry weight in water have been incorporated into urban agricultural systems to help reduce the stress of irrigation in drought-wrought environments by improving soil moisture.^{51,113,114} Other hydrogel matrixes have been modified with target-specific functional monomers to selectively capture heavy metal contaminants in water such as Pb^{2+} and Cd^{2+} .^{35,115,116} In these instances where the recovery of the hydrogel contents is desired

to isolate the contaminants, stimuli-responsive polymers such as poly(N-isopropylacrylamide) (pNIPAm) have been widely utilized due to the thermo-responsive nature. pNIPAm has a lower critical solution temperature (LCST) at 32 °C and exhibits a reversible hydrophilic to hydrophobic transition when heated above the LCST.⁶ The hydrogen bonds formed between the water molecules and the amid group of the polymer energetically dominates when the temperature is below the LCST. When heated above the LCST, the solvation of the hydrophobic regions becomes unstable forcing the rearrangement of the polymer chains to a globule conformation, breaking the hydrogen bonding, and expelling the water molecules.¹¹

Recently, the applications of hydrogels for desalination have centered around two main processes: stimuli-responsive hydrogels and polyelectrolyte hydrogels. The polyelectrolyte hydrogels exploit the high charge density contained within the gel to create an osmotic pressure gradient in which the high osmotic pressure of brackish water deters the passage of salt ions into a high charge concentrated area of the gel phase.^{7,8,73} These types of hydrogels excellent at rapid swelling achieving salt rejection up to 35% when using a polyacrylic acid gel in 10 g/L NaCl feed solutions.⁷³ The limitation of these materials is that the clean water is recovered either by mechanical means, by applying stress to the gel and squeezing the gel like a sponge, or by copolymerizing with a stimuli responsive polymer such as pNIPAm. But this lends to very low recovery rates (< 10 %) as the high charge density in the gel increases the LCST dramatically or depressing the thermo-responsive properties altogether.⁷

Combining a hydrogel material with a highly selective polyamide coating for the recovery of clean water has been explored recently for applications in aqueous sample concentration. A study by Dou et al combined a polyacrylic acid hydrogel core coated with a polyamide (PA) membrane shell typical of a TFC membranes for desalination. This material was able to achieve >96 % salt rejection but the mechanism for water recovery was by evaporation at 60 °C, and the material was not able to withstand repeat swelling/deswelling cycle for reuse.⁷⁴ To improve the PA adhesion to a hydrogel surface, Gupta and coworkers optimized a pNIPAm-co-pSA hydrogel that exploited the charge interaction between the pSA

and polyethyleneimine, the amine containing monomer for the IP reaction, acting as an anchor for the PA layer.⁷⁶ This material was able to withstand 100 swelling/deswelling cycles without any observed delamination between the PA and the hydrogel. Although, the rejection of inorganic salts was varied and was not selective to smaller Li⁺ and Cl⁻ ions.⁷⁶

In this study, a novel membrane system based on a pNIPAm hydrogel as the support material that is coated with a polyamide selective layer for enhanced separation performance is presented. The developed water treatment system shows comparable performance in terms of water flux for a non-ionic polymer and excellent selectivity for a number of solutes. Furthermore, the thermo-responsive behavior of the pNIPAm hydrogel allows for the recovery of water from the membrane system using heat and maintain performance for 3 swelling/deswelling cycles. This material can potentially reduce energy consumption and enhance the sustainability for many different wastewater or sample treatment applications. All fabrication optimization, filtration experiments, and characterization was performed by me with the exception of the FTIR, which was performed by Dr. Pooria Karami, and ESEM/cryo-TEM, which was submitted through nanoFAB.

4.2 Experimental Section

Materials: N-isopropylacrylamide (NIPAm) recrystallized from hexanes, N,N'-methylenebisacrylamide (BIS), ammonium persulfate (APS, >98%), tetramethylethylenediamine (TEMED), toluene, chloroform, ethanol, m-phenylenediamine (MPD), trimesoyl chloride (TMC, >98%), triethylamine (TEA), and lithium chloride (LiCl, ≥99%) purchased from Sigma-Aldrich. Sodium chloride (NaCl) and Calcium chloride (CaCl₂) purchased from Fisher Chemicals. And magnesium sulfate (MgSO₄) purchased from Caledon.

4.2.1 Preparation of Spherical Hydrogels and Polyamide Coating

The spherical hydrogels were prepared using a 1M aqueous monomer solution containing 4.9 mmol NIPA, 0.02 mmol BIS, and 0.08 mmol APS. 100 μL volumes of monomer solution were carefully placed at the interface of chloroform and toluene-2 wt% TEMED in a glass vial. The polymerization was carried out for 20 minutes at room temperature. The hydrogel spheres were dried in 100% ethanol for a minimum of 12 hours. For the polyamide

shell addition, the hydrogels were hydrated in an aqueous MPD solution of desired concentration for a minimum of 12 hours. The hydrated gels were then submerged in a mix of heptane and chloroform containing the desired concentration of TMC for 2 min. The resulting PA coated hydrogels were left in 2 M KCl overnight to remove water from the hydrogel before experiments.

4.2.2 Preparation of Flat Hydrogels

Flat hydrogels were prepared for characterization purposes by using the as-prepared monomer solution described above. 5.0 mL monomer solution and 100 μ L 1% TEMED in deionized water was added to a small petri dish and left for 30 minutes. The flat hydrogel was rinsed 3x with deionized water to remove unreacted monomer before placing in 100% ethanol to dry. Small portions of the flat hydrogel were cut using a razor blade before the polyamide coating reaction, which was the same as described above.

4.2.3 Filtration Experiments and Data Treatment

A quantitative estimation of the flux was obtained by measuring the weight and radius changes of the coated hydrogels after immersing the as-prepared PA coated hydrogels, deswollen in 2 M NaCl, in 1.0 mL volumes of a salt solution feed at regular time intervals after gently drying the surface of the gel with a wipe. The hydrogels are not perfectly spherical throughout the swelling process, as shown in Figure 4.1, but an effort to approximate the surface area of the polyamide membrane layer was made to estimate the flux was defined by Equation 4.1.

$$(4.1) \quad \text{Flux (LMH)} = \bar{t} \left(\frac{W_t - W_i}{4\pi\bar{r}^2} \right)$$

Where t is the average time between the intervals, in this case 15 min, W_i and W_t is the weight of the gel before and after the time interval had passed, \bar{r} is the mean radius of the gel before and after the time interval. Flux is typically reported as LMH (or $\text{L}\cdot(\text{m}^2\cdot\text{h})^{-1}$). Using the change in radius of the “spherical” hydrogel, the surface area of the membrane (the PA skin) can be approximated, the change in mass of the gel at each time is the amount of water

passing through the membrane, and the time is the average time between each measurement.

The corresponding water uptake of the gels over the same time scale was obtained as follows.

$$(4.2) \quad \text{Water Uptake (\%)} = \left(\frac{W_t - W_d}{W_s - W_d} \right) 100$$

Where W_d is the dry weight of the gel after drying at 60 °C overnight and W_s is the equilibrium weight of the hydrated gel after 24 h in the same feed concentration as the experiment at room temperature.

The performance of the polyamide coated hydrogels in selectively rejecting salt was determined by measuring the target salt ion concentration in the feed recovered after the first 2 h filtration, and after 1 h for subsequent filtrations. An aliquot of feed sample was diluted 20x and the concentration was measured using an Optima DV 2100 inductively coupled plasmon atomic emission spectrometer (ICP-AES). The moles of salt in the feed before and after filtration were presented as a mole ratio where selective rejection meant a ratio = 1 as defined by the following Equation 4.3.

$$(4.3) \quad \text{Mole Ratio} = \left(\frac{C_f V_f}{C_i V_i} \right)$$

Where C_i and C_f are the concentration of the target salt ion in the feed before and after the filtration, respectively. V_i and V_f are the feed volume before and after filtration, respectively, derived from the weight of the swollen hydrogel corresponding to the weight of water absorbed.

The gels were transferred into deionized water before placing in a 50 °C water bath for 60 min and allowed to shrink. To obtain the percent water recovered, the weight of the gel before and after heating was measured and compared to the total weight of water absorbed by the hydrogel in Equation 4.4.

(4.4)
$$\text{Water Recovery (\%)} = \left(\frac{W_h - W_r}{W_h - W_i} \right) 100$$

Where W_h is the weight of the hydrated gel after the filtration prior to heating, W_r is the weight of the shrunken gel after heating, and W_i is the mass of the hydrogel after dewatering in KCl. The gels were then cycled through into a fresh feed volume and allowed to rehydrate for 1 hr, determining the membrane selectivity and subsequent water recovery a total of 3 times.

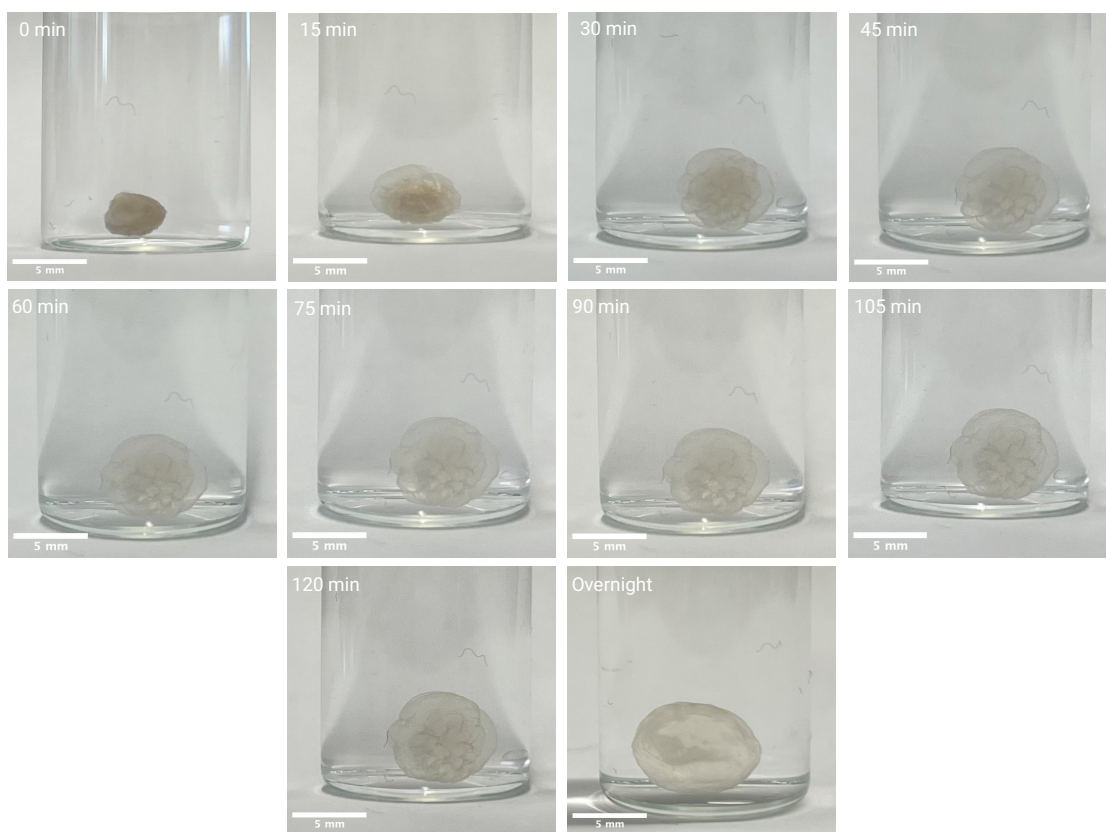


Figure 4.1 Images of a pNIPAm hydrogel with a 1% MPD-0.4% TMC PA coating swelling in water captured every 15 min for 2 h and after ~ 24 hr.

4.2.4 Characterization

Surface morphology of the bare hydrogel and the polyamide coating was characterized by several techniques. To prepare samples for SEM imaging, the PA coated hydrogel was fully hydrated to swelling equilibrium in deionized water before gently

separating the PA from the hydrogel surface using a razor blade in the water volume to minimize surface damage before collecting on the appropriate substrate for imaging. The SEM samples were sputter coated with gold before imaging done under 10 kV accelerating voltage using a Hitachi S-4800 FESEM high resolution (SEM). The collected images are presented in Figure 4.3. It was difficult to collect a sample area large enough using the described method, so flat hydrogel samples were used instead as detailed in section 4.2.2. The flat samples were allowed to air dry overnight before collecting AFM images using a Dimension 3000 AFM to calculate surface roughness. The AFM data is summarized in Figure 4.6. Chemical characterization of the polyamide and the hydrogel was done by Fourier transform infrared spectroscopy (FTIR) shown in Figure 4.2. Hydrated flat samples were imaged using to observe the film thickness of the polyamide coating via STEM (Figure 4.3)

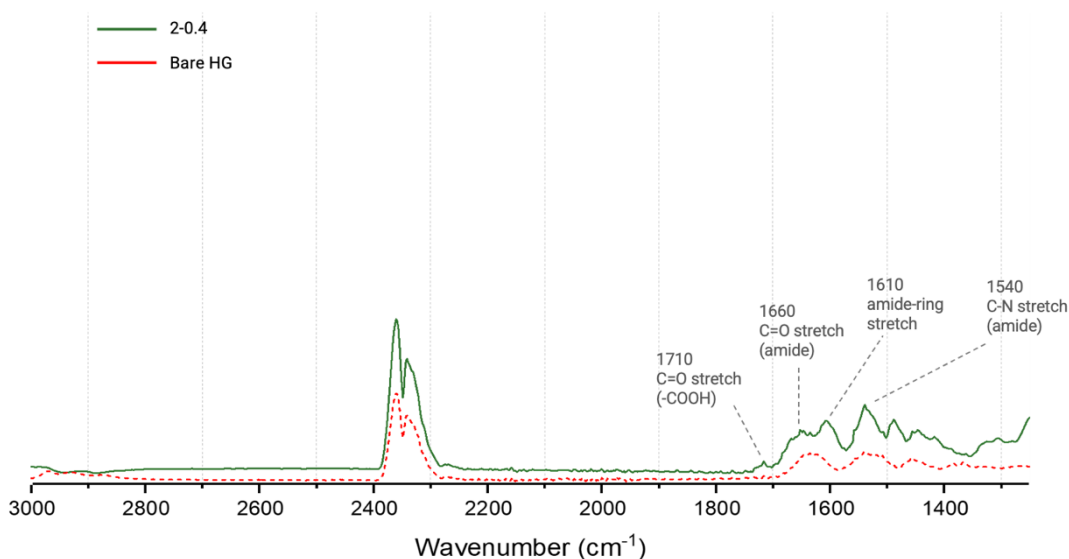


Figure 4.2 FTIR spectra of the bare hydrogel (in red) and the hydrogel coated in 2% MPD-0.4% TMC polyamide composition (in green).

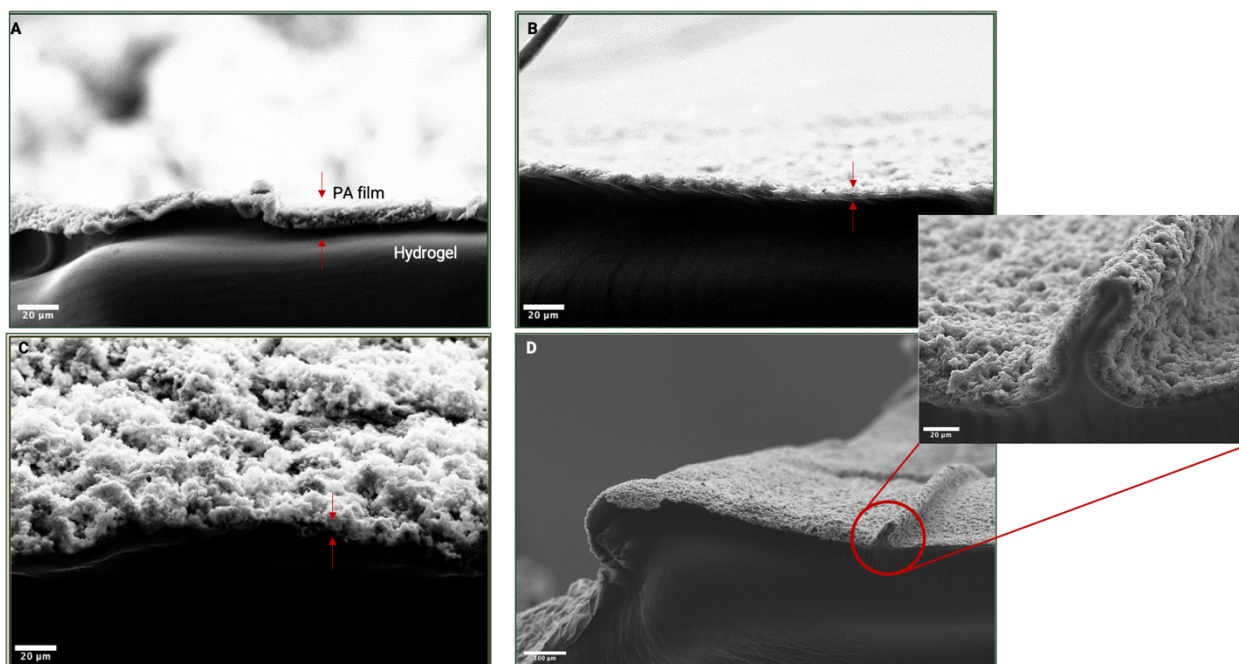


Figure 4.3 FESEM images of the polyamide layer on a dried flat hydrogel for (A) 1% MPD-0.1% TMC, (B) 1% MPD-0.4% TMC, (C) 2% MPD-0.1% TMC, and (D) 2% MPD-0.4% TMC (with high mag. Inset).

4.3 Results & Discussion

There are several approaches to making hydrogels similar in nature to those used in this study.^{7,74,117} Typically, a thermal radical initiator is employed and activated by heating the monomer solution. Details of precipitation polymerization and its benefits for the synthesis of small pNIPAm-based nano- and microgels has been discussed in previous chapters of this thesis. For this work, the goal of fabricating a more dense, macroscale spherical hydrogel required a different polymerization method. A previously reported method used the interface between tetrachloroethylene (TCE) and toluene to suspend individual aqueous monomer spheres that contained APS that was then heated to 70 °C to initiate the polymerization.⁷⁴ In that case, 8 μL droplets were used whereas in this work 100 μL droplets were used and it was observed that heating the organic fractions caused convection agitation that resulted in the monomer droplets merging before the polymerization had begun. Instead, chloroform was substituted for TCE and TEMED was added to the toluene phase to activate the APS, eliminating the need to heat the volume, and resulted in a 20 min polymerization where the size of the hydrogels could be tuned for

different scale filtrations by varying the monomer droplet volume. After drying the as-prepared spheres in ethanol, they were hydrated in an aqueous *m*-phenylenediamine (MPD) solution. The fully hydrated diameter of the spheres was ~ 8 μm . The gels were suspended in a volume of 58% heptane : 42% chloroform with trimesoyl chloride (TMC) for 2 minutes and the colourless opaque PA film was formed by interfacial polymerization. This fraction of heptane to chloroform was determined experimentally to be about the same as the density of the hydrated hydrogels so that the gels would sit submerged in the TMC solution without touching the sides of the glass vial and therefore encouraging the even and unobstructed formation of the polyamide. The PA coated hydrogels were then transferred into 2 M KCl to deswell to ~ 3 μm before filtration experiments. The polymerization and polyamide coating scheme are presented in Figure 4.4.

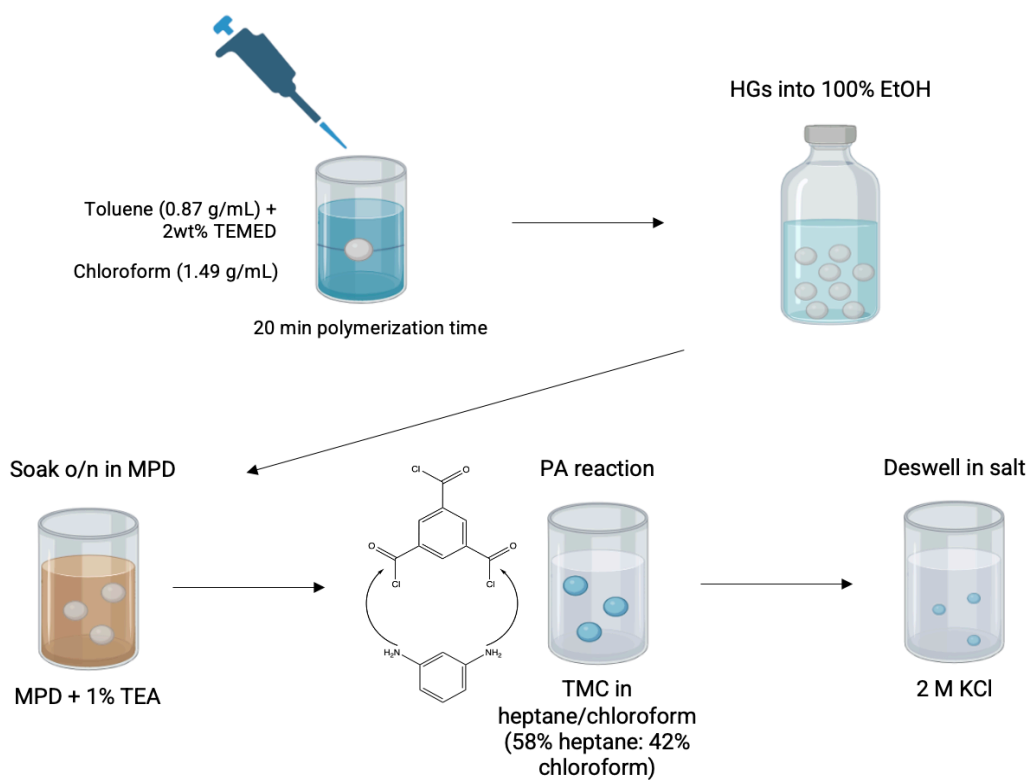


Figure 4.4 Polymerization and polyamide coating scheme. Created with BioRender.

The PA film was characterized from samples gently separated from the hydrogel surface onto the appropriate substrate for analysis. Noting that the PA samples were formed on a curved surface and then placed on a flat surface for imaging, it is expected that some amount of wrinkling and folding would occur but at the scale at which the images were taken it can be assumed that they are representative of the surface in-situ. The surface of the bare hydrogel and the separated PA films were imaged with SEM and AFM. At the lowest concentration, 1% MPD-0.1% TMC, the PA morphology was generally smoother appearance with fewer clusters of polyamide in comparison to 1% MPD-0.4% TMC, seen in Figure 4.5-(b & c). The higher 2% MPD concentration samples had a noticeable increase in surface roughness and wrinkling, with larger more dense clusters of PA that propagate outwards during the film formation, seen in Figure 4.5-(d & e). This effect is often observed in films formed by interfacial polymerization when the respective monomer concentrations are high, the rapid rate of polymerization generates local convection moments and disrupts diffusion of MPD into the nonpolar phase containing TMC, resulting in non-uniform folds and lateral growths.^{6,118} Separating a piece of the polyamide from the hydrogel surface that was large enough for AFM imaging without damage was difficult as the polyamide is strongly adhered to the hydrogel. Therefore, flat hydrogel samples were prepared as outlined in section 4.2.2 for AFM, FTIR, and FESEM. The FTIR results displayed a fair number of similar peaks due to the similar bonding nature of pNIPAm and the polyamide coating. But a few distinct peaks became more intense, particularly those at 1540 cm^{-1} (C-N stretching of the amide bond) and 1660 cm^{-1} (C=O stretching of amide bond). With the appearance of distinct peaks at 1610 cm^{-1} (aromatic amide ring stretch) and 1710 cm^{-1} (C=O stretch of terminal carboxylic acid from hydrolyzed acyl chloride groups on TMC) that are characteristic of the polyamide (Figure 4.2). The calculated surface roughness from the AFM images are shown in Figure 4.6. The bare hydrogel is very smooth, as expected. With increasing concentration of TMC, the surface roughness also increases for the 1% MPD samples. The average roughness increasing from 48.1 nm to 62.1 nm as TMC increases from 0.1% to 0.4%, respectively. As the concentration of MPD increases to 2%, the surface roughness remains largely unchanged at 88.2 nm and 85.6 nm for 0.1% and 0.4% TMC, respectively. This indicated that there is an upper threshold where increasing the TMC concentration at this MPD concentration has minimal effect on the polyamide lateral growth. At a certain point, the initial layer of

polyamide formed when the two solutions meet will impact that later diffusion of the MPD into the TMC/organic phase surrounding the hydrogel. If the concentrations of the two monomers is high, the insipient polyamide layer will be dense enough to prevent the rapid diffusion of the MPD into the TMC/organic phase surrounding the hydrogel. The results presented here would indicate that with 2% MPD, increasing the concentration from 0.1% to 0.4% has little impact of the polyamide thickness and surface roughness.

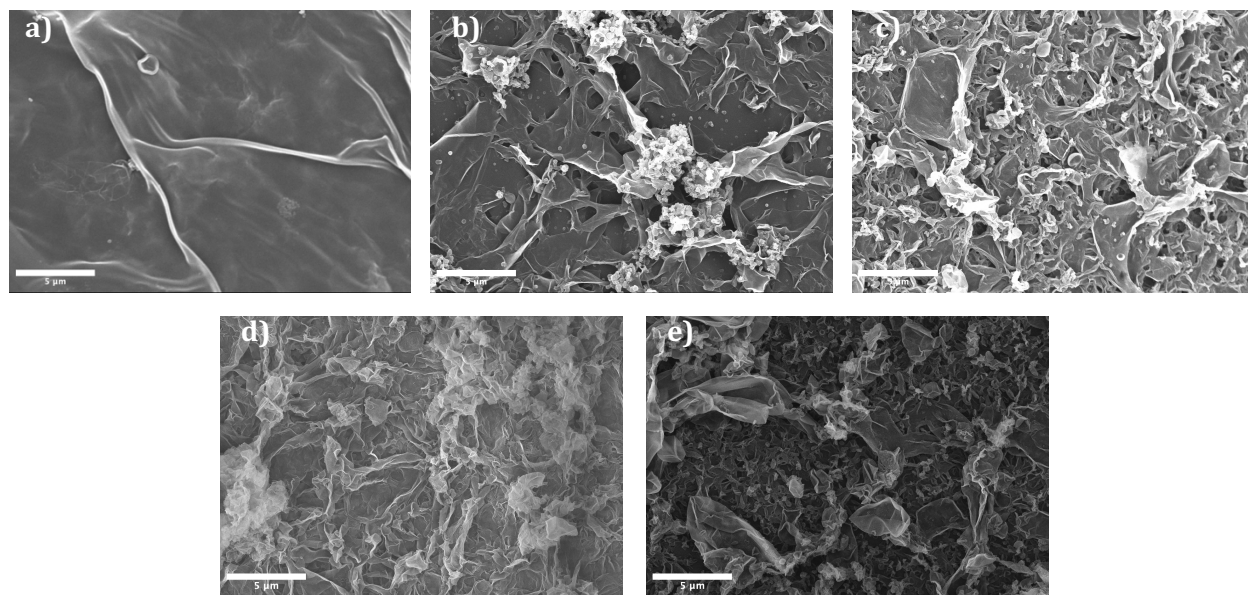


Figure 4.5 SEM images for the (a) bare hydrogel, (b) 1%MPD-0.1% TMC, (c) 1% MPD-0.4% TMC, (d) 2% MPD-0.1% TMC, and (e) 2% MPD-0.4% TMC polyamide layers separated from the spherical hydrogels.

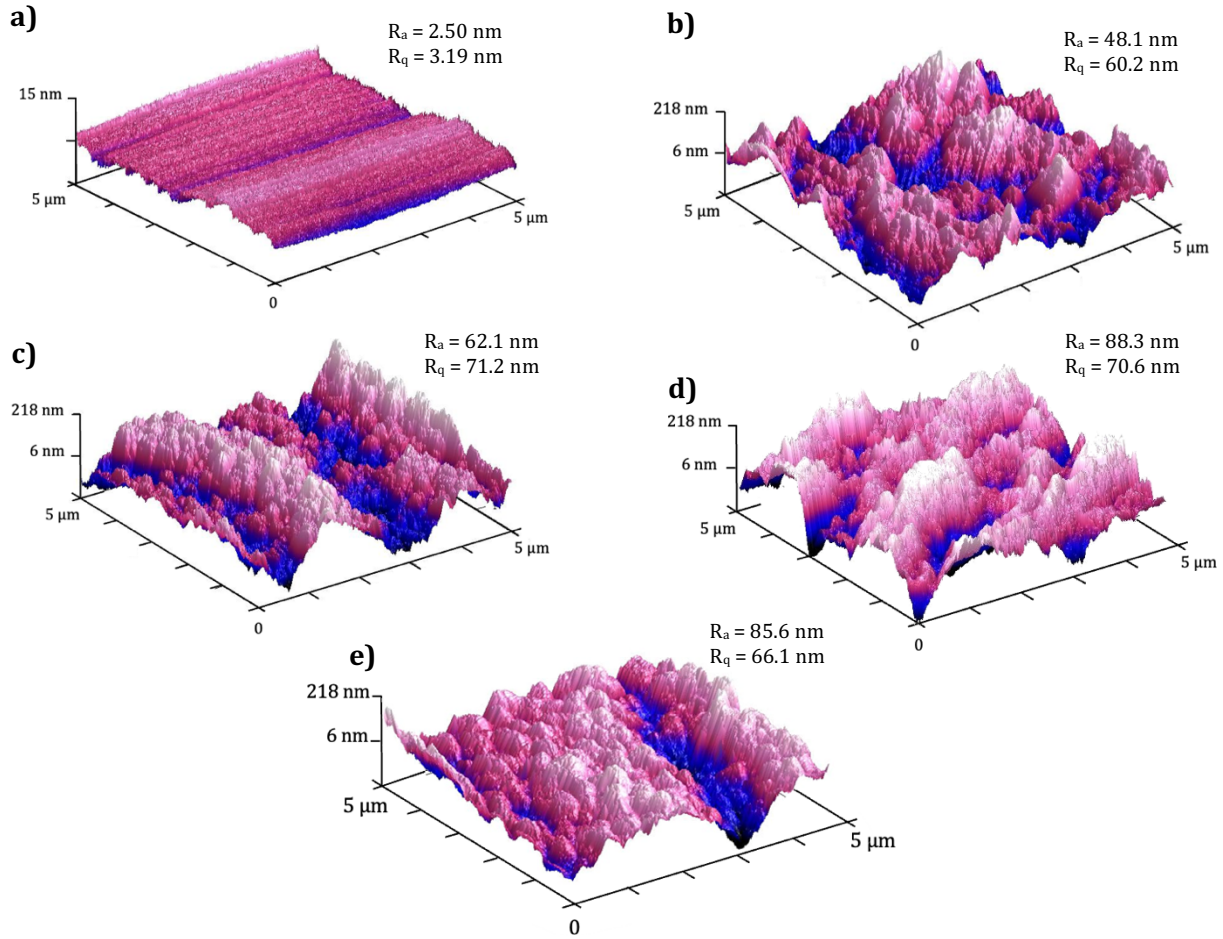


Figure 4.6 AFM images to determine surface roughness of the (a) the bare hydrogel, and the polyamide coatings of (b) 1% MPD-0.1% TMC, (c) 1% MPD-0.4% TMC, (d) 2% MPD-0.1% TMC, and (e) 2%MPD-0.4% TMC.

The hydration of hydrogels in an aqueous environment is driven by the swelling pressure of the polymer. The swelling pressure of hydrogel can be described as the difference in osmotic pressure between the two phases, the hydrogel and surrounding aqueous phase, and can be represented by the following formula;^{71,73,119}

$$(4.5) \quad \pi = \pi_{mix} + \pi_{el} + \pi_{ion}$$

Where the swelling pressure (π) is the summation of the energies of the polymer/solvent mixing, the elasticity of the polymer chains, and the ionic contribution of the mobile and bound ions in the system, represented by π_{mix} , π_{el} , and π_{ion} , respectively. The swelling

kinetics of pNIPAm hydrogels have been widely studied, by model and experiment, in organic solvent systems as well as NaCl.^{119–121} Tanveer and Chen performed thermodynamic analysis of pNIPAm hydrogel swelling in NaCl solutions and concluded that when the mass fraction of salt in the bulk feed increases above 0.03, the dominant ion hydration between water and salt ions is cause for the deswelling of the hydrogel, at which point the osmotic dewatering can occur as it does in the first step of the filtration experiments.¹²¹ Although determining the swelling pressure of the hydrogel was not explored within the scope of this work, the effects of external osmotic pressure applied by increasing the concentration of salt in the feed on the flux can be seen in Figure 4.7 and is consistent with the model trends represented in the literature.¹¹⁹ For both 1% MPD-0.4% TMC (Figure 4.7-a) to 2% MPD-0.4% TMC (Figure 4.7-b) samples, as the salt concentration increases from deionized water to 1000 ppm, the flux and rate of water absorption behaviour for both gel samples are relatively similar. When the feed concentration was increased to 10 000 ppm NaCl, both the flux and % water uptake with time is decreased. The flux and rate of water uptake is dependent on the film thickness as they decreased from ~4.5 LMH and 50% to ~2.4 LMH and 40% as the MPD monomer concentration increased from 1% to 2%, respectively.

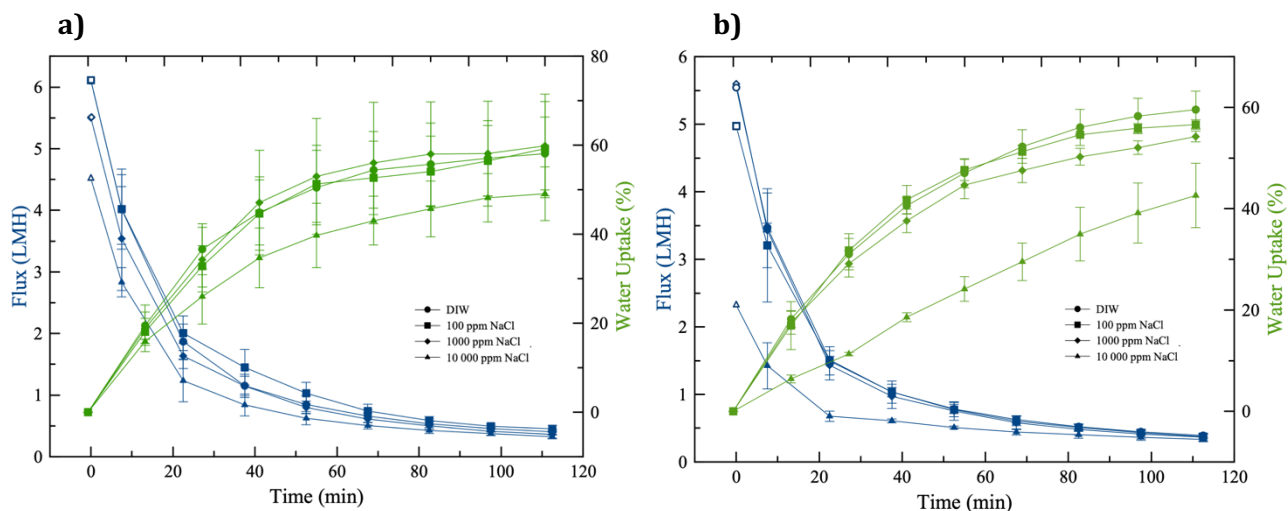


Figure 4.7 Calculated flux of the hydrogels with (a) 1% MPD-0.4% TMC and (b) 2% MPD-0.4% TMC PA coating in various feed concentrations (in blue) and the percent water taken up by the gel within the time scale (in green).

Following the IP reaction and dewatering step in 2 M KCl, the deswollen PA coated hydrogels were used in a preliminary filtration experiment with reactive red (MW 1338.1 g•mol⁻¹) to validate the selectivity of polyamide membrane layer. Herein, the successful rejection of dissolved species in the feed solution is presented as a ratio of the moles of the analyte in the feed before and after the filtration. In the case where the PA film successfully rejects the analyte from passing into the gel, the number of moles in the feed should remain the same after the filtration, resulting in a mole ratio = 1. If the PA film fails, due to cracks or delamination from the gel, the analyte will enter the gel and the ratio will be < 1. UV-Vis measurements of the concentrated dye feed after allowing the gels to hydrate for 2 hrs was done to calculate the rejection of RR based on the change in mass, and therefore mass of water absorbed by the gels in that time. The hydrogel without the PA coating and the lower concentration TMC PA films (0.1% & 0.2%) allowed the dye molecules to enter the gel as it hydrated, shown in the bar graph in Figure 4.8 (in red). The negative rejection is indicative of significant dye absorption into the gel, resulting in a decreased dye concentration in the feed after the experiment. Whereas a positive rejection is a result of the dye concentration increasing in the feed after filtration. The polyamide compositions with 0.4% TMC both selectively rejected the dye (Figure 4.8, in blue). This proof-of-concept indicated that the thinner, and perhaps more brittle, PA shells were not appropriate for filtration experiments.

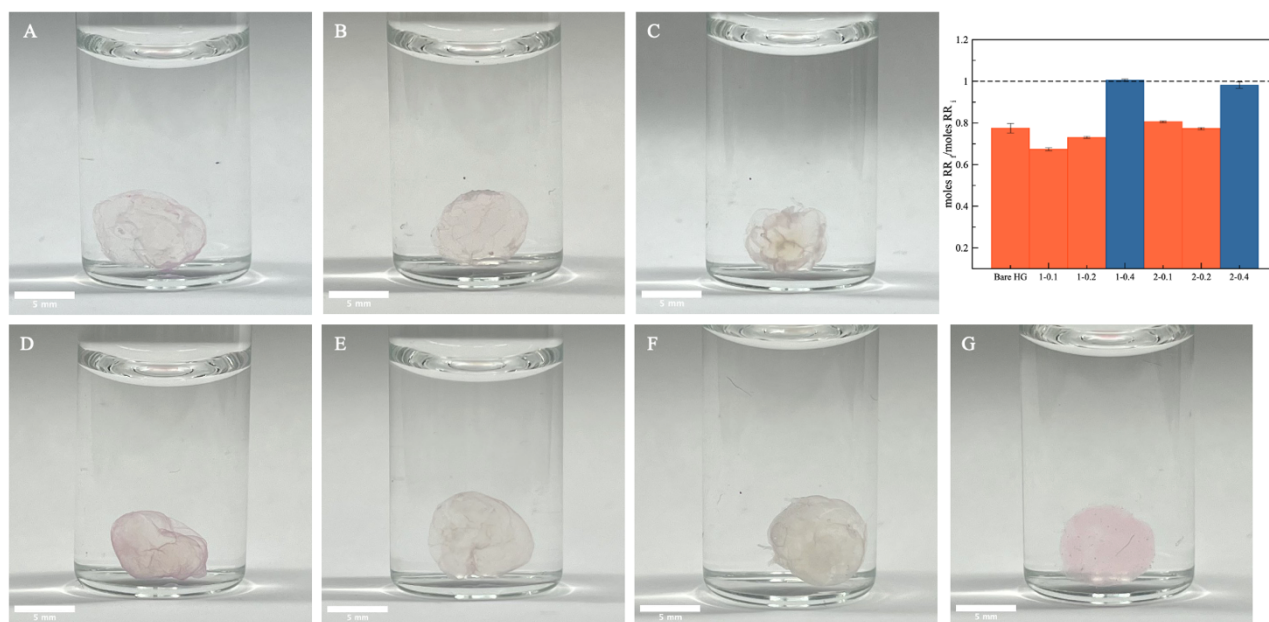


Figure 4.8 Images of PA coated hydrogels in (A) 1% MPD-0.1% TMC, (B) 1% MPD-0.2% TMC, (C) 1% MPD-0.4% TMC, (D) 2% MPD-0.1% TMC, (E) 2% MPD-0.2% TMC, (F) 2% MPD-0.4% TMC, and (G) a bare hydrogel after 2 h in 10 ppm reactive red solution. Bar graph is rejection plot of reactive red for each gel.

The selective permeability of the PA coating was further demonstrated in filtration experiments of different aqueous salts. The volume of water absorbed by the gel was determined by measuring the weight of gel before and after the filtration experiment after gently removing any remaining water on the surface with a lab wipe. The first filtration is done using the dehydrated gels hydrate in 100 ppm NaCl for 2 hr. After the first filtration, the gels are weighed and transferred to DI water and heated in a 50 °C water bath for 1 hour to allow the hydrogel core to collapse and expel clean water. The mass of the same collapsed gel was weighed before cycling again into new 100 ppm NaCl solution, allowing the gel to rehydrate for 1 hour at room temperature. After this filtration cycle, the PA film composed of 0.1% and 0.2% TMC failed as the gel took up salt ions and the resulting mole ratio was <1, likely due to cracks occurring during the rapid collapse of the hydrogel core, seen in Figure 4.9-a. This is consistent with the results of the experiments with reactive red. The denser 0.4% TMC PA films were able to withstand the heat induced deswelling to recover the clean water without experiencing any decline in rejection.

The average volume of clean water recovered from 3 samples of the 1% MPD – 0.4% TMC samples was about $38 \pm 5\%$ of the total clean water in gel (Figure 4.9-c, in green) after

one cycle compared to the $15 \pm 4\%$ of the total water volume in the gel recovered from the 2% MPD-0.4% TMC gel (Figure 4.9-d, in green). While both membranes performed, the thicker PA film hindered the recovery of clean water when heated. Therefore, it was determined that 1% MPD-0.4% TMC was the optimal PA composition. The cycling of this gel was repeated 3 times and the selectivity and rejection performance of the gel remained consistent the mole ratio of salt in the feed remained close to 1 (Figure 4.9-(c & d)). In some cases that the mole ratio of salt is > 1 , particularly in the first cycle and in the experiments with the different salt species. As there is no route to introduce more salt ions in the system, this can be attributed to small deviations between the measured mass of water taken up by the gel and the actual mass. As the hydrogel hydrates from the dewatered state, as it does in the first cycle, the density of the polymer is changing slightly which is difficult to correct for.

A control experiment was done with a bare hydrogel core and the decrease in the concentration of salt after the filtration results in an average mole ratio of 0.87 ± 0.03 after each heat cycle shown in both Figure 4.9-(c & d) (red bar graph). Not only is the salt entering freely without the membrane film, but the small negative charge carried in the gel imparted by the any residual APS initiator could be attracting Na^+ ions. It is important to note that the time allowed to swell in the feed from its deswollen state from 2 M KCl was 2 hours before taking the hydrated weight and then continuing to the next heat cycling experiment with the same gel. As discussed above, the total water uptake for the optimized hydrogel, the total water uptake percent is approximately 60% after 2 hours (Figure 4.9-a). As the gel has not reached equilibrium swelling, the recovery of the gel may be inflated somewhat in the first cycle as it is in the following cycles. By the 3rd heat cycle, the % water recovery has decreased from 38% to 15% for the optimized polyamide sample. Therefore, with each cycling experiment, the gel is allowed to sit in the feed solution for an additional 1 hour, and it is approaching equilibrium swelling. Because of this, the percent recovery in relation to the total volume of water taken up by the gel after three cycles is expected to decline. Even so, comparing 1%-0.4% to 2%-0.4%, the percent water recovery is still greater after 3 heating cycles for the optimized membrane.

The selectivity of this gel was evaluated against 100 ppm feed solutions of LiCl, CaCl₂, and MgSO₄. The optimized 1%-0.4% PA membrane was selective to both the larger divalent Ca²⁺ Mg²⁺ ions as well as the smaller Li⁺ ions. These results are promising as the optimized gel is selectively permeable against a wide range of tested solutes of varying size and charge. The recovery of the clean water is simple and efficient and if the gel further optimized to be less dense/crosslinked, the % recovery of clean water would stand to increase per cycle. These hydrogels have potential for applications in aqueous environmental sample pre-concentration prior to analysis. It may also be possible to scale up the hydrogels to achieve larger volumes of water recovery for water treatment or remediation purposes.

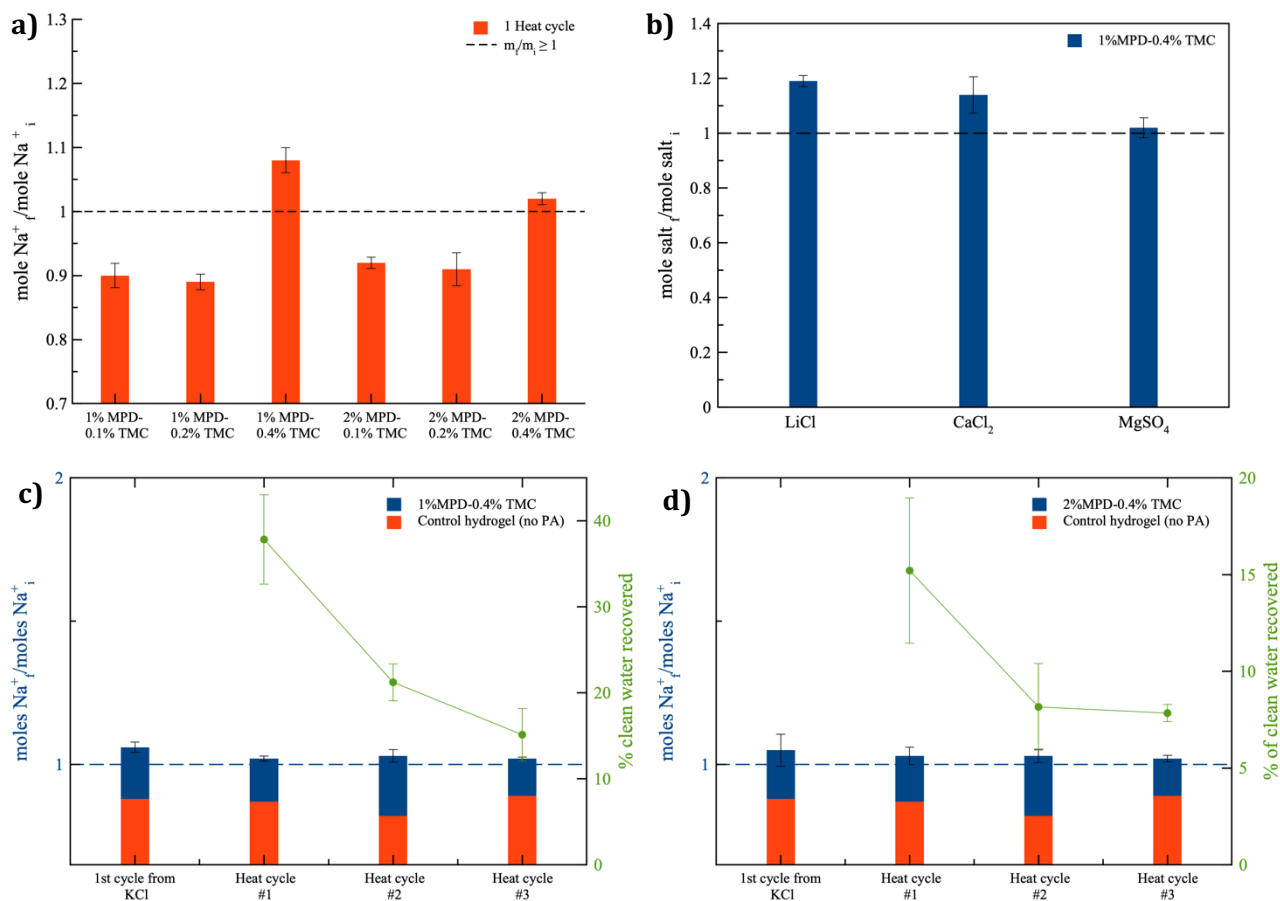


Figure 4.9 (a) The performance of different PA compositions after one filtration and recovery cycle. (b) The selectivity of 1% MPD-0.4% TMC against different salts. The mole ratio of salt of the PA coated hydrogel (in blue) and a bare hydrogel control (in red) bar graph, where a ratio ≥ 1 is indicative of a selective PA. Both 1% MPD-0.4% TMC (c) and 2% MPD-0.4% TMC (d) were able to withstand 3 filtration and heat recovery cycles. The % water recovered in presented in green on for each respective heat cycle.

4.4 Conclusion

The work presented in this chapter details the use of thermo-responsive pNIPAm hydrogels with a polyamide skin coating to yield a reusable material that is selective to both reactive red dye and a variety of smaller salt species where up to 40% of the clean absorbed water can be recovered by heating the gel above the LCST. A novel polymerization method for fabricating large spherical hydrogels was optimized by utilizing an activator to initiate polymerization in a layered solvent system using the density of chloroform and toluene to suspend the aqueous monomer solution at the interface. The addition of the polyamide to hydrogel materials has been previously reported but none have achieved both good rejection of small salt ions (ie Na^+ or Li^+) as well as reusability. While the rate of hydration of a neutral polymer like pNIPAm is slower when compared to a polyelectrolyte like pAAc, the added thermo-responsive recovery potential is simpler than a mechanical recovery system. Increasing the concentration of the polyamide monomers resulted in a thicker, more flexible polyamide that can withstand 3 repeated cycles of swelling and deswelling without the appearance of cracks or delamination from the hydrogel.

Chapter 5 Conclusions and Future Work

The focus of the thesis is centered around the thermo-responsive polymer pNIPAm and how core-shell morphologies of this polymer can be modified and functionalized for water treatment applications. In Chapter 2, a systematic study of functionalized core-pNIPAm shell microgels with increasing shell thicknesses were investigated for the uptake and pH triggered release of target dye molecules when free in solution and immobilized on a gold surface at room temperature and at 40 °C. The copolymerization of pNIPAm with some functional monomer will incorporate an acidic (AAc) or a basic (APMA) moiety. These added functionalities will impart a negative or positive charge within the polymer matrix that is dependent on the pK_a of that group. This charge will electrostatically attract and retain dye molecules of opposing charge within the polymer until the pH is changed as to neutralize the charge, at which point the dye molecules will be released from the polymer into the surrounding environment. The addition of thin pNIPAm shell (AAc-5 and AAc-10) had a larger release of CV when immobilized and free in solution compared the AAc-core and AAc-20 samples. This indicates that there may be some threshold where the thinner shell will help in dye uptake and retention where a thick shell will hinder the uptake, the release, or both. The APMA samples behaved in a more linear fashion where the APMA-core generally had a larger dye release profile which decreased with increasing shell thickness for all samples below and above the LCST. There are several factors that could contribute to the different behaviour between the two sample sets including the size of the microgels, the incorporation efficiency of the copolymer, and the carrying shell thickness.

Chapter 3 focused on using similar pNIPAm-based core-shell nanogels to couple them to a TFC membrane to observe their effects on rejection during high-temperature filtration and for antifouling purposes. The pNIPAm core and APMA shell resulted in a thermo-responsive particle that could covalently crosslink to the selective polyamide layer through residual acyl chloride groups remaining after the IP reaction. Incorporating the nanogels during the IP reaction allowed for the nanogels to be dispersed throughout the polyamide layer so that during high temperature filtration. Where the flux would typically increase and salt rejection would decrease in response to the lowered viscosity of water and relaxation of

the polyamide chains, the nanogels instead were able to pull the bound polyamide around in tighter when the cores collapsed as the temperature rose above the LCST. So, as the concentration of the nanogels incorporated increased, the flux improvement with temperature declined and salt rejection increased.

The localization of the nanogels on the surface of the polyamide following the IP was investigated for antifouling purposes. Typically, a TFC membrane is modified to be either highly charged or to have increased hydrophilicity/hydrophobicity to improve antifouling. In this system, sodium alginate (SA) crosslinked with Ca^{2+} ions was used as a model foulant, which is hydrophilic and net positively charged. Extensive surface characterization was performed to confirm the successful coating of the nanogels and found that the modified membranes were both more hydrophobic, from the contact angle, and more positively charged, from the zeta potential measurements. As detailed in the chapter discussion, the nanogels themselves are hydrophilic polymer materials and therefore should not have increased the contact angle so significantly and it is assumed that there is some inflation due to the added roughness and texture of the nanogel aggregates on the surface. With this information, it would stand to reason that the fouling of the modified membrane would be worse given the increased electrostatic and hydrophilic-hydrophilic interactions. However, the opposite was observed where the modified membranes experience far less fouling and improved flux recovery when washed at high temperature. This is attributed to the actuation and additional hydrophilic to hydrophobic transition of the pNIPAM cores during high temperature washing. Due to time restraints this combined project was not developed further, but these interesting results can be investigated further and perhaps the two modification methods can be combined and the separation of smaller species such as Li^+ could be explored, which is a major interest for battery research and manufacturing.¹¹⁰

In Chapter 4, the fabrication of a polyamide coated thermo-responsive hydrogel was developed and optimized for a self-driven filtration material that is selective against reactive red dye and a variety of salt ions. The mixed organic suspension phase polymerization method was tailored to fabricate the large pNIPAM hydrogel spheres which were then impregnated with the aqueous monomer used in the interfacial polymerization reaction with

TMC. The swelling pressure of the polymer hydrating from a dry state drives the filtration. The PA coatings made with 0.4% TMC were able to reject salt ions from the feed and were robust enough to withstand 3 heating and filtration cycles without losing any selectivity. The optimized polyamide composition was determined to be 1% MPD-0.4% TMC as it showed a higher % water recovery upon heating as well as a higher % water uptake and flux in high salt concentrations. The practical applications of these materials in environmental sample concentration or larger scale filtrations experiments were not performed and therefore it is not known if this polyamide could experience fouling. In which case, there has not been a study published to date, to the best of my knowledge, of any modifications made to the polyamide coatings of hydrogels. Additionally, the hydrogels could be optimized further to improve the swelling rate by coupling pNIPAm with a polyionic material like tri-n-alkyl(vinylbenzyl)phosphonium chloride that will still deswell when heated above the LCST.⁷⁵

References

- (1) Zhong, W.; Zhang, X.; Duan, X.; Liu, H.; Fang, Y.; Luo, M.; Fang, Z.; Miao, C.; Lin, D.; Wu, J. Redox-Responsive Self-Assembled Polymeric Nanoprodrug for Delivery of Gemcitabine in B-Cell Lymphoma Therapy. *Acta Biomater.* **2022**, *144*, 67–80. <https://doi.org/10.1016/j.actbio.2022.03.035>.
- (2) Oroojalian, F.; Babaei, M.; Taghdisi, S. M.; Abnous, K.; Ramezani, M.; Alibolandi, M. Encapsulation of Thermo-Responsive Gel in pH-Sensitive Polymersomes as Dual-Responsive Smart Carriers for Controlled Release of Doxorubicin. *J. Controlled Release* **2018**, *288*, 45–61. <https://doi.org/10.1016/j.jconrel.2018.08.039>.
- (3) Zhang, Q.; Zhang, Y.; Wan, Y.; Carvalho, W.; Hu, L.; Serpe, M. J. Stimuli-Responsive Polymers for Sensing and Reacting to Environmental Conditions. *Prog. Polym. Sci.* **2021**, *116*, 101386. <https://doi.org/10.1016/j.progpolymsci.2021.101386>.
- (4) Kobayashi, K.; Oh, S. H.; Yoon, C.; Gracias, D. H. Multitemperature Responsive Self-Folding Soft Biomimetic Structures. *Macromol. Rapid Commun.* **2018**, *39*(4), 1700692. <https://doi.org/10.1002/marc.201700692>.
- (5) Li, S.; Liu, X.; Huang, W.; Li, W.; Xia, X.; Yan, S.; Yu, J. Magnetically Assisted Removal and Separation of Cationic Dyes from Aqueous Solution by Magnetic Nanocomposite Hydrogels. *Polym. Adv. Technol.* **2011**, *22*(12), 2439–2447. <https://doi.org/10.1002/pat.1782>.
- (6) Xu, X.; Bizmark, N.; Christie, K. S. S.; Datta, S. S.; Ren, Z. J.; Priestley, R. D. Thermoresponsive Polymers for Water Treatment and Collection. *Macromolecules* **2022**, *55*(6), 1894–1909. <https://doi.org/10.1021/acs.macromol.1c01502>.
- (7) Ali, W.; Gebert, B.; Hennecke, T.; Graf, K.; Ulbricht, M.; Gutmann, J. S. Design of Thermally Responsive Polymeric Hydrogels for Brackish Water Desalination: Effect of Architecture on Swelling, Deswelling, and Salt Rejection. *ACS Appl. Mater. Interfaces* **2015**, *7*(29), 15696–15706. <https://doi.org/10.1021/acsami.5b03878>.

- (8) Flory, P. J.; Rehner, J. Statistical Mechanics of Cross-Linked Polymer Networks I. Rubberlike Elasticity. *J. Chem. Phys.* **1943**, *11* (11), 512–520.
<https://doi.org/10.1063/1.1723791>.
- (9) Yuan, Z.; Ding, J.; Zhang, Y.; Huang, B.; Song, Z.; Meng, X.; Ma, X.; Gong, X.; Huang, Z.; Ma, S.; Xiang, S.; Xu, W. Components, Mechanisms and Applications of Stimuli-Responsive Polymer Gels. *Eur. Polym. J.* **2022**, *177*, 111473.
<https://doi.org/10.1016/j.eurpolymj.2022.111473>.
- (10) Audureau, N.; Coumes, F.; Rieger, J.; Stoffelbach, F. Poly(*N*-Cyanoethylacrylamide), a New Thermoresponsive Homopolymer Presenting Both LCST and UCST Behavior in Water. *Polym. Chem.* **2022**, *13* (8), 1075–1083. <https://doi.org/10.1039/D2PY00032F>.
- (11) Schild, H. G. Poly(*N*-Isopropylacrylamide): Experiment, Theory and Application. *Prog. Polym. Sci.* **1992**, *17* (2), 163–249. [https://doi.org/10.1016/0079-6700\(92\)90023-R](https://doi.org/10.1016/0079-6700(92)90023-R).
- (12) Liu, H. Y.; Zhu, X. X. Lower Critical Solution Temperatures of *N*-Substituted Acrylamide Copolymers in Aqueous Solutions. *Polymer* **1999**, *40* (25), 6985–6990.
[https://doi.org/10.1016/S0032-3861\(98\)00858-1](https://doi.org/10.1016/S0032-3861(98)00858-1).
- (13) Cho, E. C.; Lee, J.; Cho, K. Role of Bound Water and Hydrophobic Interaction in Phase Transition of Poly(*N*-Isopropylacrylamide) Aqueous Solution. *Macromolecules* **2003**, *36* (26), 9929–9934. <https://doi.org/10.1021/ma034851d>.
- (14) Ye, Y.; Shangguan, Y.; Song, Y.; Zheng, Q. Influence of Charge Density on Rheological Properties and Dehydration Dynamics of Weakly Charged Poly(*N*-Isopropylacrylamide) during Phase Transition. *Polymer* **2014**, *55* (10), 2445–2454.
<https://doi.org/10.1016/j.polymer.2014.03.057>.
- (15) Santhamoorthy, M.; Vy Phan, T. T.; Ramkumar, V.; Raorane, C. J.; Thirupathi, K.; Kim, S.-C. Thermo-Sensitive Poly (*N*-Isopropylacrylamide-Co-Polyacrylamide) Hydrogel for pH-Responsive Therapeutic Delivery. *Polymers* **2022**, *14* (19), 4128.
<https://doi.org/10.3390/polym14194128>.

- (16) Kim, H.; Kim, K.; Lee, S. J. Nature-Inspired Thermo-Responsive Multifunctional Membrane Adaptively Hybridized with PNIPAm and PPy. *NPG Asia Mater.* **2017**, *9* (10), e445–e445. <https://doi.org/10.1038/am.2017.168>.
- (17) Ahiabu, A.; Serpe, M. J. Rapidly Responding pH- and Temperature-Responsive Poly (*N* -Isopropylacrylamide)-Based Microgels and Assemblies. *ACS Omega* **2017**, *2* (5), 1769–1777. <https://doi.org/10.1021/acsomega.7b00103>.
- (18) Cui, G.; Wang, H.; Long, S.; Zhang, T.; Guo, X.; Chen, S.; Kakuchi, T.; Duan, Q.; Zhao, D. Thermo- and Light-Responsive Polymer-Coated Magnetic Nanoparticles as Potential Drug Carriers. *Front. Bioeng. Biotechnol.* **2022**, *10*, 931830. <https://doi.org/10.3389/fbioe.2022.931830>.
- (19) Yin, J.; Guan, X.; Wang, D.; Liu, S. Metal-Chelating and Dansyl-Labeled Poly(*N* -Isopropylacrylamide) Microgels as Fluorescent Cu²⁺ Sensors with Thermo-Enhanced Detection Sensitivity. *Langmuir* **2009**, *25* (19), 11367–11374. <https://doi.org/10.1021/la901377h>.
- (20) Tsai, H.-Y.; Lee, A.; Peng, W.; Yates, M. Z. Synthesis of Poly(*N*-Isopropylacrylamide) Particles for Metal Affinity Binding of Peptides. *Colloids Surf. B Biointerfaces* **2014**, *114*, 104–110. <https://doi.org/10.1016/j.colsurfb.2013.09.060>.
- (21) Peng, L.; Wu, C. S.; You, M.; Han, D.; Chen, Y.; Fu, T.; Ye, M.; Tan, W. Engineering and Applications of DNA-Grafted Polymer Materials. *Chem. Sci.* **2013**, *4* (5), 1928. <https://doi.org/10.1039/c2sc21198j>.
- (22) Costa, M. C. M.; Silva, S. M. C.; Antunes, F. E. Adjusting the Low Critical Solution Temperature of Poly(*N*-Isopropyl Acrylamide) Solutions by Salts, Ionic Surfactants and Solvents: A Rheological Study. *J. Mol. Liq.* **2015**, *210*, 113–118. <https://doi.org/10.1016/j.molliq.2015.02.008>.
- (23) Hiruta, Y.; Nagumo, Y.; Suzuki, Y.; Funatsu, T.; Ishikawa, Y.; Kanazawa, H. The Effects of Anionic Electrolytes and Human Serum Albumin on the LCST of Poly(*N* -

- Isopropylacrylamide)-Based Temperature-Responsive Copolymers. *Colloids Surf. B Biointerfaces* **2015**, *132*, 299–304. <https://doi.org/10.1016/j.colsurfb.2015.05.032>.
- (24) Ferrand-Drake Del Castillo, G.; Hailes, R. L. N.; Dahlin, A. Large Changes in Protonation of Weak Polyelectrolyte Brushes with Salt Concentration—Implications for Protein Immobilization. *J. Phys. Chem. Lett.* **2020**, *11* (13), 5212–5218. <https://doi.org/10.1021/acs.jpcllett.0c01289>.
- (25) Carvalho, W. S. P.; Wei, M.; Ikpo, N.; Gao, Y.; Serpe, M. J. Polymer-Based Technologies for Sensing Applications. *Anal. Chem.* **2018**, *90* (1), 459–479. <https://doi.org/10.1021/acs.analchem.7b04751>.
- (26) Islam, M.; Ahiabu, A.; Li, X.; Serpe, M. Poly (N-Isopropylacrylamide) Microgel-Based Optical Devices for Sensing and Biosensing. *Sensors* **2014**, *14* (5), 8984–8995. <https://doi.org/10.3390/s140508984>.
- (27) Kennedy, C. Ionic Strength and the Dissociation of Acids. *Biochem. Educ.* **1990**, *18* (1), 35–40. [https://doi.org/10.1016/0307-4412\(90\)90017-I](https://doi.org/10.1016/0307-4412(90)90017-I).
- (28) Carvalho, W. S. P.; Lee, C.; Zhang, Y.; Czarnecki, A.; Serpe, M. J. Probing the Response of Poly (N-Isopropylacrylamide) Microgels to Solutions of Various Salts Using Etalons. *J. Colloid Interface Sci.* **2021**, *585*, 195–204. <https://doi.org/10.1016/j.jcis.2020.11.045>.
- (29) Galogahi, F. M.; Zhu, Y.; An, H.; Nguyen, N.-T. Core-Shell Microparticles: Generation Approaches and Applications. *J. Sci. Adv. Mater. Devices* **2020**, *5* (4), 417–435. <https://doi.org/10.1016/j.jsamd.2020.09.001>.
- (30) Misra, S.; Pandey, P.; Dalbhat, C. G.; Mishra, H. N. Emerging Technologies and Coating Materials for Improved Probiotication in Food Products: A Review. *Food Bioprocess Technol.* **2022**, *15* (5), 998–1039. <https://doi.org/10.1007/s11947-021-02753-5>.
- (31) Baxani, D. K.; Morgan, A. J. L.; Jamieson, W. D.; Allender, C. J.; Barrow, D. A.; Castell, O. K. Bilayer Networks within a Hydrogel Shell: A Robust Chassis for Artificial Cells

- and a Platform for Membrane Studies. *Angew. Chem. Int. Ed.* **2016**, *55* (46), 14240–14245. <https://doi.org/10.1002/anie.201607571>.
- (32) Zhao, S.; Agarwal, P.; Rao, W.; Huang, H.; Zhang, R.; Liu, Z.; Yu, J.; Weisleder, N.; Zhang, W.; He, X. Coaxial Electrospray of Liquid Core–Hydrogel Shell Microcapsules for Encapsulation and Miniaturized 3D Culture of Pluripotent Stem Cells. *Integr. Biol.* **2014**, *6* (9), 874–884. <https://doi.org/10.1039/c4ib00100a>.
- (33) Suzuki, D.; Kawaguchi, H. Gold Nanoparticle Localization at the Core Surface by Using Thermosensitive Core–Shell Particles as a Template. *Langmuir* **2005**, *21* (25), 12016–12024. <https://doi.org/10.1021/la0516882>.
- (34) Jia, H.; Roa, R.; Angioletti-Uberti, S.; Henzler, K.; Ott, A.; Lin, X.; Möser, J.; Kochovski, Z.; Schnegg, A.; Dzubiella, J.; Ballauff, M.; Lu, Y. Thermosensitive Cu₂O–PNIPAM Core–Shell Nanoreactors with Tunable Photocatalytic Activity. *J. Mater. Chem. A* **2016**, *4* (24), 9677–9684. <https://doi.org/10.1039/C6TA03528K>.
- (35) Liu, Y.-M.; Ju, X.-J.; Xin, Y.; Zheng, W.-C.; Wang, W.; Wei, J.; Xie, R.; Liu, Z.; Chu, L.-Y. A Novel Smart Microsphere with Magnetic Core and Ion-Recognizable Shell for Pb²⁺ Adsorption and Separation. *ACS Appl. Mater. Interfaces* **2014**, *6* (12), 9530–9542. <https://doi.org/10.1021/am501919j>.
- (36) Karg, M.; Wellert, S.; Prevost, S.; Schweins, R.; Dewhurst, C.; Liz-Marzán, L. M.; Hellweg, T. Well Defined Hybrid PNIPAM Core-Shell Microgels: Size Variation of the Silica Nanoparticle Core. *Colloid Polym. Sci.* **2011**, *289* (5–6), 699–709. <https://doi.org/10.1007/s00396-010-2327-2>.
- (37) Zhang, L.; Daniels, E. S.; Dimonie, V. L.; Klein, A. Mechanism for the Formation of PNIPAM/PS Core/Shell Particles. *J. Appl. Polym. Sci.* **2014**, *131* (8), n/a–n/a. <https://doi.org/10.1002/app.40124>.
- (38) Ding, J.; Liu, G. Polystyrene- *b* Lock -Poly(2-Cinnamoyl ethyl Methacrylate) Nanospheres with Cross-Linked Shells. *Macromolecules* **1998**, *31* (19), 6554–6558. <https://doi.org/10.1021/ma980710d>.

- (39) Matsumoto, K.; Hasegawa, H.; Matsuoka, H. Synthesis of Sodium-Polystyrenesulfonate-Grafted Nanoparticles by Core-Cross-Linking of Block Copolymer Micelles. *Tetrahedron* **2004**, *60* (34), 7197–7204. <https://doi.org/10.1016/j.tet.2004.05.057>.
- (40) Jones, C. D.; Lyon, L. A. Synthesis and Characterization of Multiresponsive Core-Shell Microgels. *Macromolecules* **2000**, *33* (22), 8301–8306. <https://doi.org/10.1021/ma001398m>.
- (41) Blackburn, W. H.; Lyon, L. A. Size-Controlled Synthesis of Monodisperse Core/Shell Nanogels. *Colloid Polym. Sci.* **2008**, *286* (5), 563–569. <https://doi.org/10.1007/s00396-007-1805-7>.
- (42) Yang, X.-L.; Ju, X.-J.; Mu, X.-T.; Wang, W.; Xie, R.; Liu, Z.; Chu, L.-Y. Core-Shell Chitosan Microcapsules for Programmed Sequential Drug Release. *ACS Appl. Mater. Interfaces* **2016**, *8* (16), 10524–10534. <https://doi.org/10.1021/acsami.6b01277>.
- (43) Galogahi, F. M.; Zhu, Y.; An, H.; Nguyen, N.-T. Formation of Core-Shell Droplets for the Encapsulation of Liquid Contents. *Microfluid. Nanofluidics* **2021**, *25* (10), 82. <https://doi.org/10.1007/s10404-021-02483-2>.
- (44) Ke, H.; Wang, J.; Dai, Z.; Jin, Y.; Qu, E.; Xing, Z.; Guo, C.; Yue, X.; Liu, J. Gold-Nanoshelled Microcapsules: A Theranostic Agent for Ultrasound Contrast Imaging and Photothermal Therapy. *Angew. Chem. Int. Ed.* **2011**, *50* (13), 3017–3021. <https://doi.org/10.1002/anie.201008286>.
- (45) Serra, C. A.; Chang, Z. Microfluidic-Assisted Synthesis of Polymer Particles. *Chem. Eng. Technol.* **2008**, *31* (8), 1099–1115. <https://doi.org/10.1002/ceat.200800219>.
- (46) Zhou, X.; Sun, Y.; Finne-Wistrand, A.; Van Der Wijngaart, W.; Haraldsson, T. Core-Shell Microparticle Synthesis in Droplet Microfluidics Using a Single Step Polymerization. In *2015 28th IEEE International Conference on Micro Electro Mechanical Systems (MEMS)*; IEEE: Estoril, Portugal, 2015; pp 472–475. <https://doi.org/10.1109/MEMSYS.2015.7050994>.

- (47) Mao, X.; Wang, M.; Jin, S.; Rao, J.; Deng, R.; Zhu, J. Monodispersed Polymer Particles with Tunable Surface Structures: Droplet MICROFLUIDIC-ASSISTED Fabrication and Biomedical Applications. *J. Polym. Sci.* **2022**, *60* (11), 1653–1669. <https://doi.org/10.1002/pol.20210909>.
- (48) Kim, J. H.; Jeon, T. Y.; Choi, T. M.; Shim, T. S.; Kim, S.-H.; Yang, S.-M. Droplet Microfluidics for Producing Functional Microparticles. *Langmuir* **2014**, *30* (6), 1473–1488. <https://doi.org/10.1021/la403220p>.
- (49) Li, W.-H.; Stöver, H. D. H. Monodisperse Cross-Linked Core-Shell Polymer Microspheres by Precipitation Polymerization. *Macromolecules* **2000**, *33* (12), 4354–4360. <https://doi.org/10.1021/ma9920691>.
- (50) Ottewill, R. H.; Schofield, A. B.; Waters, J. A.; Williams, N. St. J. Preparation of Core-Shell Polymer Colloid Particles by Encapsulation. *Colloid Polym. Sci.* **1997**, *275* (3), 274–283. <https://doi.org/10.1007/s003960050081>.
- (51) Palanivelu, S. D.; Armir, N. A. Z.; Zulkifli, A.; Hair, A. H. A.; Salleh, K. M.; Lindsey, K.; Che-Othman, M. H.; Zakaria, S. Hydrogel Application in Urban Farming: Potentials and Limitations—A Review. *Polymers* **2022**, *14* (13), 2590. <https://doi.org/10.3390/polym14132590>.
- (52) *Reviews of Environmental Contamination and Toxicology Volume 237*; De Voogt, W. P., Ed.; Reviews of Environmental Contamination and Toxicology; Springer International Publishing: Cham, 2016; Vol. 237. <https://doi.org/10.1007/978-3-319-23573-8>.
- (53) Karami, P.; Khorshidi, B.; McGregor, M.; Peichel, J. T.; Soares, J. B. P.; Sadrzadeh, M. Thermally Stable Thin Film Composite Polymeric Membranes for Water Treatment: A Review. *J. Clean. Prod.* **2020**, *250*, 119447. <https://doi.org/10.1016/j.jclepro.2019.119447>.
- (54) Daufin, G.; Escudier, J.-P.; Carrère, H.; Bérot, S.; Fillaudeau, L.; Decloux, M. Recent and Emerging Applications of Membrane Processes in the Food and Dairy Industry. *Food Bioprod. Process.* **2001**, *79* (2), 89–102. <https://doi.org/10.1205/096030801750286131>.

- (55) Khorshidi, B.; Hosseini, S. A.; Ma, G.; McGregor, M.; Sadrzadeh, M. Novel Nanocomposite Polyethersulfone- Antimony Tin Oxide Membrane with Enhanced Thermal, Electrical and Antifouling Properties. *Polymer* **2019**, *163*, 48–56. <https://doi.org/10.1016/j.polymer.2018.12.058>.
- (56) Dong, H.; Qu, X.-Y.; Zhang, L.; Cheng, L.-H.; Chen, H.-L.; Gao, C.-J. Preparation and Characterization of Surface-Modified Zeolite-Polyamide Thin Film Nanocomposite Membranes for Desalination. *Desalination Water Treat.* **2011**, *34* (1–3), 6–12. <https://doi.org/10.5004/dwt.2011.2789>.
- (57) Kayvani Fard, A.; McKay, G.; Buekenhoudt, A.; Al Sulaiti, H.; Motmans, F.; Khraisheh, M.; Atieh, M. Inorganic Membranes: Preparation and Application for Water Treatment and Desalination. *Materials* **2018**, *11* (1), 74. <https://doi.org/10.3390/ma11010074>.
- (58) Huang, K.; Quan, X.; Li, X.; Tezel, F. H.; Li, B. Improved Surface Hydrophilicity and Antifouling Property of Nanofiltration Membrane by Grafting NH₂-Functionalized Silica Nanoparticles. *Polym. Adv. Technol.* **2018**, *29* (12), 3159–3170. <https://doi.org/10.1002/pat.4438>.
- (59) Soltannia, B.; Islam, M. A.; Cho, J.-Y.; Mohammadtabar, F.; Wang, R.; Piunova, V. A.; Almansoori, Z.; Rastgar, M.; Myles, A. J.; La, Y.-H.; Sadrzadeh, M. Thermally Stable Core-Shell Star-Shaped Block Copolymers for Antifouling Enhancement of Water Purification Membranes. *J. Membr. Sci.* **2020**, *598*, 117686. <https://doi.org/10.1016/j.memsci.2019.117686>.
- (60) Wang, G.; Xie, R.; Ju, X.-J.; Chu, L.-Y. Thermo-Responsive Polyethersulfone Composite Membranes Blended with Poly(*N*-Isopropylacrylamide) Nanogels. *Chem. Eng. Technol.* **2012**, *35* (11), 2015–2022. <https://doi.org/10.1002/ceat.201200235>.
- (61) Zhijuan, S.; Fengkai, D.; Qian, W.; Yilian, T.; Yaoyao, Z.; Congjie, G.; Lixin, X. High Water Permeating Thin Film Composite Polyamide Nanofiltration Membranes Showing Thermal Responsive Gating Properties. *J. Water Process Eng.* **2020**, *36*, 101355. <https://doi.org/10.1016/j.jwpe.2020.101355>.

- (62) Tripathi, B. P.; Dubey, N. C.; Simon, F.; Stamm, M. Thermo Responsive Ultrafiltration Membranes of Grafted Poly(N-Isopropyl Acrylamide) via Polydopamine. *RSC Adv* **2014**, *4* (64), 34073–34083. <https://doi.org/10.1039/C4RA03485F>.
- (63) Luo, F.; Zhao, Q.; Xie, R.; Cao, Y.; Ju, X.-J.; Wang, W.; Liu, Z.; Chu, L.-Y. Effects of Fabrication Conditions on the Microstructures and Performances of Smart Gating Membranes with in Situ Assembled Nanogels as Gates. *J. Membr. Sci.* **2016**, *519*, 32–44. <https://doi.org/10.1016/j.memsci.2016.07.045>.
- (64) Wu, D.; Liu, X.; Yu, S.; Liu, M.; Gao, C. Modification of Aromatic Polyamide Thin-Film Composite Reverse Osmosis Membranes by Surface Coating of Thermo-Responsive Copolymers P(NIPAM-Co-Am). I: Preparation and Characterization. *J. Membr. Sci.* **2010**, *352* (1–2), 76–85. <https://doi.org/10.1016/j.memsci.2010.01.061>.
- (65) Drikvand, H. N.; Golgoli, M.; Zargar, M.; Ulbricht, M.; Nejati, S.; Mansourpanah, Y. Thermo-Responsive Hydrophilic Support for Polyamide Thin-Film Composite Membranes with Competitive Nanofiltration Performance. *Polymers* **2022**, *14* (16), 3376. <https://doi.org/10.3390/polym14163376>.
- (66) Karami, P.; Aktij, S. A.; Khorshidi, B.; Firouzjaei, M. D.; Asad, A.; Elliott, M.; Rahimpour, A.; Soares, J. B. P.; Sadrzadeh, M. Nanodiamond-Decorated Thin Film Composite Membranes with Antifouling and Antibacterial Properties. *Desalination* **2022**, *522*, 115436. <https://doi.org/10.1016/j.desal.2021.115436>.
- (67) Mo, Y.; Tiraferri, A.; Yip, N. Y.; Adout, A.; Huang, X.; Elimelech, M. Improved Antifouling Properties of Polyamide Nanofiltration Membranes by Reducing the Density of Surface Carboxyl Groups. *Environ. Sci. Technol.* **2012**, *46* (24), 13253–13261. <https://doi.org/10.1021/es303673p>.
- (68) Zhang, X.; Xiong, S.; Liu, C.-X.; Shen, L.; Wang, S.-L.; Lang, W.-Z.; Wang, Y. Smart TFC Membrane for Simulated Textile Wastewater Concentration at Elevated Temperature Enabled by Thermal-Responsive Microgels. *Desalination* **2021**, *500*, 114870. <https://doi.org/10.1016/j.desal.2020.114870>.

- (69) ElSherbiny, I. M. A.; Khalil, A. S. G.; Ulbricht, M. Tailoring Surface Characteristics of Polyamide Thin-Film Composite Membranes toward Pronounced Switchable Wettability. *Adv. Mater. Interfaces* **2019**, *6* (5), 1801408.
<https://doi.org/10.1002/admi.201801408>.
- (70) Yu, C.; Wang, Y.; Lang, X.; Fan, S. A Method for Seawater Desalination via Squeezing Ionic Hydrogels. *Environ. Sci. Technol.* **2016**, *50* (23), 13024–13031.
<https://doi.org/10.1021/acs.est.6b03193>.
- (71) Razmjou, A.; Liu, Q.; Simon, G. P.; Wang, H. Bifunctional Polymer Hydrogel Layers As Forward Osmosis Draw Agents for Continuous Production of Fresh Water Using Solar Energy. *Environ. Sci. Technol.* **2013**, *47* (22), 13160–13166.
<https://doi.org/10.1021/es403266y>.
- (72) Cai, Y.; Shen, W.; Loo, S. L.; Krantz, W. B.; Wang, R.; Fane, A. G.; Hu, X. Towards Temperature Driven Forward Osmosis Desalination Using Semi-IPN Hydrogels as Reversible Draw Agents. *Water Res.* **2013**, *47* (11), 3773–3781.
<https://doi.org/10.1016/j.watres.2013.04.034>.
- (73) Höpfner, J.; Klein, C.; Wilhelm, M. A Novel Approach for the Desalination of Seawater by Means of Reusable Poly(Acrylic Acid) Hydrogels and Mechanical Force. *Macromol. Rapid Commun.* **2010**, *31* (15), 1337–1342. <https://doi.org/10.1002/marc.201000058>.
- (74) Dou, Z.; Wang, T.; Chen, W.; Lin, B.; Dong, H.; Sun, W.; Xie, X. Self-Driven Membrane Filtration by Core–Shell Polymer Composites. *J. Mater. Chem. A* **2020**, *8* (31), 15942–15950. <https://doi.org/10.1039/D0TA03617J>.
- (75) Yuan, X.; Cai, Y.; Jiang, J.; Zhou, Z.; Wang, C.; Hu, J.; Liu, L.; Li, B.; Liu, M. Membrane-Free Osmotic Desalination at near-Room Temperatures Enabled by Thermally Responsive Polyionic Liquid Hydrogels. *J. Mater. Chem. A* **2022**, *10* (46), 24453–24461.
<https://doi.org/10.1039/D2TA06869A>.
- (76) Gupta, N.; Liang, Y. N.; Chew, J. W.; Hu, X. Highly Robust Interfacially Polymerized PA Layer on Thermally Responsive Semi-IPN Hydrogel: Toward On-Demand Tuning of

- Porosity and Surface Charge. *ACS Appl. Mater. Interfaces* **2021**, *13* (50), 60590–60601.
<https://doi.org/10.1021/acsami.1c16639>.
- (77) Parasuraman, D.; Serpe, M. J. Poly (*N*-Isopropylacrylamide) Microgels for Organic Dye Removal from Water. *ACS Appl. Mater. Interfaces* **2011**, *3* (7), 2732–2737.
<https://doi.org/10.1021/am2005288>.
- (78) Parasuraman, D.; Serpe, M. J. Poly (*N*-Isopropylacrylamide) Microgel-Based Assemblies for Organic Dye Removal from Water. *ACS Appl. Mater. Interfaces* **2011**, *3* (12), 4714–4721. <https://doi.org/10.1021/am201132x>.
- (79) Gao, Y.; Wong, K. Y.; Ahiabu, A.; Serpe, M. J. Sequential and Controlled Release of Small Molecules from Poly(*N*-Isopropylacrylamide) Microgel-Based Reservoir Devices. *J. Mater. Chem. B* **2016**, *4* (30), 5144–5150. <https://doi.org/10.1039/C6TB00864J>.
- (80) Ribeiro, A. R.; Umbuzeiro, G. D. A. Effects of a Textile Azo Dye on Mortality, Regeneration, and Reproductive Performance of the Planarian, *Girardia Tigrina*. *Environ. Sci. Eur.* **2014**, *26* (1), 22. <https://doi.org/10.1186/s12302-014-0022-5>.
- (81) Gao, F. Poly (*N*-Isopropylacrylamide)-Based Microgels for Contaminant Removal from Water, University of Alberta, 2021.
- (82) Jiang, Y.; Colazo, M. G.; Serpe, M. J. Poly(*N*-Isopropylacrylamide) Microgel-Based Sensor for Progesterone in Aqueous Samples. *Colloid Polym. Sci.* **2016**, *294* (11), 1733–1741. <https://doi.org/10.1007/s00396-016-3926-3>.
- (83) Jiang, Y.; Colazo, M. G.; Serpe, M. J. Poly(*N*-Isopropylacrylamide) Microgel-Based Etalons for the Label-Free Quantitation of Estradiol-17 β in Aqueous Solutions and Milk Samples. *Anal. Bioanal. Chem.* **2018**, *410* (18), 4397–4407.
<https://doi.org/10.1007/s00216-018-1095-6>.
- (84) Islam, M.; Ahiabu, A.; Li, X.; Serpe, M. Poly (*N*-Isopropylacrylamide) Microgel-Based Optical Devices for Sensing and Biosensing. *Sensors* **2014**, *14* (5), 8984–8995.
<https://doi.org/10.3390/s140508984>.

- (85) Islam, M. R.; Serpe, M. J. Penetration of Polyelectrolytes into Charged Poly(*N*-Isopropylacrylamide) Microgel Layers Confined between Two Surfaces. *Macromolecules* **2013**, *46* (4), 1599–1606. <https://doi.org/10.1021/ma302637n>.
- (86) Cho, E. C.; Kim, Y. D.; Cho, K. Thermally Responsive Poly(N-Isopropylacrylamide) Monolayer on Gold: Synthesis, Surface Characterization, and Protein Interaction/Adsorption Studies. *Polymer* **2004**, *45* (10), 3195–3204. <https://doi.org/10.1016/j.polymer.2004.02.052>.
- (87) Marcisz, K.; Romanski, J.; Karbarz, M. Electroresponsive Microgel Able to Form a Monolayer on Gold through Self-Assembly. *Polymer* **2021**, *229*, 123992. <https://doi.org/10.1016/j.polymer.2021.123992>.
- (88) Bilić, A.; Reimers, J. R.; Hush, N. S.; Hafner, J. Adsorption of Ammonia on the Gold (111) Surface. *J. Chem. Phys.* **2002**, *116* (20), 8981–8987. <https://doi.org/10.1063/1.1471245>.
- (89) Hu, L.; Serpe, M. J. The Influence of Deposition Solution pH and Ionic Strength on the Quality of Poly(*N*-Isopropylacrylamide) Microgel-Based Thin Films and Etalons. *ACS Appl. Mater. Interfaces* **2013**, *5* (22), 11977–11983. <https://doi.org/10.1021/am403745k>.
- (90) Jones, C. D.; Lyon, L. A. Shell-Restricted Swelling and Core Compression in Poly(*N*-Isopropylacrylamide) Core-Shell Microgels. *Macromolecules* **2003**, *36* (6), 1988–1993. <https://doi.org/10.1021/ma021079q>.
- (91) Nigro, V.; Angelini, R.; Rosi, B.; Bertoldo, M.; Buratti, E.; Casciardi, S.; Sennato, S.; Ruzicka, B. Study of Network Composition in Interpenetrating Polymer Networks of Poly(N Isopropylacrylamide) Microgels: The Role of Poly(Acrylic Acid). *J. Colloid Interface Sci.* **2019**, *545*, 210–219. <https://doi.org/10.1016/j.jcis.2019.03.004>.
- (92) Wathukarage, A.; Herath, I.; Iqbal, M. C. M.; Vithanage, M. Mechanistic Understanding of Crystal Violet Dye Sorption by Woody Biochar: Implications for Wastewater Treatment. *Environ. Geochem. Health* **2019**, *41* (4), 1647–1661. <https://doi.org/10.1007/s10653-017-0013-8>.

- (93) Du, W.; Xu, Y.; Wang, Y. Photoinduced Degradation of Orange II on Different Iron (Hydr)Oxides in Aqueous Suspension: Rate Enhancement on Addition of Hydrogen Peroxide, Silver Nitrate, and Sodium Fluoride. *Langmuir* **2008**, *24* (1), 175–181. <https://doi.org/10.1021/la7021165>.
- (94) Saunders, B. R. On the Structure of Poly(*N*-Isopropylacrylamide) Microgel Particles. *Langmuir* **2004**, *20* (10), 3925–3932. <https://doi.org/10.1021/la036390v>.
- (95) Maity, S.; Mishra, B.; Nayak, K.; Dubey, N. C.; Tripathi, B. P. Zwitterionic Microgel Based Anti(-Bio)Fouling Smart Membranes for Tunable Water Filtration and Molecular Separation. *Mater. Today Chem.* **2022**, *24*, 100779. <https://doi.org/10.1016/j.mtchem.2022.100779>.
- (96) Zhao, G.; Chen, W. N. Design of Poly(Vinylidene Fluoride)-*g*-p(Hydroxyethyl Methacrylate-Co-*N*-Isopropylacrylamide) Membrane via Surface Modification for Enhanced Fouling Resistance and Release Property. *Appl. Surf. Sci.* **2017**, *398*, 103–115. <https://doi.org/10.1016/j.apsusc.2016.11.138>.
- (97) Liu, J.; Yu, L.; Yue, G.; Wang, N.; Cui, Z.; Hou, L.; Li, J.; Li, Q.; Karton, A.; Cheng, Q.; Jiang, L.; Zhao, Y. Thermoresponsive Graphene Membranes with Reversible Gating Regularity for Smart Fluid Control. *Adv. Funct. Mater.* **2019**, *29* (12), 1808501. <https://doi.org/10.1002/adfm.201808501>.
- (98) Andersson, M.; Maunu, S. L. Structural Studies of Poly(*N*-Isopropylacrylamide) Microgels: Effect of SDS Surfactant Concentration in the Microgel Synthesis. *J. Polym. Sci. Part B Polym. Phys.* **2006**, *44* (23), 3305–3314. <https://doi.org/10.1002/polb.20971>.
- (99) Pei, Y.; Chen, J.; Yang, L.; Shi, L.; Tao, Q.; Hui, B.; Li, J. The Effect of pH on the LCST of Poly(*N*-Isopropylacrylamide) and Poly(*N*-Isopropylacrylamide-Co-Acrylic Acid). *J. Biomater. Sci. Polym. Ed.* **2004**, *15* (5), 585–594. <https://doi.org/10.1163/156856204323046852>.

- (100) Crooks, J. E.; Robinson, B. H. Reaction between Bromophenol Blue and Aromatic Nitrogen Bases in Chlorobenzene Studied with a Laser Temperature-Jump Apparatus. *Trans. Faraday Soc.* **1970**, *66*, 1436. <https://doi.org/10.1039/tf9706601436>.
- (101) Sun, Z.; Li, L.; Wu, Q.; Zhang, Z.; Yang, L.; Jiang, G.; Gao, C.; Xue, L. Nano-Filtration Performance and Temperature Dependency of Thin Film Composite Polyamide Membranes Embedded with Thermal Responsive Zwitterionic Nanocapsules. *J. Membr. Sci.* **2022**, *656*, 120609. <https://doi.org/10.1016/j.memsci.2022.120609>.
- (102) Alsohaimi, I. H. Hybrid PSf/TNT-SO₃H Ultrafiltration Membrane Fouling by Sodium Alginate: Effect of Permeation Flux on Fouling Resistance and Desalination Efficiency. *Adsorpt. Sci. Technol.* **2022**, *2022*, 1–10. <https://doi.org/10.1155/2022/2885849>.
- (103) Zheng, Q.; Lü, C. Size Effects of Surface Roughness to Superhydrophobicity. *Procedia IUTAM* **2014**, *10*, 462–475. <https://doi.org/10.1016/j.piutam.2014.01.041>.
- (104) Li, C.; Zhang, J.; Han, J.; Yao, B. A Numerical Solution to the Effects of Surface Roughness on Water–Coal Contact Angle. *Sci. Rep.* **2021**, *11* (1), 459. <https://doi.org/10.1038/s41598-020-80729-9>.
- (105) Genzer, J.; Efimenko, K. Recent Developments in Superhydrophobic Surfaces and Their Relevance to Marine Fouling: A Review. *Biofouling* **2006**, *22* (5), 339–360. <https://doi.org/10.1080/08927010600980223>.
- (106) Ritt, C. L.; Werber, J. R.; Wang, M.; Yang, Z.; Zhao, Y.; Kulik, H. J.; Elimelech, M. Ionization Behavior of Nanoporous Polyamide Membranes. *Proc. Natl. Acad. Sci.* **2020**, *117*(48), 30191–30200. <https://doi.org/10.1073/pnas.2008421117>.
- (107) Dinari, A.; Mortazavi Farsani, S. S.; Mohammadi, S.; Najafi, F.; Abdollahi, M. A Facile Method for Morphological Characterization at Nano Scale. *Iran. J. Biotechnol.* **2020**, *18* (3). <https://doi.org/10.30498/ijb.2020.2645>.
- (108) Ma, Z.; Zhang, L.; Liu, Y.; Ji, X.; Xu, Y.; Wang, Q.; Sun, Y.; Wang, X.; Wang, J.; Xue, J.; Gao, X. Influential Mechanism of Natural Organic Matters with Calcium Ion on the

- Anion Exchange Membrane Fouling Behavior via xDLVO Theory. *Membranes* **2021**, *11* (12), 968. <https://doi.org/10.3390/membranes11120968>.
- (109) Zhang, M.; Lin, H.; Shen, L.; Liao, B.-Q.; Wu, X.; Li, R. Effect of Calcium Ions on Fouling Properties of Alginate Solution and Its Mechanisms. *J. Membr. Sci.* **2017**, *525*, 320–329. <https://doi.org/10.1016/j.memsci.2016.12.006>.
- (110) Li, X.; Mo, Y.; Qing, W.; Shao, S.; Tang, C. Y.; Li, J. Membrane-Based Technologies for Lithium Recovery from Water Lithium Resources: A Review. *J. Membr. Sci.* **2019**, *591*, 117317. <https://doi.org/10.1016/j.memsci.2019.117317>.
- (111) Shao, S.; Zeng, F.; Long, L.; Zhu, X.; Peng, L. E.; Wang, F.; Yang, Z.; Tang, C. Y. Nanofiltration Membranes with Crumpled Polyamide Films: A Critical Review on Mechanisms, Performances, and Environmental Applications. *Environ. Sci. Technol.* **2022**, *56* (18), 12811–12827. <https://doi.org/10.1021/acs.est.2c04736>.
- (112) Patel, S. K.; Biesheuvel, P. M.; Elimelech, M. Energy Consumption of Brackish Water Desalination: Identifying the Sweet Spots for Electrodialysis and Reverse Osmosis. *ACS EST Eng.* **2021**, *1* (5), 851–864. <https://doi.org/10.1021/acsestengg.0c00192>.
- (113) Louf, J.-F.; Lu, Nancy B.; O'Connell, Margaret G.; Cho, H. Jeremy; Datta, Sujit S. Under Pressure: Hydrogel Swelling in a Granular Medium. *Sci. Adv.* **2021**, *7* (7), 1–10. <https://doi.org/10.1126/sciadv.abd2711>.
- (114) Salehi, A. A.; Ghannadi-Maragheh, M.; Torab-Mostaedi, M.; Torkaman, R.; Asadollahzadeh, M. Hydrogel Materials as an Emerging Platform for Desalination and the Production of Purified Water. *Sep. Purif. Rev.* **2021**, *50* (4), 380–399. <https://doi.org/10.1080/15422119.2020.1789659>.
- (115) Ju, X.-J.; Zhang, S.-B.; Zhou, M.-Y.; Xie, R.; Yang, L.; Chu, L.-Y. Novel Heavy-Metal Adsorption Material: Ion-Recognition P(NIPAM-Co-BCAm) Hydrogels for Removal of Lead(II) Ions. *J. Hazard. Mater.* **2009**, *167* (1–3), 114–118. <https://doi.org/10.1016/j.jhazmat.2008.12.089>.

- (116) Huang, S.; Liu, X.; Hu, Q.; Wei, T.; Wang, J.; Chen, H.; Wu, C. Temperature-Driven Metalloprotein-Based Hybrid Hydrogels for Selective and Reversible Removal of Cadmium(II) from Water. *ACS Appl. Mater. Interfaces* **2020**, *12* (2), 2991–2998.
<https://doi.org/10.1021/acsami.9b19306>.
- (117) Musarurwa, H.; Tavengwa, N. T. Stimuli-Responsive Polymers and Their Applications in Separation Science. *React. Funct. Polym.* **2022**, *175*, 105282.
<https://doi.org/10.1016/j.reactfunctpolym.2022.105282>.
- (118) Tan, Z.; Chen, S.; Peng, X.; Zhang, L.; Gao, C. Polyamide Membranes with Nanoscale Turing Structures for Water Purification. *Science* **2018**, *360* (6388), 518–521.
<https://doi.org/10.1126/science.aar6308>.
- (119) Tanveer, S.; Chen, C.-C. Thermodynamic Analysis of Hydrogel Swelling in Aqueous Sodium Chloride Solutions. *J. Mol. Liq.* **2022**, *348*, 118421.
<https://doi.org/10.1016/j.molliq.2021.118421>.
- (120) Hüther, A.; Xu, X.; Maurer, G. Swelling of N-Isopropyl Acrylamide Hydrogels in Aqueous Solutions of Sodium Chloride. *Fluid Phase Equilibria* **2006**, *240* (2), 186–196.
<https://doi.org/10.1016/j.fluid.2005.12.025>.
- (121) Islam, M. R.; Tanveer, S.; Chen, C.-C. Modeling Swelling Behavior of Hydrogels in Aqueous Organic Solvents. *Chem. Eng. Sci.* **2021**, *242*, 116744.
<https://doi.org/10.1016/j.ces.2021.116744>.